THE UNIVERSITY OF CHICAGO

DEVELOPING A QUANTITATIVE DESCRIPTION OF FEEDING BEHAVIOR AND ITS RESPONSE TO PERTURBATIONS

A DISSERTATION SUBMITTED TO
THE FACULTY OF THE DIVISION OF THE PHYSICAL SCIENCES
AND
THE FACULTY OF THE DIVISION OF THE BIOLOGICAL SCIENCES
AND THE PRITZKER SCHOOL OF MEDICINE
IN CANDIDACY FOR THE DEGREE OF
DOCTOR OF PHILOSOPHY

GRADUATE PROGRAM IN BIOPHYSICAL SCIENCES

BY
MONIKA SCHOLZ

CHICAGO, ILLINOIS
AUGUST 2017

TABLE OF CONTENTS

LIST OF FIGURES

LIST OF TABLES

ACKNOWLEDGMENTS

I would like to thank my advisors, Aaron Dinner and David Biron for their support and mentorship during the past five years. I was lucky to have a lot of freedom to explore projects and seek out collaborations that might seem unusual at first. There was always an open door and a quick chat to get me back on track when I needed input. I want to acknowledge the support of my committee, Peggy Mason and Ed Munro, for their encouragement and guidance. I was lucky to get financial support through an international fellowship from HHMI. The freedom that came from that support was incredibly useful for my professional development and independence. I would like to acknowledge my long-term colleagues in the Biron and Dinner groups. We shared a lot of scientific discussions, laughs and worms. I want to thank my colleague Jarred Sanders, who is my co-author on Chapter 3. I am continually impressed by his drive to understand a system more deeply. My class mates in the biophysics program, especially my office mate Alan Hutchison, made the past years very enjoyable. Over the years, I got to work with a few talented undergraduates, visitors and lab techs. Natalie Gray and Ilaria Merutka and Rebecca Fishman helped trouble-shoot our protocols, improve image analysis code and patiently listened to my advice. Finally, I would like to thank my favorite co-author and best rubber duck debugger, Bjorn Scholz.

ABSTRACT

The regulation of food intake plays a major role in controlling energy availability in organisms. Feeding regulation needs to be robust to common perturbations, to ensure continued thriving of the organism. Here, I present the behavioral response of an animal to challenging feeding conditions: We assay low and temporally-varying levels of food, as well as feeding after stressful sleep-deprivation. I test the effect of these conditions in the nematode *Caenorhabditis elegans*, which is a model organism that shares conserved regulatory mechanisms with insects and vertebrates.

First, I describe a scalable automated method for measuring the food intake of *C. elegans* in controlled environments. This approach enables unbiased measurements for prolonged periods, high throughput, and the possibility of controlled, dynamically changing feeding environments. The automated analysis compares well with scoring pumping by visual inspection, a common practice in the field.

I then apply our automated method to investigate the regulation of feeding in response to variable food levels. Animals need to regulate their food intake in response to the availability of food in the environment. Frequently, animals have to integrate information from the environment to decide whether to expend energy feeding, or wait until conditions improve. I find that animals upregulate their feeding rate by changing the time spent in bursts of rapid pumping relative to pauses. We expose the animals to a dynamically changing environment with pulses of high and no food. We find that animals respond stochastically, only upregulating their pumping rate in response to some of the high food pulses, with no apparent pattern. This behavior cannot be explained by traditional models of feeding.

Using our newly developed tracking method, we investigate the effect of sleep deprivation on the highly active tissue of the pharynx. We show that during the last developmental stage of the organism, animals are vulnerable to damage through sleep deprivation. We find that adult animals exhibit deficits in feeding 12 hours after deprivation. Moreover, feeding defects were exacerbated when a transcription factor active during stressful periods and effective

in mitigating downstream damage was inactive. We show that these downstream effects include the mitochondrial unfolded protein response and endoplasmic reticulum stress. These observations link cellular damage directly to sleep deprivation, indicating that a protective mechanism exists to shield adult feeding behavior from damage.

Finally, I show that an information-theoretic model can recapitulate key features of the animals' feeding behavior. We find that the temporal pattern of feeding behavior is shaped by a balance between the need to obtain information about a changing environment and the exploitation of the available food. The model shows how a feeding pattern consisting of bursts and pauses can be advantageous for an animal. The model also accounts for stochastic responses to oscillating food levels, which was observed experimentally. Taken together, these results show how a quantitative description of behavior can be used to understand strategies that animals employ to ensure survival in challenging conditions.

CHAPTER 1

INTRODUCTION

1.1 Studying feeding behavior in a model organism

In 1951 the ethologist Nikolaas Tinbergen defined animal behavior as 'The total movements made by the intact animal'[1] (Tinbergen, 1951). By careful observation of an animal, one can often infer its needs, its adaptation to the environment and strategies it uses to effectively interact with that environment. Building on prior work, Tinbergen later formulated four questions that are required to understand what causes animals to behave in a certain way. First, he considers the question of 'how' a behavior is implemented. To this end, one needs to consider (i) Mechanism: how is the animal performing a behavior and (ii) Ontogeny: the temporal changes of the behavior over the lifetime of the animal. To understand 'why' a behavior exists one needs to consider (iii) Evolution: the selective forces that shaped the behavior and (iv) Real-world function: The fitness consequence of the behavior in its current form (Tinbergen, 1963). Combining these four levels of understanding provides a pluralistic view of behavior in context.

Behavioral research by careful observation and quantification has a long tradition going back to Charles Darwin, and has yielded fundamental explanations for behaviors. Recently, a group of neuroscientists argued that the top-down view of ethology, the inference of computational principles and mechanisms of behavior from observation, has been neglected (Krakauer et al., 2017). Newer studies, they argue, favor an interventionist, or bottom-up approach, which trades detailed analysis of individual neurons for a generalized understanding of behavior. The authors argue that the increase in available experimental techniques at the level of individual neurons and small circuits has caused this devaluation of careful behavioral

1. A recent update of the definition resulted from a survey of behavioral scientists: 'Behaviour is the internally coordinated responses (actions or inactions) of whole living organisms (individuals or groups) to internal and/or external stimuli, excluding responses more easily understood as developmental changes.'(Levitis et al., 2009)

experiments. Using Tinbergen's framework, this has led to a focus on the mechanism, while neglecting the other three aspects, especially the real-world function.

Ultimately, the goal of behavioral science is to establish a link between neuronal computation and behavior [2] To this end, neuronal observation has to be combined with behavioral analysis. In this thesis, I describe how one can use careful behavior experiments to infer the underlying function and physical implementation of a behavior. First, I present a method to quantify feeding behavior under relevant environmental conditions. I will show how disturbing the development of the animal affects adult behavior, thus considering ontogeny. Using the quantitative description, I define a model of feeding behavior that is motivated by the real-world function of the behavior. I then connect behavioral data with a possible implementation or mechanism of the behavior, considering the available 'hardware'. I will discuss how detailed behavioral studies can inform further studies at the neuronal and circuit level, to eventually establish a link between neuronal computation and organismal behavior. In particular, I focus on the feeding behavior of the nematode *Caenorhabditis elegans*, which serves as a model system with its quantifiable behavior and tractable genetics.

Feeding is an essential behavior for an animal. Food intake determines the energy balance of an organism which ultimately affects fitness. Food intake is highly regulated to avoid starvation, as well as diseases associated with unrestricted caloric intake. For example, in mammals failure to regulate feeding can lead to metabolic disorders, diabetes, and cardiovascular diseases (Colman et al., 2009; Fontana et al., 2010; Lin et al., 2004). In ecology, foraging behavior has been studied extensively for a number of species. Quantitative descriptions of foraging behavior and models of optimal foraging abound. However, the act of food intake (feeding) has been less well characterized and few models exist. The decision to feed and what to eat (if a choice exists) is crucial for survival, but characterizing feeding is more challenging. It requires the accurate characterization of food intake, as opposed to the

2. Typically called the brain-behavior link, which stems from a vertebrate-centric view. However, simple computations leading to behavior have been observed with animals which do not have a classical brain, but rather rely on a distributed neural network such as *Hydra vulgaris* (Dupre and Yuste, 2017).

easier task of tracking the locomotion of a whole organism. Feeding behavior depends on the animal's life history, its current metabolic state and other learned behaviors. Typically, it is highly coupled to foraging behavior, which makes studying it more challenging. The study of feeding in mammals has identified important aspects of satiety, obesity and the interaction of metabolic pathways and feeding behavior (Belsky et al., 2013; Tecott and Abdallah, 2003; Prado-Lima et al., 2006; Leibowitz, 1990; Halford et al., 2010). However, studies in mammalian systems are often limited to a small number of subjects, and behavioral studies are hard to control. Especially the dependence on life-history impedes studies in humans, often precluding generalizable conclusions and obscuring subtle effects. To transition from a correlative to a causative study, one needs to use an animal model with easily quantifiable behaviors, accessible genetics, and a controllable life-history. Recent studies in flies and worms have shown that these model systems fulfill these criteria and are amenable for large-scale studies (Lee et al., 2017; Scholz et al., 2016b; Itskov et al., 2014).

1.2 Feeding in *Caenorhabditis elegans*

Caenorhabditis elegans is a millimeter-long roundworm with a life-span of 12 - 18 days and a reproductive cycle of approximately 3 days. The animal is transparent to visible light which enables imaging of fluorescently-labeled cells within the body of the animal. *C. elegans* can rapidly reproduce either by self-fertilization or by mating. The animal then produces between 300 and 1000 offspring. Self-fertilization is particularly useful for propagating the animal in the laboratory: A homozygous animal breeds true when self-fertilized, which leads to large clonal populations that are available for experiments. *C. elegans* has been used as a model system for diverse processes ranging from development, aging, and pathogenesis to memory and learning (Leung et al., 2008; Olsen et al., 2006; Labrousse et al., 2000; Rankin et al., 1990). It is also a relevant model for feeding, metabolism and fat storage, since a number of genes involved in these processes are orthologs to human genes (a recent review can be found in (Luedtke et al., 2010)).

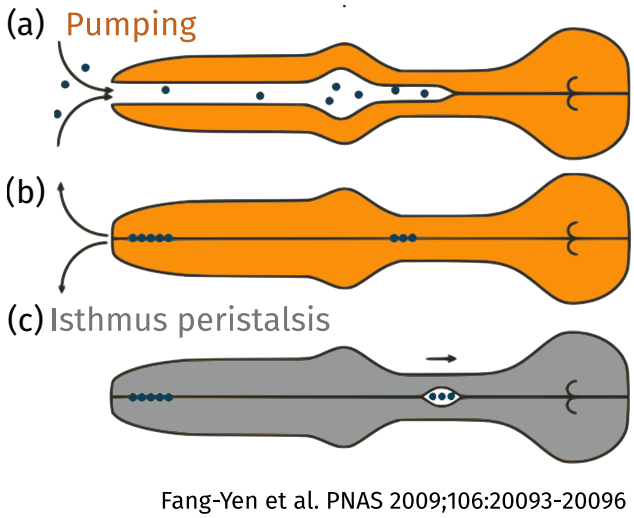

Figure 1.1: **Schematic of food intake in *C. elegans*.**

In the wild, *C. elegans* lives on rotten fruit and compost. In its natural habitat, the animal encounters bacterial colonies and small eukaryotes (Félix and Braendle, 2010). As a filter-feeder, the nematode draws in bacteria suspended in liquid. Through coordinated muscular action, it separates the liquid and only ingests the bacteria. In the laboratory, *C. elegans* can be maintained on *E. coli*(OP50) on agar plates. The approximately micron-sized bacteria are in the middle of the range of edible bacteria for the nematode (Fang-Yen et al., 2009b).However, *E. coli* would rarely be encountered by freely living animals and is thus not considered an ecologically relevant food source (Félix and Braendle, 2010). Comparative studies have investigated feeding on alternative strains of bacteria and found that *C. elegans* can thrive on a variety of food sources (Shtonda and Avery, 2006). Since the animal is a filter feeder, it can only consume particles in a small range of sizes. Studies found that effective growth depends on bacterial size, and only a specific range of sizes is consumed effectively by the animal (Fang-Yen et al., 2009b). Besides filtering by size, the animal also adapts its feeding preference to other internal and external cues. For example, the animal will favor familiar food over unfamiliar food, and preferentially seek out food of higher nutritional value (Song et al., 2013; Shtonda and Avery, 2006). Another aspect of food choice behavior is the avoidance of pathogenic bacteria. Initially, animals preferentially consume *Pseuodomonas*

aeruginosa over their standard diet of *E. coli*(OP50). *P.aeruginosa* are pathogenic to the animal by causing an intestinal infection. However, after a few hours, the animals return to their standard food and leave the pathogenic bacterial lawn.

C. elegans feeding consists of two muscular motions, pumping and isthmus peristalsis (Fig. 1.1). Pumping is a contraction-relaxation cycle of the pharynx that leads to ingestion, food concentration, and grinding of the bacteria. The contraction opens the pharyngeal lumen and creates suction that leads to the intake of a bacteria-liquid mixture (Fig. 1.1(a)). During relaxation, liquid and bacteria are separated by mechanical action and the liquid is spit out (Fig. 1.1(b)). After a few pumps, the collected bacteria are moved towards the intestine through isthmus peristalsis (Fig. 1.1(c)). While isthmus peristalsis helps to propagate bacteria through the narrow lumen of the pharynx, it does not contribute to the amount of food that is ingested. At a given concentration of bacteria in the environment, the product of pumping rate and bacteria concentration therefore fully determines the total amount of food consumed. The largest pumping rate observed is 6 Hz, which is the fastest possible muscle contraction and thus represents a physiological maximum.(Avery, 1993b). Isthmus peristalsis only occurs every few pumps, at about 1 Hz. The timing of isthmus peristalsis is coupled to the preceding pump, and regulated by separate but coupled molecular pathways (Song and Avery, 2012). The coordinated action of these two processes is required for efficient trapping of bacteria in the pharynx (Avery and Shtonda, 2003a).

The pharynx of the worm is an organ that is separated from the rest of the body by a basal lamina. The organ consists of around 80 cells, of which 20 are muscle cells and 20 are neurons. The remaining cells are arcade cells, epithelia, glands, marginal cells and valves. The 20 neurons form a small neuronal network, which receives inputs from the body via a single connection, the RIP interneuron. This reduces the complexity of studying the connection between behavior and its neuronal regulation from the 302 neurons of the whole body to a mere 20 neurons. However, it has been suggested that small molecules can cross the basal lamina and enter the pharynx from the pseudocoelic fluid. These interactions have only

been considered recently, and are likely relevant to the function of the organ. An important example of this is the regulation of feeding by the bioamine serotonin (5-hydroxytryptophane or 5-HT) (Lee et al., 2017; Song and Avery, 2012; Hobson et al., 2006). Feeding can be stimulated in the absence of food by administering serotonin. Serotonin is only produced in 3 types of neurons in the worm. Only one such type of neuron exists in the pharynx, the pair of neurosecretory neurons NSM. A loss of function in *tph-1* abolishes the production of 5-HT in the animal and results in a drastic loss of pumping activity. However, stopping the production of 5-HT in NSM only does not result in the full phenotype, suggesting that 5-HT produced in the body enters the pharynx (Lee et al., 2017). This example illustrates the importance of small-molecule signaling. This type of signaling has to be considered for a full understanding of feeding regulation and can be seen as a 'shadow wiring diagram' in addition to neuronal regulation.

The 20 pharyngeal neurons comprise 14 different types. They are connected to the rest of the animal via a gap junction between I1 and RIP. Of the pharyngeal neurons, only the MC cholinergic motorneurons are required for rapid pumping in the presence of food (Avery and Horvitzt, 1989; Raizen et al., 1995a). The pharynx shows myogenic activity even in the absence of neuronal control (Avery and Horvitzt, 1989). This unregulated activity has been reported to discharge at approximately 1 Hz. The cholinergic neurons M2, M4, MC, and I1 form a degenerate network, excitatory for pumping and robust, where I1 can activate both MC and M2 (Trojanowski et al., 2014). In addition, the glutamatergic M3 neurons regulate the termination of a pump, which determines the duration of a single pumping cycle. The M4 neuron regulates the timing of isthmus peristalsis (Avery and Horvitzt, 1989; Avery, 1993b; Raizen et al., 1995a). Under standard conditions, M3, M4, and MC are sufficient for supporting nearly normal feeding and growth (Raizen et al., 1995a; Avery and You, 2012). M4 is mainly responsible for the timing of isthmus peristalsis. The function of the other neurons are poorly understood, and previous studies using manual counting of pumping rates in saturated food found removal of these neurons to have no effect on the average

pumping rate. This leads to a minimally required regulatory network of pumping consisting of 4 neurons (Fig. 1.2).

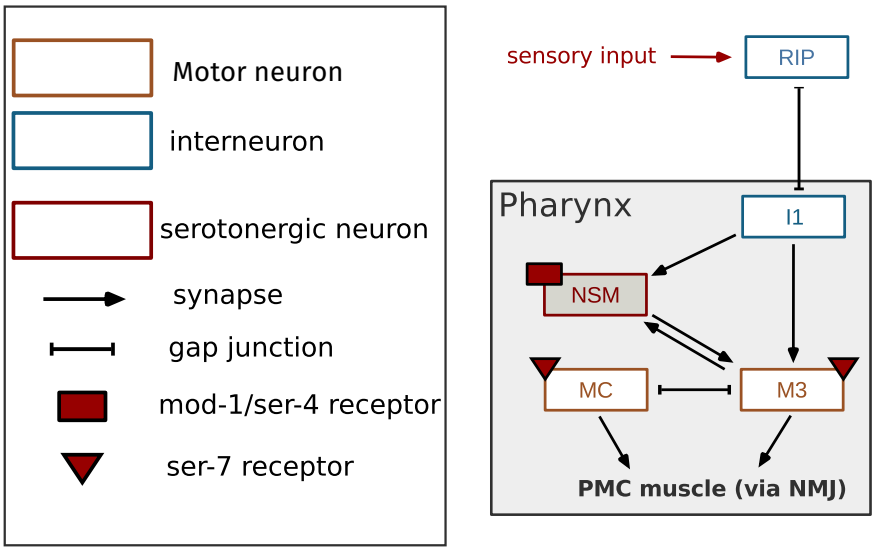

Figure 1.2: **Simplified regulatory network of pumping.** The minimal neuronal requirements for apparent normal pumping. Not included are M4 and I5, which are required for isthmus peristalsis timing and trapping of bacteria.

1.2.1 Approaches to quantifying feeding behavior

Previous studies have used manual counting of terminal bulb contractions during a finite amount of time (typically a minute) (Avery and Horvitzt, 1989; Raizen et al., 1995a; Song et al., 2013). The reduction of a potentially complex time-series to a single average rate may result in reduced information and potential bias. Timeseries of pumping show complex temporal dynamics that are not well described by such a mean rate (Lee et al., 2017; Scholz et al., 2016b). Feeding behavior has traditionally been studied either in a saturated food level, or when no food was present. To decouple foraging from feeding, animals are often placed in large homogeneous environments. Bacterial lawns on a standard cultivation plate are typically highly concentrated and large compared to the worm. A different approach is to use microfluidic chips to accurately control the food levels both in time and concentration. Microfluidic chips have been used for a range of behavioral assays. The geometry of the

chip can be designed to confine the animals, which simplifies imaging animal behavior. The temporal control of nutrients allows designing more complex assays. A specific chip design can also help to multiplex the behavioral assay. The stress-levels and longevity of animals in microfluidic chips have been assessed and are typically found to be comparable to animals on agar plates (Kopito and Levine, 2014).

Optical methods have been used to assist manual counting. By recording a short video and using a kymograph to count pharyngeal pumps, accuracy can be improved over counting without visual aids. However, automatically quantifying pumping has been challenging due to two main problems. First, a freely behaving animal explores the experimental arena. Pharyngeal pumping with a rate of around 4-5 Hz will be distorted by the head swing the animal performs while moving, which occurs at about 2 Hz. Secondly, the amplitude of contraction in the terminal bulb is relatively small. To track pumping in a freely moving animal, one needs to bridge the scales between resolving the terminal bulb (about 30 μm) while imaging or tracking the head of the animal, which is much larger and moves many bodylengths per minute. Tracking pumping in freely moving animals is to my knowledge an unsolved problem.

Electrophysiological methods for assaying pumping, such as non-invasive electrophysiology in microfluidic devices, offer the potential for a vast improvement over visual inspection (Raizen and Avery, 1994; Lockery et al., 2012; Hu et al., 2013; Hincks et al., 2016). The devices integrate the required electronics in single or few time-use microfluidic chips. However, these devices are often designed for screening purposes and do not allow long-term behavioral assays or multiplexing.

1.3 Developmentally-timed sleep in *C. elegans*

During development, *C. elegans* transitions through four larval stages. At the end of each such stage, the animal enters a two - to three-hour-long period of quiescence before molting called lethargus. This quiescent state shares many characteristics with sleep, and has thus

recently been termed 'developmentally-timed sleep' [3]. Key similarities with mammalian sleep are sensory gating, a typical posture, rebound sleep, and conserved regulatory pathways (Cho and Sternberg, 2014; Driver et al., 2013b; Iwanir et al., 2013; Nagy et al., 2014; Raizen et al., 2008; Schwarz et al., 2012; Singh et al., 2011; Tramm et al., 2014). Behaviorally, one can observe that the animals cease feeding for the entire duration of lethargus. However, a detailed study of the pair of pharyngeal neurons NSM shows that synaptic branching increases rapidly during development and continues to increase more slowly during adulthood (Axäng et al., 2008). Another study showed that the pharynx grows in bursts specifically during lethargus (George-Raizen et al., 2014).

1.4 About this dissertation

In the following chapters I present a group of studies that use quantitative behavioral observations to understand feeding behavior. In Chapter 2, I present an optical setup and quantitative imaging tools that allow automatic analysis of *C. elegans* feeding behavior. I also show how animals alter their behavior in response to the available food and to temporally varying food levels. Chapter 3 describes the effects of sleep deprivation during development on feeding behavior. The effects on sleep deprivation on the active neuro-muscular pharynx are compared with the effects on the egg-laying circuit. Chapter 4 builds on the data presented in Chapter 2 to motivate a model of feeding behavior. In that chapter, I discuss the implications of the model and its advantages compared to other possible models. In Chapter 5, I discuss future experiments that could help elucidate the role of the nervous system in regulating feeding and how the general principles developed in Chapter 4 can inform experiments. I also discuss the need for ecologically relevant behavioral experiments.

3. A review of the work on sleep in *C. elegans* and a detailed discussion of similarities with sleep in other animals can be found in (Trojanowski and Raizen, 2016)

CHAPTER 2

A SCALABLE METHOD FOR AUTOMATICALLY MEASURING PHARYNGEAL PUMPING IN *C. ELEGANS*

2.1 Overview

A key requirement to quantifying behavior is the existence of appropriate tools and methods. Before I developed the method presented in this chapter, *C. elegans* feeding behavior was typically quantified by manual counting of pumps over a minute. Alternatively, electrophysiological measurements existed, but were not widely used, mostly due to costly or complicated setups. We approached this problem from the opposite end: Can we combine an inexpensive setup with an advanced image analysis and create a setup that is easy to use and simple to implement. The resulting setup and image analysis tools have been used for the work presented in the following chapters. The key concept of the image analysis can also be used in any other context where an abrupt, stereotypical change needs to be detected.

The results presented in this chapter were published in 2016 (Scholz et al., 2016b). Co-authors: Dylan J. Lynch, Kyung Suk Lee, Erel Levine and David Biron.

2.2 Abstract

The nematode *Caenorhabditis elegans* is widely used for studying small neural circuits underlying behavior. In particular, the rhythmic feeding motions collectively termed pharyngeal pumping are regulated by a nearly autonomous network of 20 neurons of 14 types. Despite much progress achieved through laser ablation, genetics, electrophysiology, and optogenetics, key questions regarding the regulation of pumping remain open. We describe the implementation and application of a scalable automated method for measuring pumping in controlled environments. Our implementation is affordable and flexible: key hardware and software elements can be modified to accommodate different requirements. We demonstrate prolonged

measurements under controlled conditions and the resulting high quality data. We show the scalability of our method, enabling high throughput, and its suitability for measuring food intake in static and dynamic conditions. When food availability oscillated, pumping rates were low as compared to steady conditions and pumping activity was not reliably modulated in response to changes in food concentration. The prevailing method for measuring rates of pumping relies on scoring by visual inspection of short recordings. Our automated method compares well with manual scoring. It enables detailed statistical characterization under experimental conditions not previously accessible and minimizes unintentional bias. Our approach adds a powerful tool for studying pharyngeal pumping. It enhances the experimental versatility of assaying genetic and pharmacological manipulations and the ability to characterize the resulting behavior. Both the experimental setup and the analysis can be readily adapted to additional challenging motion detection problems.

2.3 Introduction

Food intake and energy expenditure are tightly regulated by a complex interplay between neurotransmitters, hormones and nutrients. Therefore feeding was extensively studied using simple model organisms (Lemieux and Ashrafi, 2015; Li et al., 2012). The nematode *Caenorhabditis elegans* feeds by drawing bacteria suspended in liquid into its pharynx, a neuromuscular organ that functions as a pump. The cycle of contraction and relaxation that draws food from the environment and filters bacteria from liquid is referred to as pharyngeal pumping. About one out of four pharyngeal pumps is followed by a posterior moving peristaltic contraction that transports food past the pharyngeal isthmus. This is referred to as isthmus peristalsis and, while coupled to pumping, it is distinctly regulated (Avery and Horvitz, 1987; Raizen and Avery, 1994; Avery and You, 2012; Song and Avery, 2013). The rate of pumping is thus the primary indicator of food intake (Avery, 1993b).

The rate of pumping depends on feeding history, quality of food, and the familiarity of food (Shtonda and Avery, 2006; Song et al., 2013; Hobson et al., 2006). Counting the

stereotypical motion observed in the terminal bulb of the pharynx enabled detailed analyses of neuronal and molecular mechanisms that regulate pumping. However, these regulatory pathways were predominantly examined in a stationary environment, containing a saturated, high abundance of (familiar) bacteria on a standard agar plate. Moreover, traditional feeding assays rely on manual scoring of the mean number of pumps over brief (typically 30 sec) intervals (Avery and Horvitzt, 1989; Raizen et al., 1995a; Song et al., 2013). The reduction of a potentially complex time-series to a single average rate may result in loss of pertinent information or even unintended bias. Electrophysiological methods for assaying pumping, such as non-invasive electrophysiology in microfluidic devices, offer a vast improvement over visual inspection (Raizen and Avery, 1994; Lockery et al., 2012; Hu et al., 2013; Hincks et al., 2016). They are complementary to the approach presented here as they may require more specialized equipment or expertise, and are less easily adaptable to alternative preparations. Bacterial lawns on a standard cultivation plate are typically highly concentrated and large compared to the worm. Under these conditions, reported pumping rates are 4-5 Hz and the duration of a single pump (constrained by the physiology of the pharynx) is approximately 170 ms (Avery, 1993b). The pharynx is separated from the rest of the body by the basal lamina, an extracellular formation of connective tissue. It contains 20 muscle cells and 20 neurons. Of these, only the MC cholinergic motorneurons were found to be individually required for rapid pumping in the presence of food (Avery and Horvitzt, 1989; Raizen et al., 1995a). The cholinergic neurons M2, M4, MC, and I1 form a degenerate network, excitatory for pumping and robust, where I1 can activate both MC and M2 (Trojanowski et al., 2014). In addition, the glutamatergic M3 neurons regulate the termination of a pump and M4 regulates isthmus peristalsis (Avery and Horvitzt, 1989; Avery, 1993b; Raizen et al., 1995a). Under standard conditions, M3, M4, and MC are sufficient for supporting nearly normal feeding and growth (Raizen et al., 1995a; Avery and You, 2012). The functions of additional pharyngeal neurons are poorly understood. In part, this may be due to the challenges of characterizing the phenomenology of pharyngeal pumping more systematically.

Here we describe an affordable and scalable method for automatically assaying pharyngeal pumping. Our method combines a previously described microfluidic device (Kopito and Levine, 2014), low cost educational microscopes, and an image analysis pipeline implemented using widely available open source tools and libraries. The image analysis code package is available for download from (Scholz, 2016a). The advantages of our approach include precise control of conditions such as the quality, uniformity, and concentration of available food, the possibility of prolonged measurement durations (hours, if required), unbiased automatic detection of pumping events, and the possibility to assay feeding conditions that change dynamically in a controlled manner. Manual scoring of pumping is arduous and limited to brief measurement periods. Automatic scoring of pumping on a high quality microscope is throughput-limited due to the cost of the imaging equipment. We found that lower quality imaging can be compensated for by rapid sampling and improved analysis without compromising the quality of the data. Using three microscopes we were able to assay up to 50 animals per day, i.e., 6 animals per objective, each for a full hour. The cost of the required equipment was $\$2,000$ (not including optional syringe pumps or other pressure sources). The setup can be further duplicated and the rate limiting step is the number of microfluidic devices that the researcher can load. The degree to which food availability can be dynamically controlled is dictated by the design of the microfluidic device used to restrict the motion of the animals and by the capabilities of the pressure source that is driving the fluid flow.

To validate our method we have compared the automatic detection to manual scoring. In addition, we characterized the phenomenology of feeding under three fixed food concentration, two velocities of fluid flow through the device, and in the presence of oscillations in food availability. We confirmed that the rate of pharyngeal pumping increases with the concentration of available food and that bursts of continuous pumping are interspersed with intervals of inactivity. In our hands, the rate of fluid flow affected the rate of pumping significantly but mildly. Finally, we measured pumping in the presence of oscillations in food availability. Interestingly, the mean rate of pumping was reduced two fold with respect to

comparable steady state conditions. When pumping dynamics of individual animals were analyzed we found that, in addition to low mean rates, shifts in food concentration could fail to evoke corresponding changes in the rate of pumping. Therefore, *C. elegans* feeding activity can persist for timescales that are longer than the rate of change in food concentration even when the latter is on the order of tens of seconds. Further work would be required to determine how pumping is regulated in response to the dynamics of the available food.

2.4 Results

2.4.1 A scalable imaging setup to record feeding behavior

We found that the image quality of commonly available educational microscopes, such as the Celestron 44104, is sufficient for assaying pharyngeal pumping. This model is equipped with 4x, 10x, and 40x air objectives, LED illumination, and a manual dual-axis translation stage. For convenience, a simple mount for the microfluidic device can be assembled from laser-cut PMMA (Poly(methyl methacrylate), acrylic). Basler acA1920-25um scientific CMOS cameras were used for imaging. Mounting the cameras can be achieved by gluing a laser-cut acrylic ring to a C-mount adapter (Thorlabs SM1A9) or by 3D printing a suitable mount. Image acquisition was controlled by a small desktop computer equipped with a three drive RAID 0 array for fast storage. Animals were assayed on WormSpa microfluidic devices (Kopito and Levine, 2014). An Elveflow OB1 Mk3 pressure controller and and MUX-D10 automated injection valve were used to dynamically change food availability.

2.4.2 Image analysis compensates for low-cost optics

Pharyngeal pumping motion is most easily detected through the motion of the grinder – a cuticle region of the pharynx inside the terminal bulb that is used to crush bacteria to aid digestion (Avery and Thomas, 1997). At low magnifications, directly tracking the position of the grinder is ineffective: the amplitude of grinder motion is small and any translation

or deformation of the head will compromise the data. Therefore, our approach relied on intensity differences between consecutive images and on the separation of timescales between head motion and pumping (Fig. 2.1A-B).

Key to this approach is a high imaging rate, 62.5 fps, more than 10 times faster than the maximal instantaneous rate of pumping. Substantially reducing the rate of acquisition would compromise the integrity of the data. The two main reasons for this are: (i) motion peaks associated with individual pumping events are $\sim$ 50 ms wide. At 60 fps, each peak is sampled by merely 3 data points. Attempting to sample less frequently would impede detection. (ii) The position of the head is maintained by mounting the animal into the WormSpa microfluidic device (Kopito and Levine, 2014). In such devices, tracking a moving animal is not required and the motion of the head is dampened without a major impact on feeding. However, the head is not fully restrained. At lower imaging rates the abrupt yet minuscule motion of the grinder would no longer dominate over motion artifacts.

Subtracting consecutive frames that were captured 16 ms apart isolates fast-changing features, i.e., the motion of the grinder. Examples of distributions of intensity differences in the presence or absence of a pump are shown in Fig. 2.1C. Notably, rapid motion affects the tail of this distribution. Therefore, a measure that preferentially weighs the tail would enhance the signal to noise ratio of motion detection. Using the entropy, $\sum_i p_i \log p_i$ (where p_i is the probability of observing intensity i in the difference image), to enhance the significance of motion achieves this goal (Jing et al., 2004). An additional advantage of this method as compared to tracking the grinder is that no model of the background needs to be calculated. In a high frame-rate movie of grinder motion, the entropy of intensity differences peaks sharply when pumping occurs while contributions of slower head motions are minor. In our hands, imaging conditions did not require fine tuning in order to maintain a signal to noise ratio that exceeded 200% (2.1D).

Peaks in the entropy were identified using a standard peak detection algorithm. To validate the correspondence between such peaks and pumping events we compared the per-

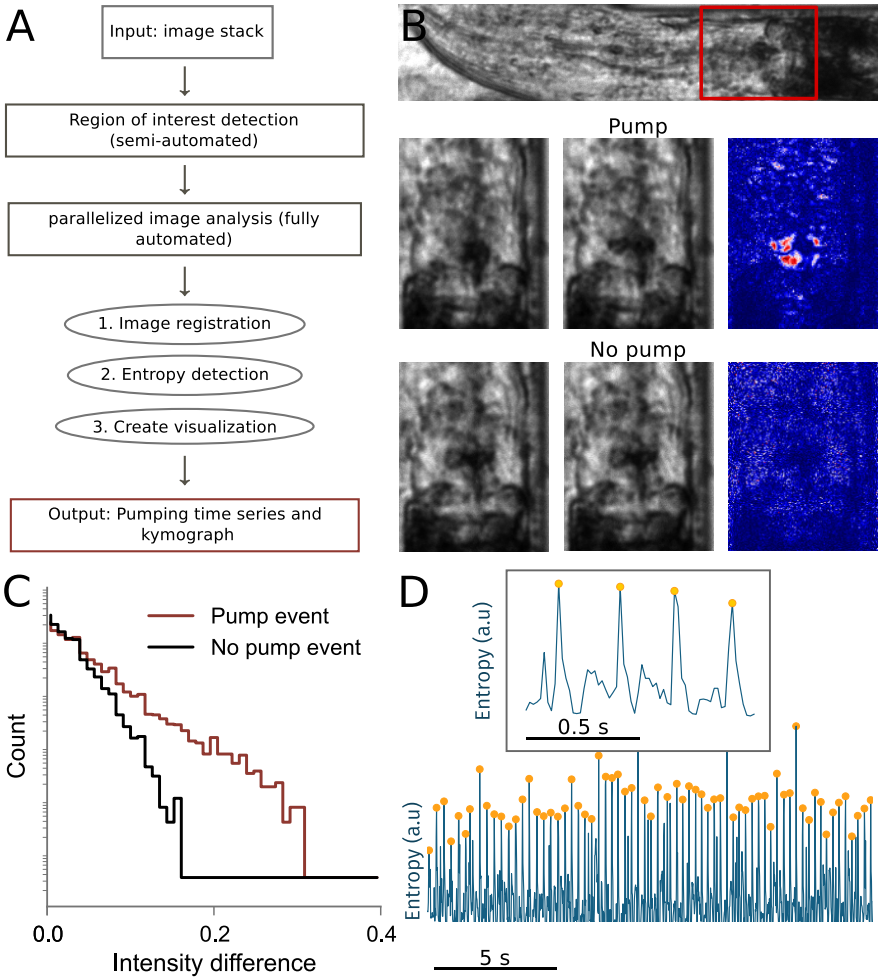

Figure 2.1: **Entropy-based detection of pumping events.** (A) An overview of the work flow from image acquisition to the time series of entropy peaks. Individual steps require little user input such that multiple animals can be analyzed in parallel. (B) Top: an image of the head of a nematode in a WormSpa microfluidic device mounted on an educational microscope (10x magnification). The terminal bulb is enclosed in a red box and the grinder appears as a dark spot at its center. Middle: a pair of consecutive frames captured during a pump and a heat map of the intensities in the corresponding difference image. Bottom: same as above for a pair of frames captured in the absence of a pump. Pumping results in a small number of high intensity pixels in the difference image. (C) The distribution of intensity values in the difference image in the presence (red) and absence (black) of a pump. The separation between the two histograms is most pronounced at the high intensity tail of the distribution. (D) A sample trace showing the dynamics of entropy during four (top) or many (bottom) pumping events. Individual events correspond to characteristic entropy peaks, which are readily identified by a standard peak detection algorithm followed by a minimal height selection criteria (orange dots) and the removal of close double peaks (less than ten frames apart).

formance of our method to identifying pumps by visual inspection. The confinement of the animals constrains head motion to the direction of the longitudinal axis of the body. We thus generated kymographs of the animal over time by summing across the lateral axis of each frame. The grinder appeared as a dark spot in each line and pumps appear as stereotypical peaks. We verified that these peaks correspond to pumping motion in the raw images and counted kymograph peaks by visual inspection. We found that manual and automatic detection of pumping highly correlated (Fig. 2.2A). To compare our measurements to previously reported pumping rates, we binned our data in 30 sec intervals. The resulting pumping rates also exhibited good agreement between manual and automatic scoring (Fig. 2.2B). Likewise, the distributions of instantaneous rates, i.e., of the reciprocal values to the periods measured between consecutive pumps, were similar (Fig. 2.2C-D). Therefore, we concluded that our assays are capable of identifying pharyngeal pumping with a high level of accuracy.

2.4.3 Pharyngeal pumping is affected by the concentration and the flow rate of bacterial food.

To demonstrate our method, we first assayed pharyngeal pumping in the presence of fixed food concentrations. In agreement with previous reports, pumping rates decreased when the concentration of bacteria was lowered but did not vanish in the absence of food (Fig. 2.3A-C). In addition, the mean rates we observed were comparable (Fig. 2.3C) to the values reported previously (Avery, 1993b; Hobson et al., 2006; Raizen et al., 1995a). Henceforth, unless stated otherwise the low and high food concentrations were set to $OD_{600} = 0.0$ and 4.0 [1], respectively. Fig. 2.3A-B depict typical distributions of instantaneous pumping rates under these conditions. When food was readily available, wild-type animals exhibited a peak rate of $4-5$ Hz but also a substantial tail of lower rates. In our hands, changing the flow rate in the device from 5 to 200 $\mu l/min$ resulted in a mild yet significant reduction in pumping rates

1. OD_{600} is the optical density of a sample measured using light with a 600 nm wavelength. This is a standard technique used to establish concentration measurements of bacterial cultures.

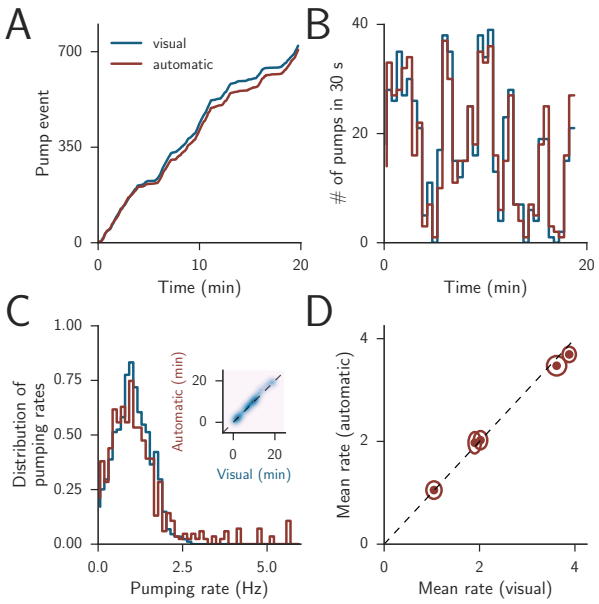

Figure 2.2: **Pumping detection at low magnification (4x)**. All panels correspond to 20 min recordings of wild-type animals in which automated and manual scoring were compared. Unless stated otherwise, the concentration of bacterial food (*E. coli* OP50) was $OD_{600} = 2.5$. In panels A-C, automated and manual scoring are plotted as red and blue lines, respectively. (A) An example of the cumulative number of pumps as a function of time ($R^2 = 0.98$). (B) The data from panel A binned in 30 sec bins ($R^2 = 0.90$). (C) An example of a distribution of instantaneous pumping rates (intervals between consecutive pumps). Inset: correlation between the automatically detected and manually detected pump events. The dashed line denotes unity. Intensity corresponds to the density of pumping events. (D) Mean pumping rates from 5 animals (one per data point). Here, the instantaneous pumping rates were smoothed with a median filter of width 15 peaks. The dashed line denotes unity, the major and minor axes of the ellipsoids represent the standard deviations of the two rates. To obtain a range of mean rates, we assayed 5 animals at food concentrations between $OD_{600} = 3$ and $OD_{600} = 5$ and scored 500 pumping events per animal.

(Fig. 2.3A, C). Our measurements were performed continuously and therefore invariably included periods devoid of pumping events, as indicated by the low frequency tail in Fig. 2.3A. Therefore, we also measured the duration of continuous pumping, defined as a series of consecutive pumps that were separated by no longer than 250 ms. The fraction of time spent in continuous pumping was defined as the pharyngeal duty ratio, which also increased with food concentration (Fig. 2.3D). These results indicate that our method provides an unbiased and efficient approach for characterizing pharyngeal pumping at precisely controlled steady

state conditions.

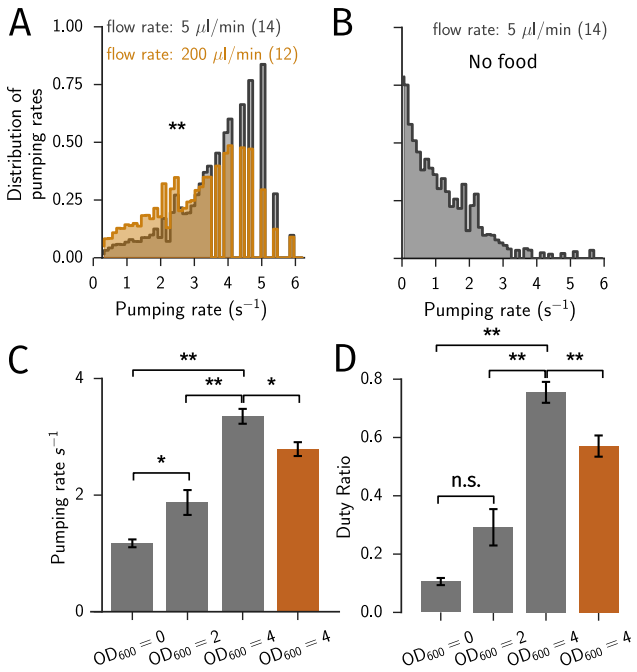

Figure 2.3: **Pumping at variable food levels.** All panels correspond to recordings from wild-type animals at 4x magnification. In A-D each animal was assayed for 30 min at a constant concentration of food (*E. coli* OP50). (A) Wild-type instantaneous pumping rates at a food concentration of $OD_{600} = 4.0$ were affected by the flow rate in the device. Flow rates of 5 $\mu l/min$ and 200 $\mu l/min$ are plotted in grey and orange, respectively. $N_{5\ \mu l/min} = 14$, $N_{200\ \mu l/min} = 12$ animals (B) Instantaneous pumping rates in the absence of bacterial food ($OD_{600} = 0.0$). $N = 14$ (C-D) Mean pumping rates and duty ratios for the data presented in panels A-B. The duty ratio was defined as the fraction of time during which consecutive pumps were ≤ 250 ms apart. $N_{OD=0} = 14$, $N_{OD=2} = 12$, $N_{OD=4,\ 5\mu l/min} = 14$, $N_{OD=4,\ 200\mu l/min} = 12$.

2.4.4 Pumping rates are reduced and exhibit long correlations in a dynamic environment.

Combined, controlling food availability and prolonged measurements enable assaying pharyngeal pumping in a dynamic environment. To demonstrate this, we have oscillated the concentration of available food between its high ($OD_{600} = 4.0$) and low (0.0) values with a period of 360 sec. Switching between the two food reservoirs was performed using a small

volume rotative valve, which eliminates back-flow and cross contamination and minimizes flow disruptions. As a result, we could not detect a response to switching between two reservoirs containing the same concentration of food (data not shown).

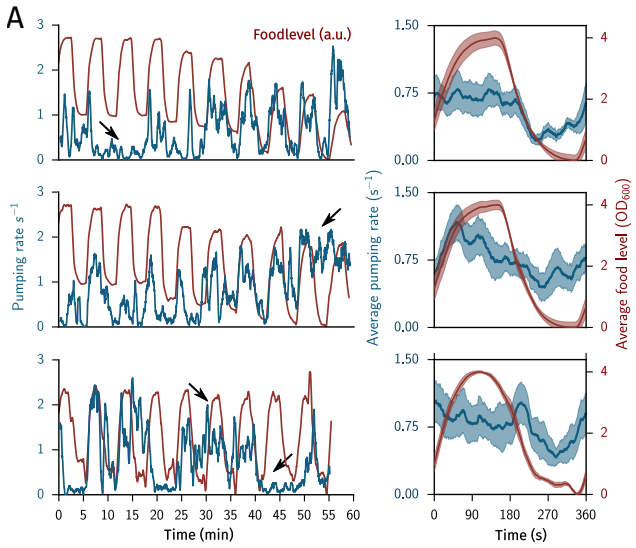

Figure 2.4: **Pumping in dynamically changing environments.** All panels correspond to recordings from wild-type animals at 4x magnification.. Each animal was assayed for 60 min, pumping rates and food levels were denoted in blue and red, respectively, and bacterial food flowed at 200 $\mu l/min$ and oscillated between high ($OD_{600} = 4.0$) and low ($OD_{600} = 0.0$) levels with a period of 360 sec. (A) Left: representative examples of pumping dynamics of individual animals in the presence of oscillating food availability. Pumps were grouped in bins of 1 *sec* and the time-series was smoothed using a moving average with 20 *sec* width. Arrows denote periods where the animal maintained high or low pumping activity regardless of the oscillations in food concentration. Right: mean pumping rates and food levels per animal: data were averaged over the nine periods of the stimuli for each of the animals on the left.

Fig. 2.4 depicts examples of instantaneous pumping rates of individual animals and the corresponding food levels, as well as averaged data. Our analysis could readily detect changes in pumping rates that occurred over $\leq$ 10 sec and in this assay the animals experienced a plateau of high food availability for 90 sec during each period. We thus predicted that pumping rates would track the changes in food availability and that their highest and lowest mean pumping rates would be comparable to those measured at the corresponding fixed concentrations (Fig. 2.3C). However, mean pumping rates in the dynamic environment

were approximately 2−fold lower than the corresponding steady state rates (Fig. 2.5A-B). Moreover, it was not uncommon for animals to maintain low or high pumping activity regardless of oscillations in the concentration of food for up to 10 min (see arrows in Fig. 2.4 and the inset in Fig. 2.5).

Due to the variability of the behavioral responses, we also calculated the response-triggered average to the periodic stimuli. We identified the time points when the instantaneous pumping rate exceeded a threshold value of 2 Hz. Food concentration data from the 180 sec periods that immediately preceded these time points were aligned and averaged. We found that the mean concentration of food increased from $OD_{600} \simeq 0.7$ at earlier times to $OD_{600} \simeq 2.2$ when high activity was detected (Fig. 2.5C). This result indicates that high pumping rates are exercised preferentially in response to an increase in food availability. Combined, our results suggest that *C. elegans* readily detects dynamic changes in food availability and can respond to them rapidly, yet their behavior is more complex than simply tracking the external conditions.

2.5 Discussion

We described an efficient, unbiased, and scalable method for measuring pharyngeal pumping of *C. elegans* under controlled and reproducible conditions. Our method exhibits good agreement with previously reported data under comparable conditions, as well as good agreement between manual and automatic scoring of pumps. Moreover, it extends the conditions of pumping assays to prolonged measurements and dynamic yet controlled environments. Consequently, we found that *C. elegans* responds to dynamic changes in food availability with unexpected complexity: the overall rate of pumping is suppressed and periods of high or low pumping activity can persist for several minutes regardless of the changes in available food.

As compared to locomotion-based behaviors, extensively studied under a wide range of circumstances, pharyngeal pumping assays were by and large performed under a restricted set of conditions. The combination of rapid and spatially minuscule motion limited the through-

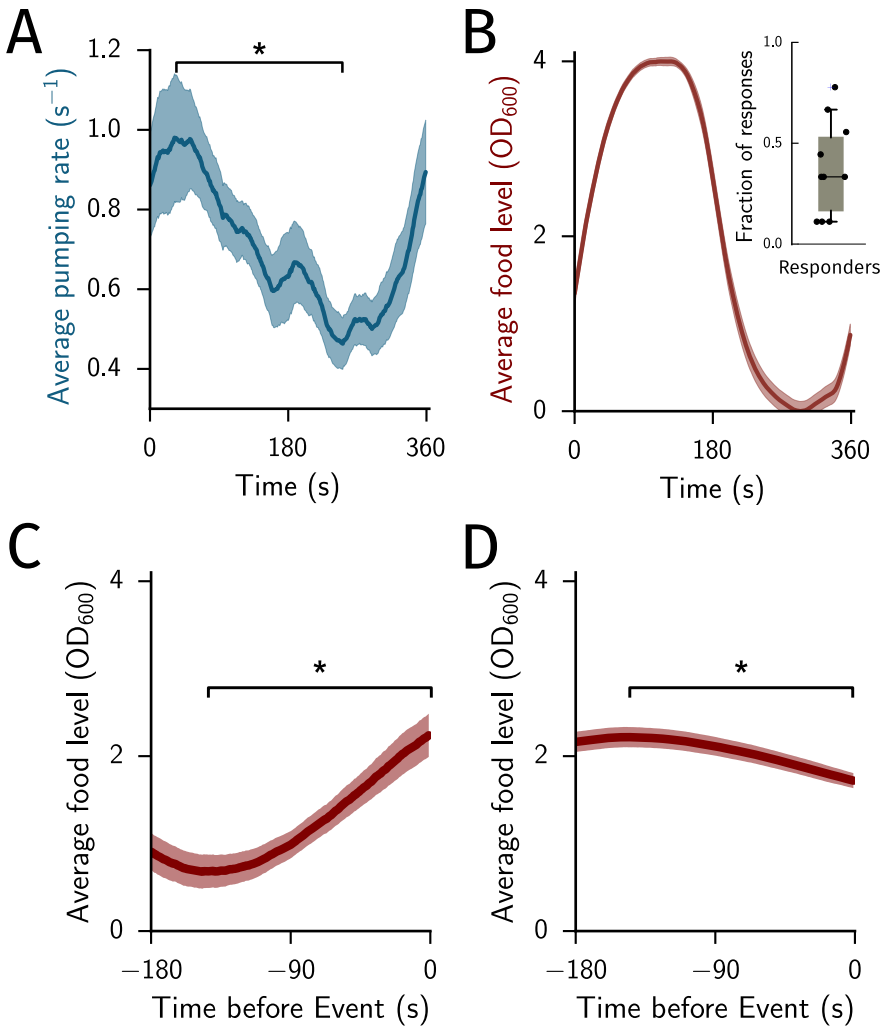

Figure 2.5: **Response-triggered averages show behavioral output corresponding to food changes.** (A-B) Mean pumping rates and food levels averaged over stimuli and all animals. Shaded areas denote ± s.e.m. Inset: Fraction of responses per animal. A response was defined as an increase in pumping rate during high food levels that was at least 2 s.e.m higher than the mean rate at the preceding $OD_{600} = 0.0$ period.(C-D) Response-triggered averages: food concentrations were averaged during all 180 sec periods that preceded $t = 0$, defined as the time-points when the pumping rate exceeded 2 Hz (C) or fell below 1 Hz (D). The red lines depict the population means and the shaded area denote ± s.e.m. In all panels $N = 10$ animals.

put of pumping assays, shortened the duration of individual measurements, and served as an additional barrier to challenging the animal with dynamic environments. Therefore, our approach can be used to address a variety of questions that were minimally studied previously. These include the quantitative relations between food availability and the instantaneous rate

of pumping or the impact of external dynamics on pumping responses.

Our methodology can be easily adapted and modified to accommodate varying experimental needs. For instance, the image analysis can be combined with a worm tracker (at the expense of throughput) to assay pumping in freely locomoting animals. Alternatively, any microfluidic device used for trapping worms would be compatible with our imaging setup and alterations to existing devices can enhance the flexibility of the assay.

An alternative to tracing grinder motion altogether is to assay pumping based on electrophpharyngeograms. The resulting data are detailed and manual scoring is not required. Traditional electrophysiological methods require specialized equipment and have limited throughput (Raizen and Avery, 1994). Microfluidic electrophysiological devices offer improved convenience and throughput with respect to the traditional method (Lockery et al., 2012; Hu et al., 2013; Hincks et al., 2016). Overall, however, cost, throughput, and ease of adaptation of such devices depend on the specific implementation. Automated tracking of the motion of the grinder complements electrophysiological methods with minimal requirements for specialized equipment and high adaptability, e.g., for different preparations. At its heart, our approach trades image quality for frame rate while preserving the integrity of the data. Due to its low cost, it can be considerably scaled up in size. As the cost of electronics such as low-end desktop computers and CMOS[2] cameras continues to drop, the limiting factor would likely be the schedule of the researcher performing the assays.

2.6 Additional materials and methods

2.6.1 Animal handling

C. elegans N2 animals were cultivated with OP50 bacteria according to standard protocols at 20°C. To measure the statistics of pumping in detail, we use a microfluidic device that enables continuous measurements of pumping and control of the feeding conditions (Kopito

2. CMOS: complementary metal-oxide semiconductor, a type of sensor for a camera.

and Levine, 2014). Young adults were picked into liquid NGM and loaded into the WormSpa microfluidic device. An *E. coli* OP50 overnight culture, concentration-adjusted to the desired OD_{600} in NGM was flown through the device at a constant rate throughout the assay. After an hour of acclimation in the device, the animals were imaged for one hour at a magnification of 4x and 62.5 frames per second using the optical setup.

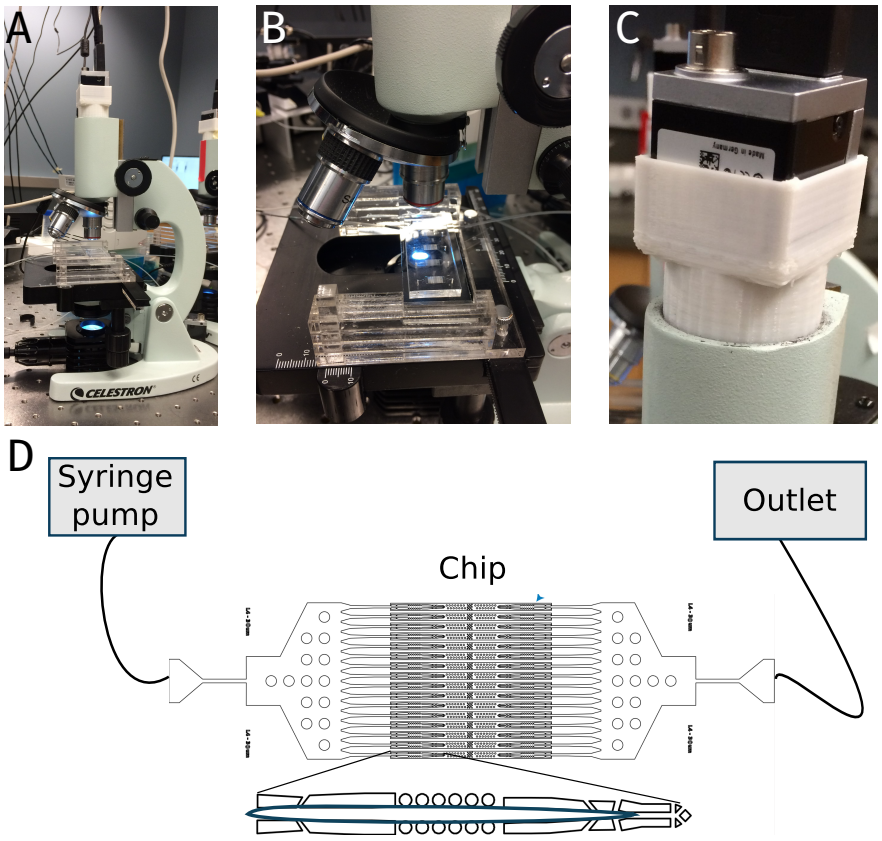

Figure 2.6: **A low-cost imaging setup and microfluidics to record feeding behavior.** (A) Celestron microscope with custom laser-cut slide holder and 3D-printed camera mount. (B) View of the microfluidic device in the custom slide holder. (C) Detailed view of the camera mount. (D) Schematic of the microfluidic chip used. Each animal sits in a small clamp with posts to allow unhindered egg-laying (see box).

2.6.2 Monitoring oscillating food levels

Food levels were oscillated using a programmable pressure regulator (Elveflow Inc., Paris, France). High and low food levels were measured prior to the assay. Food coloring (Mc-

Cormick & Co., Hunt Valley, 21031, MD) was filtered through a 0.22 μm filter and diluted to a final concentration of 1 : 60 in the tube containing the low food concentration. In preliminary assays we observed that oscillating between two sources containing identical concentrations of food, one of which supplemented with food coloring, did not evoke a correlated response (data not shown). Thus, our assay could not detect a response to either the food coloring or the switching between the two sources. The food coloring shifted the mean brightness of our images, which indicated the concentration of food flowing through the device, without obscuring the anatomy of the pharynx.

2.6.3 Statistics

In Figs 3C, D, F and H significance was calculated using an unequal-variance t-test and the Bonferroni post-hoc correction for multiple comparisons (3C and 3D). In 3F and 3G values at the minimum and maximum of the average curves were compared. The distributions in 3A were compared using a χ^2-test with 35 classes (non-zero bins).

2.6.4 Acquisition setup

Given a high frame rate, our approach does not depend on the specific design of the acquisition setup. Components such as the educational microscope, camera, or microfluidic device can be readily exchanged. By way of example, our designs for the camera and microscope stage mounts, as well as our peak detection code, are available for download from (Scholz, 2016b). Additional details are described in (Lynch and Biron, 2015).

2.7 Supplementary data

2.7.1 Imaging setup

The imaging setup is based on an entry-level microscope. The basic microscope is modified with a custom camera mount and stage to accommodate the USB3 camera and the

microfluidic chip (Fig. 2.6A-C). The camera mount is 3D printed to fit the Basler cameras. The small, cube-sized cameras can be adjusted from an open-source image acquisition tool (Basler, Pylon). The animals are kept in place by the geometry of the microfluidic chip. Each animal sits in a narrow channel separated from the other animals (Fig. 2.6D).

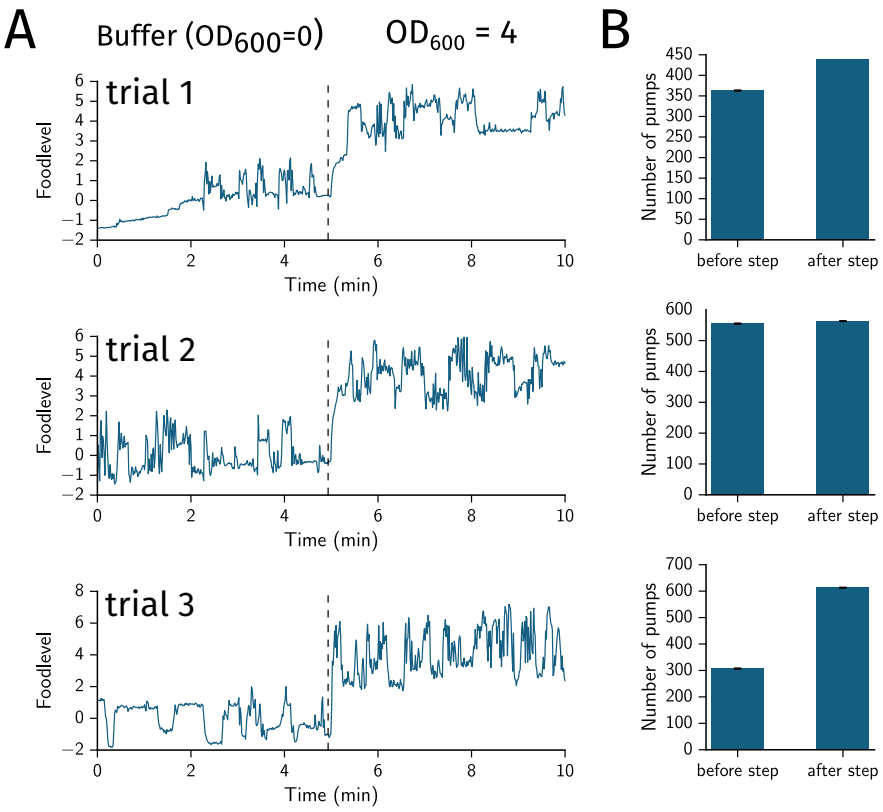

Figure 2.7: **Rapid food switches in the olfactory chip.** (A) Three trials of switching between buffer and a food solution. The food is tracked by labeling the buffer with food coloring. The noise in the food level is due to the analysis rather than representing actual fluctuations. The dashed line denotes where the switch should occur. (B) The number of pumps before and after the switch. Each segment (before and after) is 5 minutes long.

2.7.2 Alternative microfluidic technology

For the work presented in this thesis, the WormSpa chip was used for all pumping experiments (Kopito and Levine, 2014). The chip is easy to load and the parallel arrangement of many animals allows imaging multiple worms at once (Fig. 2.6D). Due to the partic-

ular geometry, the chip can not be used to rapidly switch between fluids at a sub-second timescale. Figs. 2.4 and 2.5 show the response to more gradual changes over tens of seconds. To test if the response is qualitatively different if the changes in food level are delivered more rapidly, we used the 'olfactory chip' (Albrecht and Bargmann, 2011). In this case, the fluids can be switched rapidly, however only a single animal can be imaged at a time. As a proof-of-principle, we imaged a single animal during three switches. The animal was kept in buffer without food for an hour. Imaging was started and the behavior in buffer was recorded for five minutes. After five minutes, the solution was switched to a high food concentration ($OD_{600} = 4$) and the behavior was recorded for another five minutes. The switch in food level occurred in less than ten seconds Fig. 2.7A in two trials and rapidly, but delayed in one trial. The animal responded to the switch by pumping more in two trials, but not in all Fig. 2.7B. The number of cumulative pumps and the instantaneous rate show no striking increase after the up-step (2.8A,B). These observations are consistent with our previous observation that animals respond stochastically to changes in food concentration. These preliminary observations indicate that the olfactory chip can be used to generate fast switches in food levels and is thus better suited to investigate the animals feeding behavior in response to an abrupt change in environmental conditions. However, the low throughput makes it unsuitable for genetic screening or similar experiments that require large groups.

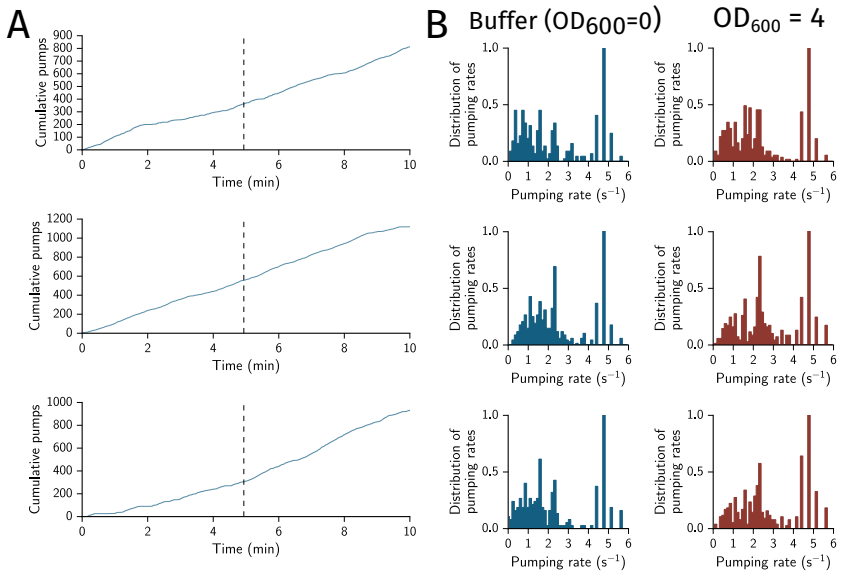

Figure 2.8: **Pumping in response to rapid food switches.** (A) Cumulative number of pumps in time. The dashed line denotes the switch in food level. (B) The instantaneous pumping rate at buffer and high food concentrations.

CHAPTER 3

DISTINCT UNFOLDED PROTEIN RESPONSES MITIGATE EFFECTS OF NONLETHAL DEPRIVATION OF *C. ELEGANS* SLEEP IN DIFFERENT TISSUES

3.1 Overview

Sleep is an essential behavior, and severe sleep deprivation can have extreme health consequences. More subtle question can be asked by looking at the effects of mild sleep deprivation. Mild sleep deprivation does not lead to the death of an organism and can mostly be compensated for. Using mild sleep deprivation in the nematode *C. elegans*, we asked what effects this deprivation has on key neural circuits and the reproductive organs. Looking at the feeding circuit and the egg-laying circuit allowed us to measure the effects of deprivation on a developing neural circuit. Both circuits operate under different constraints: The feeding circuit has to generate high frequency muscle contractions for feeding, whereas the egg–laying circuit has to synchronize the action of two vulva muscles to enable the expulsion of an egg. Our results reflect these differences, in that different protective pathways are required to shield the circuits from damage after sleep deprivation. These experiments allow us to find a better understanding of the core function of sleep. Different hypotheses have been brought forward to explain the need for sleep, especially during development. This work is a step towards finding the underlying function of sleep and will lead to an explanation why we spend so much time of our life with our eyes closed.

The work presented in this chapter was done in collaboration with Jarred Sanders, who worked on the egg-laying circuit and germ line, while I focused on the feeding circuit. Other co-authors are Ilaria Merutka, and David Biron. A detailed description of the calcium-imaging software I built to analyze physiological imaging data presented here can be found in the Appendix.

3.2 Abstract

Disrupting sleep during development leads to lasting deficits in chordates and arthropods. To address lasting impacts of sleep deprivation in *C. elegans*, we established a nonlethal deprivation protocol. Deprivation triggered protective insulin-like signaling and two unfolded protein responses (UPRs): the mitochondrial (UPR^{mt}) and the endoplasmic reticulum (UPR^{ER}) responses. While the latter is known to be triggered by sleep deprivation in rodent and insect brains, the former was not strongly associated with sleep deprivation previously. We show that deprivation results in a feeding defect when the UPR^{mt} is deficient. In contrast, deprivation causes germ cell apoptosis and excess twitching in vulval muscles when the UPR^{ER} is deficient, mirroring a trend caused by loss of egg-laying command neurons. These data show that nonlethal deprivation of *C. elegans* sleep causes proteotoxic stress. Unless mitigated, distinct types of deprivation-induced proteotoxicity can lead to anatomically and genetically separable lasting defects. The relative importance of different UPRs post-deprivation likely reflects functional, developmental, and genetic differences between the respective tissues and circuits.

3.3 Introduction

Disrupting mammalian sleep during development correlates with negative effects on physical, cognitive, and social health, thereby supporting the widely accepted notion that sleep is important for appropriate development (Halbower et al., 2006; Jan et al., 2010; Owens et al., 2014). Nonlethal sleep deprivation was also shown to cause lasting neurological and behavioral deficits in *D. melanogaster* (Kayser et al., 2014). However, a mechanistic grasp of why inadequate sleep during development is particularly deleterious is lacking.

Caenorhabditis elegans exhibits developmentally timed sleep during lethargus, a 2-3 hour long period at the termination of each larval stage (Byerly et al., 1976; Raizen et al., 2008; Singh and Sulston, 1978). Similar to mammalian sleep, lethargus is characterized by loco-

motion and feeding quiescence, sensory gating, a typical posture, rebound sleep, and deeply conserved regulation (Cho and Sternberg, 2014; Driver et al., 2013b; Iwanir et al., 2013; Nagy et al., 2014; Raizen et al., 2008; Schwarz et al., 2012; Singh et al., 2011; Tramm et al., 2014). Disruption of developmentally timed worm sleep activates DAF-16/FoxO, the *C. elegans* Forkhead box O (FoxO) stress activated transcription factor, whose nuclear translocation is inhibited by the Insulin/Insulin-like growth factor signaling (IIS) pathway (Lee et al., 2001; Lin et al., 1997). In response to prolonged and continuous deprivation, DAF-16 translocates to the nucleus to mitigate or delay lethality (Driver et al., 2013b) and in the presence of much weaker disruptions DAF-16 is required for rebound sleep (Nagy et al., 2014). Sleep deprivation is broadly known to be a stressor. In all species examined, expression of immunoglobulin binding protein (BiP), an endoplasmic reticulum (ER) chaperone, is upregulated upon sleep deprivation (Cirelli, 2009; Cirelli and Tononi, 2000; Naidoo, 2012, 2009; Shaw et al., 2000, 2002). BiP upregulation requires the action of the ribonuclease inositol requiring protein-1 (IRE-1): a key receptor for sensing ER, proteotoxic stress and triggering the ER unfolded protein response (UPR^{ER}) (Calfon et al., 2002; Mori, 2009; Shen et al., 2001; Taylor and Dillin, 2013; Urano et al., 2002; Zhang and Kaufman, 2006). Upon sensing proteotoxicity, IRE-1 signaling activates the XBP-1 transcription factor which upregulates BiP, a member of the heat shock 70 (Hsp70) protein family, and other UPR^{ER} genes. Such activation of the UPR^{ER} by sleep deprivation is conserved from flies to mammals. In contrast, the connection between sleep deprivation and the mitochondrial UPR (UPR^{mt}) is less clear (Haynes and Ron, 2010). Energy requirements offer a possible connection: prolonged wakefulness increases daily energy expenditure (Dworak et al., 2010; Everson et al., 1989; Jung et al., 2011). For instance, increased neural activity during sleep deprivation increases the energy consumption of the brain (Steriade, 2001; Timofeev et al., 2001). Consequently, energy production by the mitochondrial oxidative phosphorylation system is upregulated (Cirelli and Tononi, 2000; Hardie et al., 2006; Jing and Ismail-Beigi, 2006; Nikonova et al., 2010; Saraste, 1999; Shaw et al., 2000). Upon proteotoxic stress, ex-

pression of ubl-5, encoding a ubiquitin-like protein, is upregulated and UBL-5 plays a key role in activating dedicated chaperones and proteases of the UPR^{mt} (Benedetti et al., 2006; Haynes and Ron, 2010; Yoneda et al., 2004). One study found that the mitochondrial chaperones Hsp60 and Grp75 were induced (to a lesser degree than BiP) by sleep deprivation in rat cerebral cortexes (Cirelli and Tononi, 2000). However, the impact of mitochondrial stress during sleep deprivation is unclear. Tractable model organisms have been prominently used to study responses to environmental stressors, such as oxidation or heat. Protective signaling triggered by such factors is complex and highly conserved (Mardones et al., 2015; Carvalhal Marques et al., 2015). In contrast, the stress inflicted by deprivation of *C. elegans* developmentally timed sleep was minimally explored and deprivation-induced deficits, other than lethality, were never characterized. Here we establish an automated approach to inflicting severe yet nonlethal deprivation of developmentally timed sleep in *C. elegans*. Next, we characterize lasting impacts of deprivation on behavior and physiology and identify distinct UPRs that mitigate these ill effects in different tissues. Our automated deprivation protocol resulted in a 50% reduction in quiescence during worm sleep while never forcing locomotion for continuous periods longer than a few minutes. Under these conditions, deprivation was nonlethal but negatively impacted feeding, fecundity, and egg-laying physiology. Deprivation upregulated the expression of UPR^{mt} genes and disrupting the UPR^{mt} specifically affected feeding, likely through an impact of deprivation on pharyngeal neurons. Disrupting worm sleep also triggered the UPR^{ER}, which was required for deprivation-induced reduction in brood size through germ cell apoptosis (Aballay and Ausubel, 2001; Ellis and Horvitz, 1986; Yuan and Horvitz, 1990). Independently, the egg-laying circuit exhibited a post-deprivation defect similar to the outcome of genetically ablating an egg-laying command neuron (Collins et al., 2016). Opposite to the case of the feeding circuit, the UPR^{ER} (but not the UPR^{mt}) mitigated the impact of deprivation in the egg-laying circuit. Loss of DAF-16/FoxO function exacerbated impacts of deprivation. Collectively, these findings implicate two UPRs and IIS in mitigating the impacts of disrupting worm sleep. They show that developmentally timed

sleep is a vulnerable period: external stimuli that are benign outside of lethargus inflict lasting deficits when administered during lethargus. Appropriate quiescence during this period promotes normal functions in tissues differing in developmental dynamics and physiological activity. Different protective responses mitigate distinct effects of deprivation, depending on the function of the tissue in question and perhaps on its developmental state.

3.4 Results

3.4.1 Substantial deprivation of lethargus quiescence can be automatically inflicted.

Forced locomotion during C. elegans sleep by manually delivering harsh touch was previously shown to be lethal (Driver et al., 2013b; Raizen et al., 2008). Considerably more gentle mechanical vibrations can transiently force motion. We previously identified rebound sleep when vibrations were applied infrequently (Nagy et al., 2014). and found that worms desensitized to vibrations delivered too frequently. In response to a 3 minute on/off cycle of vibrations we measured a 50% reduction in mean quiescence (Fig. 3.1A-B) [1]. This indicated that, in contrast to previously published conditions, the 3 minute on/off cycle robustly overwhelmed the capacity of the worms to compensate for excess motion. We further found that this disruption affected wild-type animals and *daf-16* mutants similarly. Manually forced locomotion during worm sleep drives translocation of DAF-16 to nuclei of intestinal and body wall muscle cells (Driver et al., 2013b). We asked whether our 3 minute on/off disruptions would induce similar translocation of DAF-16. To address this, we exposed animals expressing fluorescently labeled DAF-16 to one hour of the vibration stimuli during the first half of the fourth lethargus stage (L4 lethargus). In agreement with the manual (lethal) deprivation protocol, we observed nuclear localization in intestinal cells (Fig. 3.1C). Translocation

1. Both *daf-16* alleles are null alleles, however the genetic disruption is a deletion or a substitution (*daf-16*(mu86) and *daf-16*(mgDf50), respectively).

was not observed following a mock perturbation protocol, where vibrations were not applied during an equivalent one-hour period. In our hands, a clear translocation response was not observed in body wall muscles. In contrast to the consequences of continuous manual deprivation (Driver et al., 2013b), we did not observe any molting defects or lethality following our deprivation conditions. Possibly, this was a consequence of not depriving the animals of quiescence for a continuous period that exceeded 3 minutes. Collectively, these data demonstrate the ability to automatically and severely disrupt quiescence to a stressful yet nonlethal degree. Considering these results, the experiments described throughout the manuscript employ three types of deprivation conditions: one hour of disruptions for acute responses in individual animals expressing fluorescent markers ('mock' animals were loaded to identical observation chambers), 4 hours of disruptions for gene expression assays in small groups of tightly synchronized animals, and 12 hours of disruptions for lasting effects of deprivation assayed in large groups of animals. To control for non-specific effects of the prolonged stimulation period, we compared sleep deprived animals to those exposed to vibrations outside of lethargus. These groups were labeled 'control' (see methods section for details). In the latter two protocols (4 hours and 12 hours), sleep was disrupted for no more than the 3-hour duration of lethargus. To identify effects of vibrations that are non-specific to lethargus, we assayed a subset of strains without exposing them to any vibrations. These groups were labeled 'unperturbed' and they consistently exhibited similar phenotypes to 'control' animals. Thus, non-specific effects of vibrations were found to be minor and genetically separable from impacts of sleep deprivation.

3.4.2 Nonlethal deprivation results in a DAF-16/FoxO dependent deficit in pharyngeal pumping.

The pharynx of *C. elegans* is a simple neuromuscular organ with a well-defined function that requires speed and regularity. Therefore, we asked whether sleep deprivation would affect its operation. The pharyngeal nervous system consists of 20 neurons isolated from the rest

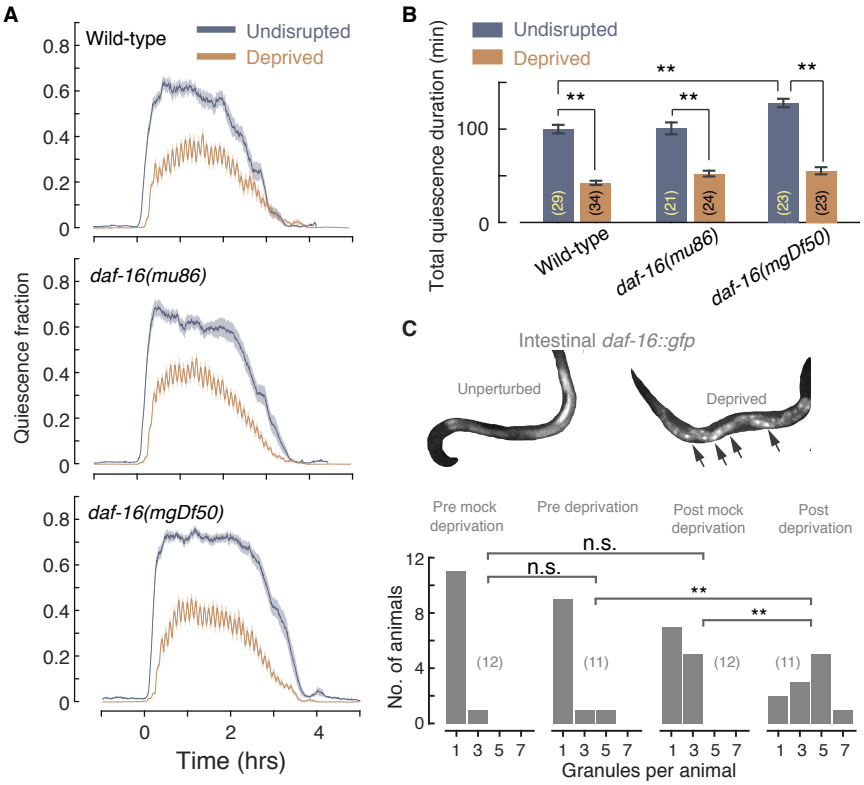

Figure 3.1: **A periodic mechanical stimulus can partially and nonlethally reduce lethargus quiescence and induce translocation of DAF-16.** (A) The fraction of quiescence measured during L4 lethargus of undisrupted (grey) and deprived (orange) wild-type animals and *daf-16* mutants. Locomotion was forced using a square wave of mechanical vibrations with a 6 minute period and 50% duty cycle. Shaded areas depict mean±s.e.m. (B)The total time in which quiescence was observed integrated over the data presented in panel A. Error bars depict mean±s.e.m. (C) DAF-16::GFP fluorescence in the intestine after one hour of partial deprivation. Top: examples of GFP fluorescence in unperturbed and partially deprived animals. Arrowheads point to bright particles indicating concentration of DAF-16::GFP. Bottom: Histograms of the number of bright particles per animal identified under each set of conditions. Sample sizes are denoted in parentheses. Single and double asterisks denote significant differences with $p<0.05$ and $p<0.01$, respectively.

of the animal by a basal lamina, and operating independently (Albertson and Thomson, 1976; Raizen et al., 1995b). The contraction and relaxation cycle of pharyngeal pumping takes in bacterial food, expels excess liquid, and traps the food (Avery, 1993a; Avery and Horvitzt, 1989). Pumping rates depend on feeding history, quality of food, and endogenous serotonin levels (Hobson et al., 2006; Scholz et al., 2016a; Song et al., 2013; Shtonda and

Avery, 2006). In the absence of food, pumping can be stimulated with exogenous serotonin (Hobson et al., 2003; Song and Avery, 2012). To characterize the effects of deprivation on pharyngeal function, we measured pumping continuously for 60 minutes at a food concentration corresponding to an optical density $OD_{600} = 2.5$, where pumping activity was found to be intermediate (Fig. 3.9). We then compared between the deprived animals and the control group, exposed to the vibrations stimuli before and after lethargus (see methods). Pharyngeal pumping can be adequately described as a time series of discrete stereotypical events (Avery and Horvitzt, 1989). These time series are composed of bursts of rapid pumping interspersed by pauses (Scholz et al., 2016a). Based on data obtained from optical tracking, we calculated the mean instantaneous pumping rate and the duty ratio of continuous rapid pumping (Lee et al., 2017). These summary statistics did not reveal significant differences between deprived and control wild-type animals. However, forced locomotion specifically during lethargus significantly affected *daf-16* mutants and the native promoter rescue of DAF-16 function restored the wild-type phenotype (Fig. 3.2A). These results suggest that worm sleep deprivation can negatively impact feeding by shortening the persistence of rapid pharyngeal pumping and that DAF-16 mitigates this adverse effect. Optical tracking of pumping motion enabled high-throughput measurements over prolonged periods, beneficial for statistical characterization. Complementarily, electropharyngeograms (EPGs) revealed the dynamics of contraction and relaxation of the pharyngeal corpus and terminal bulb in more detail. EPG data independently confirmed our key findings regarding mean rates of pumping (Fig. 3.9) and enabled precise measurements of durations of single pumps. We found that repeated mechanical stimuli extended the duration of individual pumps and could alter the shape of the contraction peak (Fig. 3.2B-C). However, the extension of single pumps was not specifically associated with sleep deprivation: deprived animals and controls exposed to the mechanical stimuli before and after lethargus exhibited similar pump durations (Fig. 3.2B-C). Thus our assays differentiated between deprivation related and nonspecific impacts of mechanical stimuli.

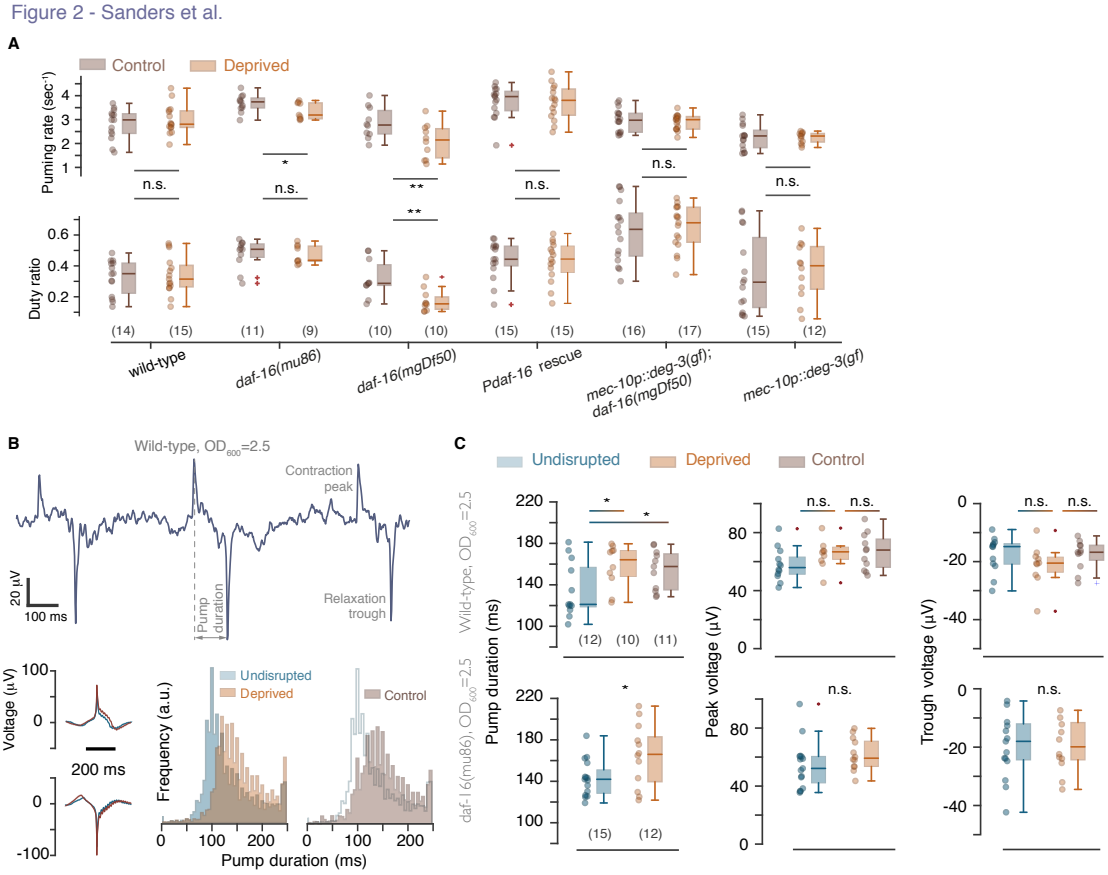

Figure 3.2: **Pharyngeal pumping is negatively impacted by nonlethal deprivation in a DAF-16 dependent manner.** (A) Box plots of average pumping rates and duty ratio for control (i.e., stimulated outside of lethargus) and deprived animals obtained with the optical tracking method. Loss of DAF-16 or *mec-10* expressing neurons confer a broad defect in stress responses or the loss of gentle mechanosensation, respectively. The duty ratio is the fraction of time spent in continous pumping. Continuous pumping was defined as a period in which the delay between pumps did not exceed 500 ms.(B) Top: a sample EPG trace of a wild-type animal in the presence of food at $OD_{600} = 2.5$ concentration. Peaks correspond to corpus and terminal bulb contraction. Troughs correspond to corpus relaxation. Bottom: average contraction and relaxation EPG traces for undisrupted and deprived wild-type animals. Distributions of pump durations are shown for undisrupted, deprived, and control (exposed to vibrations outside of lethargus) animals. The outline of the distribution for undisrupted animals was duplicated as a guide to the eye. (C) The mean (per animal) pump durations and amplitudes of EPG peaks and troughs for wild-type animals (top) and *daf-16(mu86)* mutants (bottom). Horizontal lines, boxes, and bars depict medians, 1st and 3rd quartiles, and 5 and 95 percentiles, respectively. Sample sizes are noted in parentheses, asterisks and double asterisks denote significant differences ($p<0.05$ and $p<0.01$, respectively).

3.4.3 The UPR^{mt} plays a role in mitigating effects of nonlethal deprivation on pumping.

The ubiquitin-like protein UBL-5 is required for UPR^{mt} promotion of expression of the mitochondrial chaperone genes. Expression of ubl-5 was shown to be upregulated in response to mitochondrial stress (Benedetti et al., 2006; Haynes et al., 2007; Haynes and Ron, 2010; Yoneda et al., 2004). While mitochondrial turnover may be correlated with the sleep-wake cycle, as sleep is a period of fasting (Gottlieb and Stotland, 2015), a connection between lasting impacts of sleep loss and the mitochondrial unfolded protein response (UPRmt) is not well established. The ubl-5 translational reporter expresses broadly at low levels and brightly in the posterior bulb of the pharynx, the posterior of the intestine, and the anterior edge of the intestine near the pharyngeal-intestinal valve (Benedetti et al., 2006). After exposure to one hour of sleep disruption (see methods), we observed a small but significant upregulation of *Publ-5::ubl-5::gfp* expression. No increase in, reporter fluorescence was observed following the mock protocol or when vibrations were applied at the mid L4 larval stage (Fig. 3.3A). We similarly assayed two additional indicators of the UPR^{mt}: the *hsp-6* and *hsp-60* transcriptional reporters. HSP-6 and HSP-60 are the *C. elegans* mitochondrion-specific chaperones belonging to the Hsp70 and Hsp10/16 superfamilies, respectively. Both are upregulated by chemically induced mitochondrial stress (Kimura et al., 2007; Yoneda et al., 2004). Expression of *hsp-6* was broad and most clearly visible in the intestine. Strong expression of *hsp-6* or an accumulation of the reporter brightly stained the posterior segment of the intestine and sleep deprivation did not affect this posterior bright patch. However, expression in the rest of the intestine was upregulated after one-hour of deprivation while mock deprivation did not affect *hsp-6* expression (Fig. 3.3B). In contrast to the case of the pharmacologically induced UPR^{mt}, we could not detect a similar upregulation of *hsp-60* expression (Fig. 3.11). However, we cannot rule out the possibility that upregulation of this chaperone in our hands was below the detection threshold, e.g., due to tissue specificity. We used real-time PCR to assay the relative expression of these genes after a four-hour period of

administering the disruptive stimuli that included L4 lethargus. Consistently, we observed elevated expression of *ubl-5* and *hsp-6* in deprived animals (Fig. 3.3C). To test whether the *C. elegans* UPR^{mt} plays a role in mitigating consequences of nonlethal sleep deprivation we examined feeding in *ubl-5* mutants. Deprived *ubl-5* mutants exhibited a defect in pumping rate as compared to the control group. This pumping defect was rescued by expressing the *Publ-5::ubl-5::gfp* translational reporter (Figs. 3.3D and S2). The elongation of durations of individual pumps in *ubl-5* mutants was comparable to that of wild-type animals and *daf-16* mutants (Fig. 3.3E). Thus, we did not identify a role for the UPR^{mt} in mitigating this non-specific effect of mechanical stimulation. Taken together, our results indicate that the UPR^{mt} is triggered by deprivation of *C. elegans* sleep and plays a role in mitigating the effects of deprivation on pumping.

3.4.4 Deprivation impacts pharyngeal pumping likely through affecting regulatory neurons.

The pharynx is isolated from the rest of the animal and can exhibit pumping tens of minutes after it has been dissected out (Albertson and Thomson, 1976; Raizen et al., 1995b). Pumping defects induced by sleep deprivation can thus originate from pharyngeal regulatory neurons or pharyngeal muscles. We note that our mechanical stimuli do not noticeably affect the buccal plug, a cap of extracellular material which prevents food from entering the pharynx during lethargus (Singh and Sulston, 1978), and they do not induce pumping. Consequently, the stimuli do not activate the pharyngeal muscles during lethargus and 'wear and tear' damage caused by anachronistic muscle activation is unlikely. To address this, we induced pharyngeal pumping in young adults using 10mM serotonin (5-HT) instead of food. Serotonin is known to robustly activate rapid pumping through the action of the neuronally expressed SER-7/ 5-HT7 receptor (Hobson et al., 2003, 2006; Song and Avery, 2012). We found that pumping rates in the presence of 5-HT were high in undisrupted and deprived *daf-16(mgDf50)*and *ubl-5 mutants* (Fig. 3.4A-B and 3.12). The serotonin receptor SER-1/5-

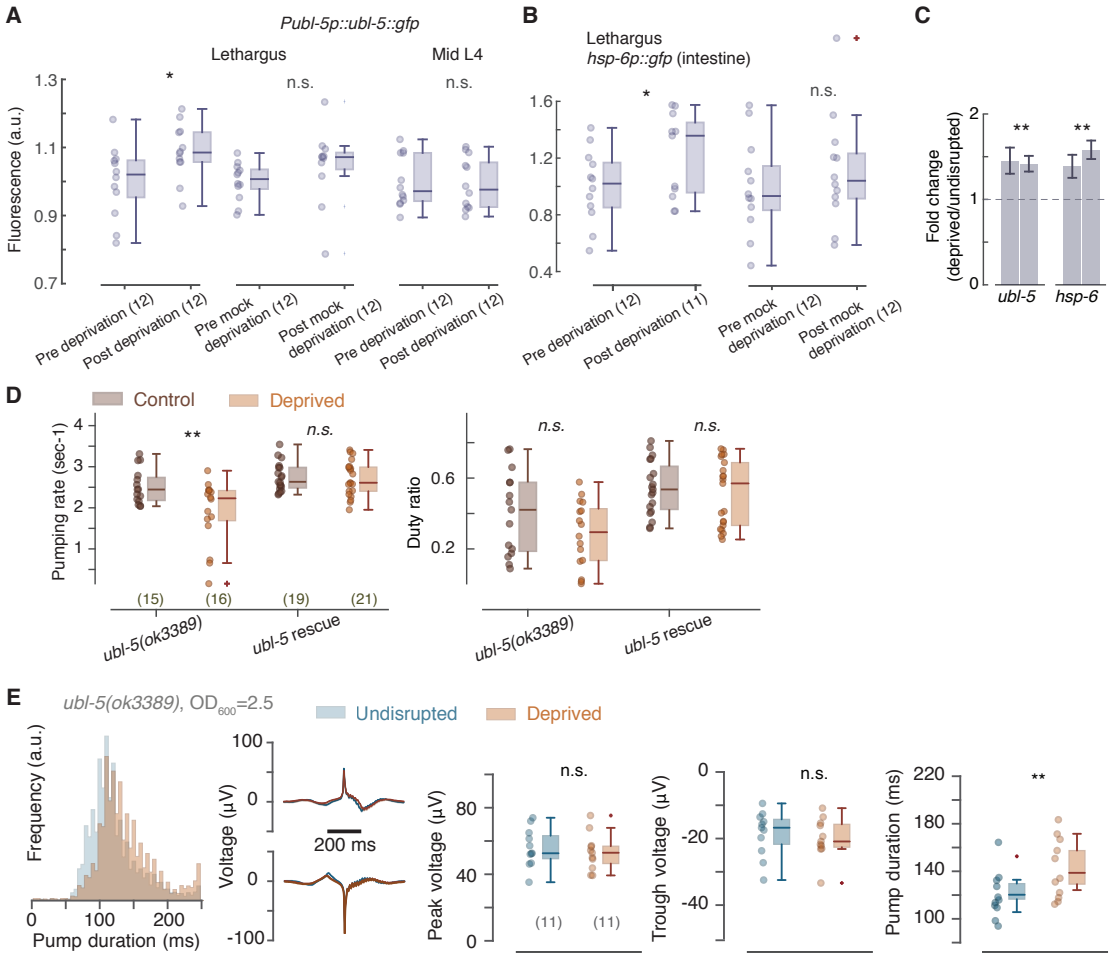

Figure 3.3: **Post-deprivation feeding is protected by the UPR^{mt}.** (A) Intestinal fluorescence of the *ubl-5p::ubl-5::gfp* UPR^{mt} reporter before and after deprivation, mock deprivation, and stimulating mid L4 larvae. (B) Intestinal fluorescence of the mitochondrial chaperone *hsp-6::gfp* reporter after deprivation and mock deprivation. (C) Relative expression of *ubl-5* and *hsp-6* in deprived as compared to undisrupted wild-type animals (2 biological replicates). The mechanical stimulus was applied for 4 hours (which included L4 lethargus) and RNA was prepared immediately after this period. Error bars depict mean±s.e.m. from 6 technical replicates and asterisks denote significant differences from a ratio of 1.0 ($p<0.05$). (D) Average pumping rates and duty ratios for control and deprived animals obtained from high-throughput optical measurements (see methods). Horizontal lines, boxes, and bars depict medians, 1st and 3rd quartiles, and 5 and 95 percentiles, respectively. (E) Distributions of pump durations, average contraction and relaxation EPG traces, mean (per animals) EPG peak and trough amplitudes, and mean (per animal) duration of individual pump for *ubl-5* mutants. Sample sizes are noted in parentheses, asterisks and double asterisks denote significant differences ($p<0.05$ and $p<0.01$, respectively).

HT2 is expressed in pharyngeal muscles (Tsalik et al., 2003). However, SER-1 was found to have a mild or no contribution to pharyngeal pumping rates, whether induced by food or by 5-HT (Dernovici et al., 2007; Hobson et al., 2006). To assess the potential impact of activation of SER-1 we assayed mutants carrying the putative null allele *ser-1(ok345)*. In our hands, loss of SER-1 mildly affected the shape of individual contractions and relaxations and did not affect the rate of 5-HT induced pumping (Fig. 3.4C and 3.12). The ability of *ser-1* mutants to pump rapidly suggests that 5-HT triggers pumping through activating pharyngeal neurons. The ability of deprived *daf-16* and *ubl-5* mutants to pump rapidly suggests that their deficits, exhibited in the presence of food, are the result of regulation rather than a biomechanical limit. In addition, neuronal rescue of DAF-16 function abolished the post-deprivation phenotype (Fig. 3.4D). Combined, these data indicate that rapid pumping is mechanically possible even in sleep deprived mutants upon activation of pharyngeal neurons. Thus, sleep deprivation likely results in lasting deficits in the neural circuit regulating pumping.

3.4.5 Nonlethal deprivation results in DAF-16/FoxO dependent reduction in brood size.

Sleep deprivation was recently shown to adversely affect fertility in rodents (Alvarenga et al., 2015; Torres et al., 2014). To address whether nonlethal deprivation impacts *C. elegans* fecundity, we compared brood sizes of deprived and control animals. We found that brood size in the control group (where stimuli were delivered outside of lethargus) was indistinguishable from that of undisrupted animals. However, sleep deprivation reduced wild-type brood size by 10% (Fig. 3.5A). The negative impact of nonlethal deprivation was exacerbated in *daf-16(mu86)* mutants, where brood size was reduced by 29% (Fig. 3.5A). In *daf-16(mgDf50)* null mutants, where brood size was markedly lower in the control group, we observed an 18% reduction (Fig. 3.5B). To address the possibility of a floor effect, we increased the brood size of *daf-16(mgDf50)* mutants through male mating (Ward and Carrel, 1979). In our hands,

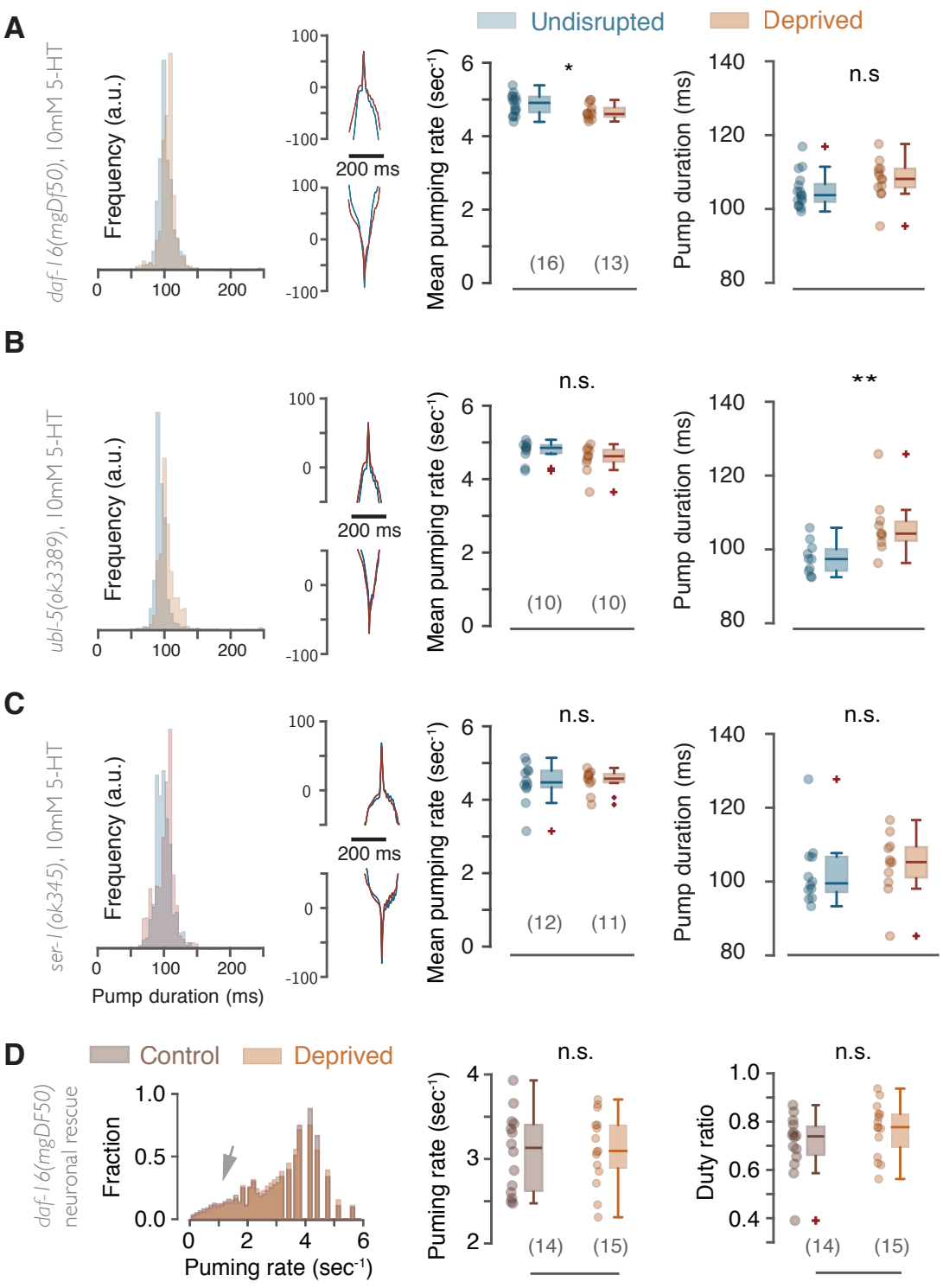

Figure 3.4: **A neuronal regulation deficiency underlies the post-deprivation slow-down of feeding.**

Figure 3.4: **A neuronal regulation deficiency underlies the post-deprivation slowdown of feeding (cont.).** (A) Distributions of pump durations, mean (per animal) contraction and relaxation EPG traces, mean pumping rates, and mean (per animal) durations of individual pumps for 5-HT triggered pumping in undisrupted and deprived *daf-16(mgDf50)* mutants. (B-C) Same as panel A for *ubl-5* and *ser-1* mutants. (D) Left: distributions of pumping rates deprived and control *daf-16* mutants where neuronal function of DAF-16 was restored. Right: mean pumping rates and duty ratios of burst of rapid pumping under these conditions. Shaded areas depict mean±s.e.m. Horizontal lines, boxes, and bars depict medians, 1st and 3rd quartiles, and 5 and 95 percentiles, respectively. Sample sizes are noted in parentheses, asterisks and double asterisks denote significant differences ($p<0.05$ and $p<0.01$, respectively).

the frequency of mating encounters was not affected by our deprivation protocol (data not shown). By the third day of adulthood, we observed a 21% increase in the brood size of the control group as compared to self-fertilization, and a 24% reduction in brood size following forced locomotion during lethargus of both hermaphrodites and males. Disrupting quiescence of either hermaphrodites or males resulted in intermediate phenotypes (Fig. 3.5B). When the function of DAF-16 was restored by driving expression with the native promoter, brood size was not reduced following forced locomotion during lethargus (Fig. 3.5C). Next, we assayed worms expressing *deg-3(u662)*, a degeneration-causing constitutively active nicotinic acetylcholine receptor (nAChR) channel subunit, in touch neurons (Albeg et al., 2011; Huang and Chalfie, 1994; Sanders et al., 2013; Treinin et al., 1998; Treinin and Chalfie, 1995). These animals did not respond to vibrations. As expected, failure to respond abolished the reduction in brood size in the presence of the stimuli (Figs. 3.5D and 3.13). In contrast to brood size, forced locomotion did not appreciably increase the number of retained eggs (Fig. 3.14). Collectively, these results suggest that nonlethal sleep deprivation in *C. elegans* negatively impacts brood size but not through a pronounced egg-laying defect and that DAF-16/FoxO mitigates this adverse effect.

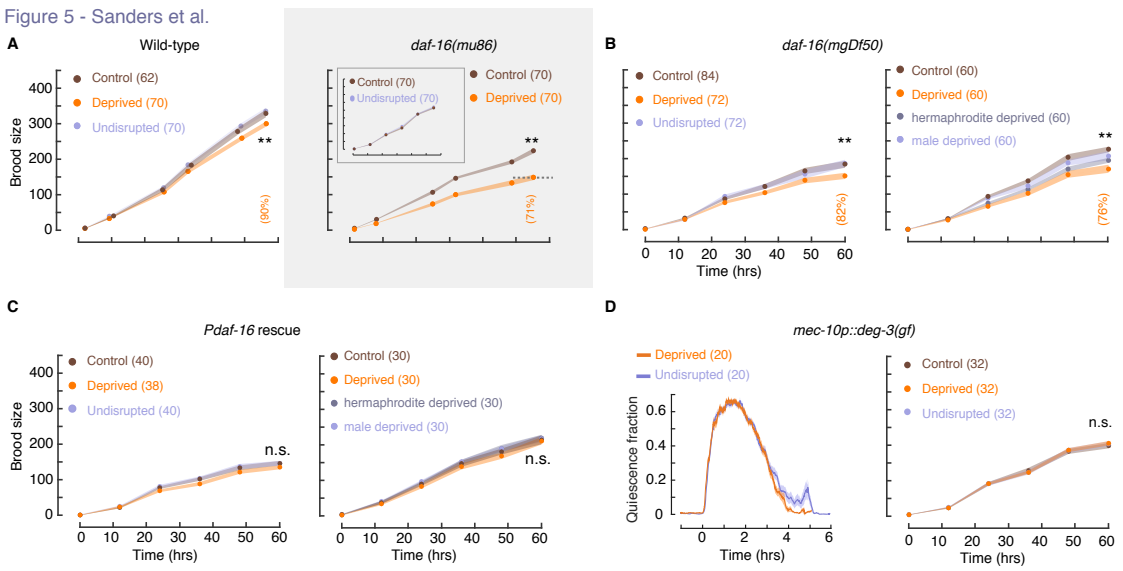

Figure 3.5: **Post-deprivation brood size is reduced in a DAF-16 dependent manner.** (A) Brood sizes of wild-type animals and *daf-16(mu86)* mutants during the first three days after L4 lethargus (t=0 is 10-12 hours after the fourth molt). Deprived animals were exposed to the stimulus before, during, and after L4 lethargus. Control animals were exposed to the stimulus before and after L4 lethargus. Inset: undisrupted animals which were never exposed to the stimulus were indistinguishable from the control group. The dotted line depicts the brood size of deprived animals at the latest time point âĂŞ see also Fig. 3.7A. (B) The same as panel A for *daf-16(mgDf50)* mutants that either self-fertilized (left) or mated with males (right). In the latter case, either the males, the hermaphrodites, or both were deprived of quiescence. (C) The same as panel A for *daf-16(mgDf50)* mutants in which expression of *daf-16* cDNA was driven using the *daf-16* native promoter. (D) Left: quiescence fraction during L4 lethargus of animals deficient in touch sensation (*mec-10p::deg-3(gf)*), whose responses to vibrations were mostly or entirely abolished (see also Fig. 3.13). Right: the same as panel A for transgenic animals deficient for touch sensation. Shaded areas depict mean±s.e.m., sample sizes are noted in parentheses, and double asterisks denote a significant difference in brood size at t=60 hours ($p<0.01$).

3.4.6 Germ cell apoptosis causes the DAF-16 dependent reduction in brood size following nonlethal deprivation.

The key determinant of *C. elegans* brood size is the number of available sperm (Ward and Carrel, 1979). Germ cell apoptosis can be triggered to protect sperm against DNA damage or environmental stressors that are not directly genotoxic, e.g., oxidative stress, heat shock, or pathogens. In both cases, core apoptotic genes are strictly required for the initiation

of programmed cell death (Aballay and Ausubel, 2001; Alpi et al., 2003; Gartner et al., 2000; Haskins et al., 2008; Salinas et al., 2006). We reasoned that stress induced germ cell apoptosis may explain the effect of *C. elegans* sleep deprivation on fecundity. To address this, we explored three lines of evidence. Developmental cell death in *C. elegans* requires a highly conserved pathway. This apoptotic core machinery includes CED-3, a cysteine-aspartate protease essential for execution of apoptosis (Conradt and Horvitz, 1998; Ellis and Horvitz, 1986; Hengartner et al., 1992; Lettre and Hengartner, 2006; Xue et al., 1996; Yuan and Horvitz, 1990). We therefore crossed *daf-16(mu86)* mutants, which exhibited the most pronounced effect on fecundity, with *ced-3(n1286)* mutants. On the *daf-16; ced-3* double mutant background, the post-deprivation reduction in brood size was completely eliminated (Fig. 3.6A). Moreover, the number of eggs counted in deprived, control, and undisrupted animals were indistinguishable from those of undisrupted *daf-16(mu86)* mutants. This suggested that the *ced-3* mutation did not affect fecundity independently of sleep deprivation. CED-1 is a transmembrane receptor that mediates the engulfment of cell corpses (Zhou et al., 2001). It is found in sheath cells surrounding the germline, where it clusters around engulfed early apoptotic corpses of germ cells (Schumacher et al., 2005). A translational *ced-1::gfp* reporter can be used for visualizing germ cell apoptosis when the number of cell deaths is not too large (Gartner et al., 2008). We imaged animals expressing this reporter and subjected to our one-hour deprivation protocol. Deprivation resulted in a significant increase in *ced-1::gfp* fluorescence. In contrast, the control group subjected to a mock deprivation protocol, i.e., where vibrations were not applied, did not exhibit a change in reporter fluorescence during the equivalent period (Fig. 3.6B). Next, we counted fluorescently labeled sperm in self-fertilized deprived and control hermaphrodites as previously described (Hansen et al., 2015; Zeiser et al., 2011). We observed reductions in sperm count following forced locomotion during L4 lethargus as compared to the control groups in all three strains assayed (Fig. 3.6C). The reduced sperm counts were sufficient to explain the corresponding reductions in brood sizes. However, the reduction in sperm count of *daf-16(mgDf50)* was as

large as that of *daf-16(mu86)*. This may have been indicative of the variability of the measurement, of our 3-day assay having fallen short of revealing the full extent of the brood size deficiency in *daf-16(mgDf50)* hermaphrodites, or of further loss of sperm during adulthood (e.g., in the *daf-16(mgDf50)* control group). These results suggest that forced locomotion specifically during L4 lethargus induces germ cell apoptosis and that this deleterious effect of sleep deprivation is mitigated by DAF-16.

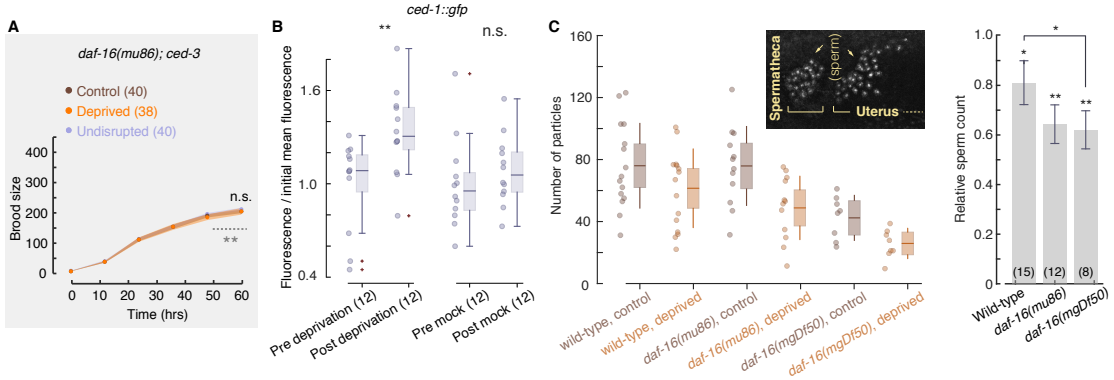

Figure 3.6: **Worm sleep deprivation causes germ cell apoptosis.** (A) Brood sizes of *daf-16(mu86); ced-3(n1286)*double mutants during the first three days after L4 lethargus (t=0 is 10-12 hours after the fourth molt). Deprivation failed to induce a reduction in brood size. The dotted line depicts the brood size of deprived *daf-16(mu86)* mutants at t=60 hours from Fig. 3.6A. (B) Box plots of the CED-1::GFP fluorescence after deprivation (left) or mock deprivation (right), normalized by the mean pre-treatment fluorescence. Horizontal lines, boxes, and bars depict medians, 1st and 3rd quartiles, and 5 and 95 percentiles, respectively. Sample sizes denoted in parentheses, double asterisks depict a significant difference ($p<0.01$). (C) Left: the number of sperm detected in a single gonad per animal. Horizontal lines, boxes, and bars depict means, 95% confidence intervals, and standard deviations, respectively. Inset: a confocal image of adult hermaphrodite sperm nuclei, specifically labeled by GFP-histone fusion driven by the *Pcomp-1* promoter. Right: the ratio between the sperm count of deprived and control animals. Error bars depict mean ±s.e.m. Sample sizes are denoted in parentheses, double asterisks depict mean values significantly different than 1 ($p<0.01$) and the single asterisk depicts a significant difference between genotypes ($p<0.05$).

3.4.7 The UPR^{ER} mitigates the effects of nonlethal deprivation on germ cells.

Germ cell apoptosis was shown to be enhanced by pharmacologically or genetically induced ER stress (Levi-Ferber et al., 2014). Moreover, nonlethal sleep deprivation triggers the UPR^{ER} in all animals previously examined (Naidoo et al., 2005b; Cirelli et al., 2004; Shaw et al., 2000; Terao et al., 2003). We therefore hypothesized that the UPR^{ER} may be triggered by nonlethal deprivation of worm sleep and that it may be required for the effect of deprivation on fecundity. HSP-4 is a *C. elegans* homolog chaperone of mammalian Grp78/BiP, upregulated in response to ER stress (Calfon et al., 2002; Heschl and Baillie, 1990; Shen et al., 2001). Expression of BiP is upregulated in fly and rodent brains in response to nonlethal sleep deprivation (Cirelli et al., 2004; Cirelli and Tononi, 2000; Naidoo et al., 2007; Naidoo, 2009; Naidoo et al., 2005b; Shaw et al., 2000; Terao et al., 2003). To address whether HSP-4/BiP is upregulated in sleep deprived worms, we subjected animals expressing the transcriptional reporter *Phsp-4::gfp* (zcIs4), a key indicator of the UPR^{ER} (Calfon et al., 2002), to the one hour deprivation protocol. We observed that *hsp-4* was notably expressed in the epithelial seam of undisrupted animals during L4 lethargus (Fig. 3.7A). This array of hypodermal stem cells, termed seam cells, regulate hypodermal/cuticle formation and transform to their adult fate at the time of the fourth molt (Ambros, 1989; Liu and Ambros, 1989). The timing of *hsp-4* expression coincided with the generation of the adult alae - longitudinally oriented cuticular ridges - by the seam cells (Singh and Sulston, 1978; Thein et al., 2003). Animals subject to the one-hour sleep deprivation protocol significantly upregulated the expression of *hsp-4*. In contrast, mock deprivation or exposing the animals to one hour of vibrations during the mid L4 larval stage did not affect hsp-4 expression (Fig. 3.7B). Consistently, *hsp-4* expression remained elevated after a 4-hour period of disruptions, as indicated by quantitative PCR (Fig 3.7C). Upregulation of *hsp-4* requires essential components of the UPR^{ER} machinery: it is mediated non cell-autonomously by the transmembrane protein kinase and endoribonuclease IRE-1, which activates the bZIP transcription factor XBP-1 (Calfon et al.,

2002; Hou et al., 2014; Urano et al., 2002). Consistent with pharmacological or genetic induction of ER stress, nonlethal sleep deprivation failed to upregulate *hsp-4* expression on *ire-1* or *xbp-1* mutant backgrounds (Fig. 3.7D). Combined, these results show that nonlethal sleep deprivation is proteotoxic and induces ER stress in *C. elegans*. Next, we asked whether IRE-1 function was essential for germ cell apoptosis caused by sleep deprivation. To address this, we compared the brood sizes of deprived, control (exposed to vibrations outside of lethargus), and undisrupted *ire-1(ok799)* mutants. Loss of IRE-1 function abolished the reduction in brood size (Fig. 3.7E). In contrast, *ubl-5* mutants, deficient in the UPR^{mt}, exhibited an identical reduction in brood size to wild-type (Fig. 3.7F). Therefore, the UPR^{ER} was essential for germ cell apoptosis induced by sleep deprivation, but the UPR^{mt} did not affect fecundity under identical conditions. Does the UPR^{ER} invoked by sleep deprivation affect pharyngeal pumping? To address this, we assayed two *ire-1* mutant alleles. Both mutants exhibited no significant change in the mean pumping rate post-deprivation. However, the duty ratio of bursts of rapid pumping was affected, indicating a potentially mild contribution of the UPR^{ER} to mitigating the deprivation-induced pumping deficiency (Fig. 3.7G). We could not detect a deprivation-induced pumping deficiency in *hsp-4* mutants, perhaps due to redundancy of downstream protective mechanisms. These results demonstrate that ER proteotoxic stress plays a secondary role in post-deprivation pumping deficiency as opposed to the prominent role played by mitochondrial stress. Combined, our data demonstrate that nonlethal deprivation of worm sleep (at the severity enabled by our assays) induced distinct types of proteotoxic stress that trigger distinct UPRs in different tissues.

3.4.8 The UPR^{ER} (but not the UPR^{mt}) mitigates the effects of nonlethal deprivation on activity in the egg-laying circuit.

Germ cell apoptosis due to deprivation induced ER stress does not preclude an independent impact of deprivation on the egg-laying circuit. To address this, we examined animals carrying the *egl-1(n986dm)* allele, which lack the cell bodies of the HSN egg-laying neurons

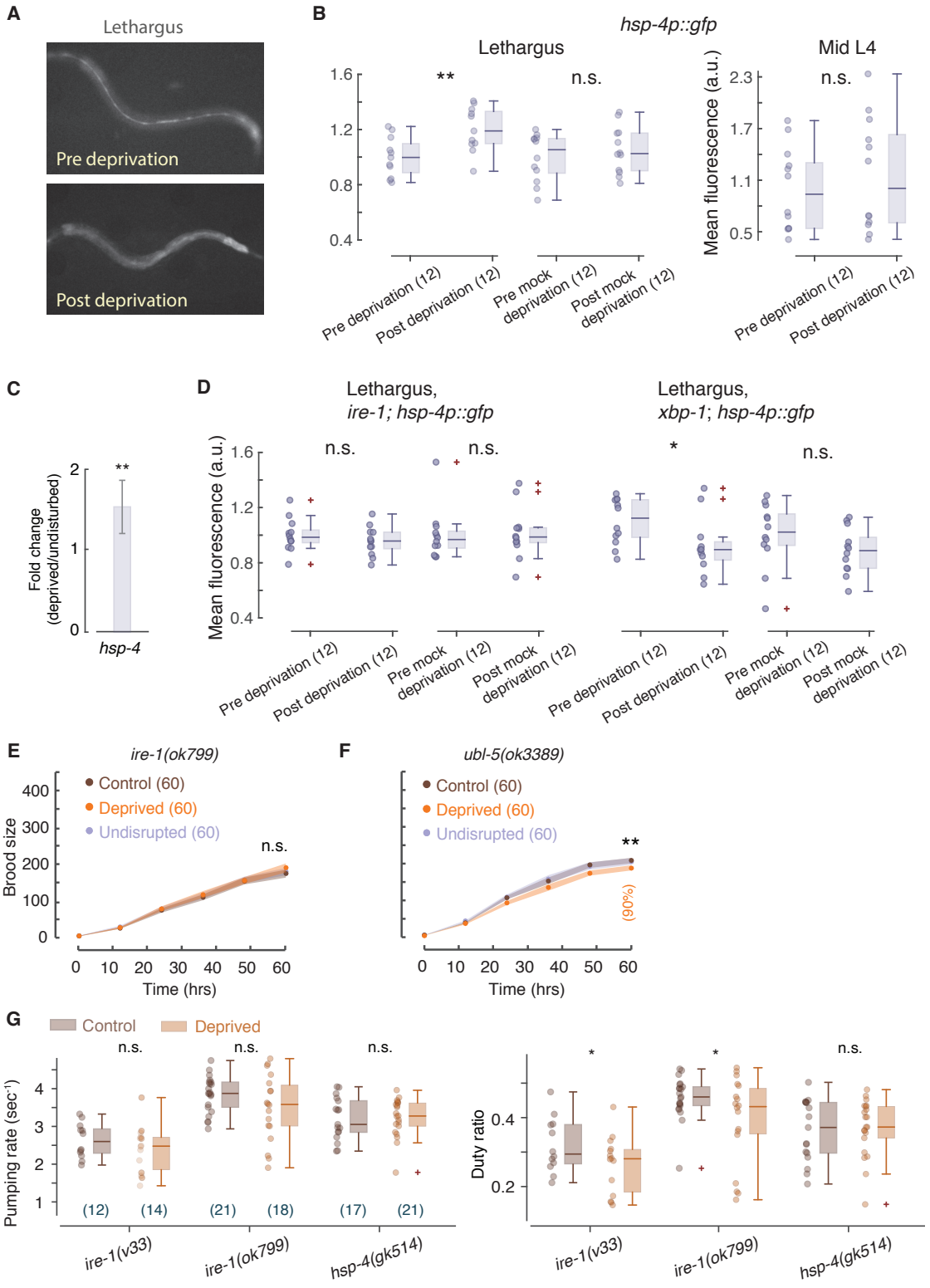

Figure 3.7: **The UPR^{ER} is required for post-deprivation germ cell apoptosis.**

Figure 3.7: **The UPR^{ER} is required for post-deprivation germ cell apoptosis (cont.)** (A) Example of pre- (top) and post- (bottom) deprivation fluorescence of the *hsp-4p::gfp* reporter. Prior to deprivation the reporter was prominently observed in the seam cells. (B) Fluorescence of the *hsp-4p::gfp* reporter before and after deprivation, mock deprivation, and stimulating mid L4 larvae. Horizontal lines, boxes, and bars depict medians, 1st and 3rd quartiles, and 5 and 95 percentiles, respectively. (C) Quantification of *hsp-4* expression using real-time PCR. Error bars depict 99% confidence intervals. (D) Fluorescence of the *hsp-4p::gfp* reporter in mutants where the function of the UPR^{ER} genes *ire-1* and *xbp-1* was lost. On these mutant backgrounds sleep deprivation did not upregulate the expression of *hsp-4*. (E) Brood sizes of *ire-1(ok799)* mutants during the first three days after L4 lethargus (t=0 is 10-12 hours after the fourth molt). Fecundity was not reduced by sleep deprivation, similar to the requirement for IRE-1 for enhanced germ cell apoptosis when ER stress is induced pharmacologically (Levi-Ferber et al., 2014). (F) Brood sizes of *ubl-5(ok3389)* mutants during the first three days after L4 lethargus (t=0 is 10-12 hours after the fourth molt). The effect of deprivation on fecundity was identical to wild-type, indicating that the UPR^{mt} does not affect germ line apoptosis under these conditions. (G) Average pumping rates and duty ratios are not and mildly affected by deprivation, respectively. Horizontal lines, boxes, and bars depict medians, 1st and 3rd quartiles, and 5 and 95 percentiles, respectively. Sample sizes denoted in parentheses, asterisk and double asterisks depict a significant difference ($p<0.05$ and $p<0.01$).

(Trent et al., 1983). The absence of HSN results in extended inactive egg-laying periods and a two-fold increase in calcium transients which correspond to twitching of the vulval muscles (vms) (Collins et al., 2016). Therefore, defects in the egg-laying circuit can be assayed by measuring the calcium transients in the vms of freely behaving animals. To do so, we sleep deprived worms co-expressing the genetically encoded calcium reporter GCaMP5 and the red fluorescent protein mCherry in their vms (Collins et al., 2016; Collins and Koelle, 2013) (Fig. 3.8A-B). Interestingly, in the egg-laying circuit, deprivation resulted in the complementing set of phenotypes to those found in the pharyngeal circuit. Neither wild-type animals nor UPR^{mt} deficient *ubl-5* mutants exhibited abnormal post-deprivation twitching. However, UPR^{ER} deficient *ire-1* mutants, when deprived, exhibited a mean increase of 30% in the number of vm twitches (Fig. 3.8C). This elevation in vm twitching mirrored the trend exhibited by *egl-1(n986dm)* mutants. Physiological activity in the egg-laying circuit is coupled with body posture and locomotion in the temporal vicinity of egg-laying events (Collins

et al., 2016; Collins and Koelle, 2013; Waggoner et al., 1998). We therefore hypothesized that differences in locomotion behavior over long timescales may also correlate with activity in the egg-laying circuit. Specifically, we asked whether a potential effect of deprivation on locomotion may indirectly cause the vm twitching phenotype in *ire-1* mutants. To address this, we calculated the mean velocity of each animal throughout the duration of our assay, compared between mean velocities of undisrupted and deprived animals, and measured the correlation of the mean velocity to the number of vm twitches. In all three genotypes assayed, the mean velocity did not vary significantly between undisrupted and deprived animals (Fig. 3.15A). While correlations between the mean velocity and vm twitching were found in all three strains, they were weakest in *ire-1* mutants. Even if the question of statistical significance was set aside, the differences between mean or median velocities was too small to plausibly account for the 30% increase in vm twitching. Thus, excess vm twitching was not an indirect consequence of elevated locomotion activity in our assays. These results are consistent with the conclusion that sleep deprivation upsets ER proteostasis and demonstrate that, if not mitigated, this stress also impacts the egg-laying circuit. Interestingly, the correlations we found between activity in the egg-laying circuit and locomotion were stronger in deprived wild-type animals and *ubl-5* mutants as compared to their respective undisrupted groups. This trend was reversed in *ire-1* mutants (Fig. 3.15B). This observation may indicate that elevating coordination between distinct behaviors during stress may require secreted proteins, such as neuropeptides, whose function depends on processing in the endoplasmic reticulum (Strand, 2003).

3.5 Discussion

The cognitive, physiological, and behavioral changes resulting from deprivation of human sleep elude superficial phenotyping. Detecting them requires functional imaging and/or proper design of the task being assayed, a clear definition of the sleep deprivation conditions, and careful measurements. Interpreting such results involves consideration of details such

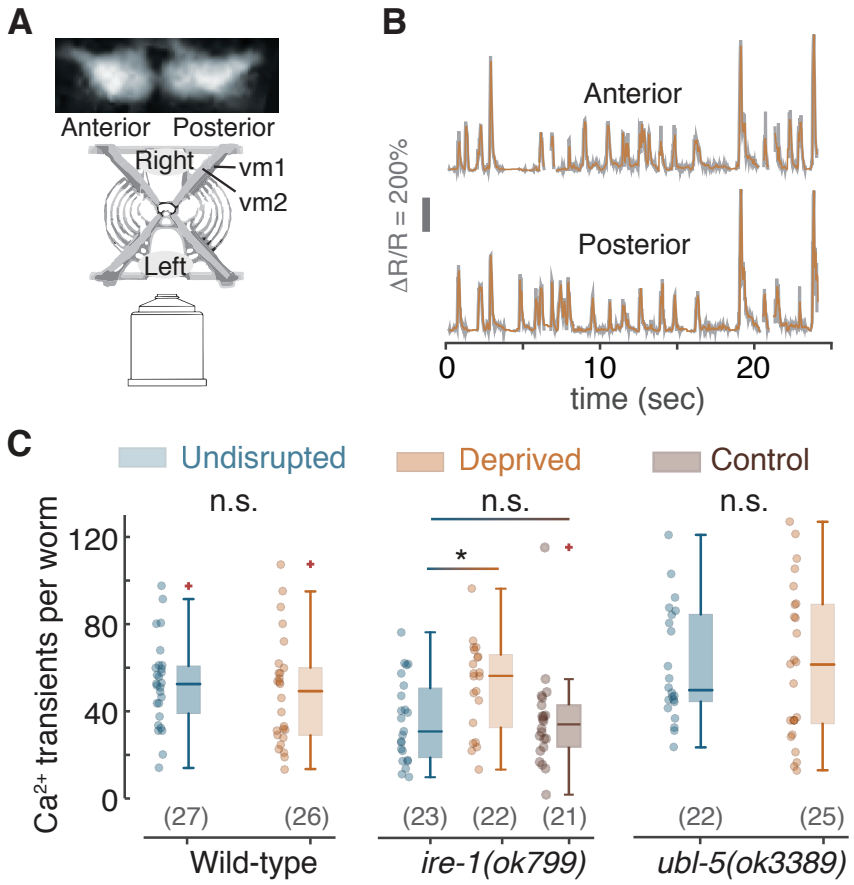

Figure 3.8: **Worm sleep deprivation results in excess twitching of vulval muscles.** (A) A schematic representation of the imaging setup. Top: fluorescently labeled anterior and posterior vulval muscle groups. Worms crawl on their left or right side such that their dorsoventral axis is parallel to the imaging plane. (B) Example traces of the ratio of GCaMP5 to mCherry fluorescence from anterior and posteriors vms. (C) The total number of calcium transients in vms of undisrupted and sleep deprived worms. An average increase of 30% in the number of vm twitches was detected in *ire-1* (UPR^{ER} deficient) mutants. No significant changes were detected in wild-type animals and *ubl-5* (UPR^{mt} deficient) mutants. Horizontal lines, boxes, and bars depict medians, 1st and 3rd quartiles, and 5 and 95 percentiles, respectively. Sample sizes are noted in parentheses and double asterisks denote significant differences ($p<0.02$).

as differences in vulnerability to deprivation between individuals and whether the task was monotonous or complex (Alhola and Polo-Kantola, 2007; Chee and Chuah, 2008; Harrison and Horne, 2000; Pilcher and Huffcutt, 1996). Similarly, wild-type rodents and insects do not typically exhibit gross defects or substantial damage to brain cells following nonlethal deprivation protocols (Cirelli et al., 1999; Gopalakrishnan et al., 2004; Kayser et al., 2014;

Vyazovskiy and Harris, 2013). Such findings suggest that the protective responses activated by deprivation have a capacity to effectively prevent or repair neuronal damage resulting from sleep deprivation.

To address the lasting impact of sleep deprivation in *C. elegans*, we established an experimental method enabling severe reduction in quiescence with no observed lethality or molting defects. Our periodic stimulus allowed for some quiescent behavior to take place throughout lethargus. Possibly, not forcing locomotion for extended continuous periods was key to avoiding a lethal outcome. In contrast, previous work assessed the impact of total sleep deprivation, i.e., consecutive forced movement for 30 minutes, which resulted in lethal molting defects. The impact on molting was interpreted to indicate a defect in metabolic regulation during lethargus as the loss of DAF-16 sensitized the animals to this effect (Driver et al., 2013a). Lasting defects in surviving animals were not previously assayed. The complete lack of lethality despite a loss of 50% of quiescence during lethargus is consistent with the hypothesis that quiescence, in and of itself, is an imperfect measure of the quality and restorative benefits of developmentally timed sleep in *C. elegans*. If homeostatic compensation can affect the quality of sleep (Singh et al., 2011), periodically allowing for rebound could confer greater restoration per unit time as compared to uninterrupted sleep. Testing this hypothesis will be key for understanding lethargus and may promote our understanding of additional quiescent states.

Next, we characterized outcomes of nonlethal deprivation and identified protective responses that mitigate them. Forced locomotion during *C. elegans* sleep negatively impacted feeding, fecundity, and the egg-laying circuit. Consistent with previous findings, our deprivation protocol triggered translocation of DAF-16/FoxO into intestinal cell nuclei (Driver et al., 2013a), and implicated it in mitigating lasting adverse effects of deprivation. In addition, several lines of evidence indicated fecundity was reduced due to germ cell apoptosis: the dependence of the effect on CED-3 and IRE-1, and the upregulation of CED-1 in sheath cells engulfing early apoptotic corpses of germ cells (Ellis and Horvitz, 1986; Levi-Ferber

et al., 2014; Schumacher et al., 2005; Yuan and Horvitz, 1990). Interestingly, sperm quality was recently shown to be negatively impacted by disruptions to sleep in rodents (Alvarenga et al., 2015; Torres et al., 2014). Identifying more specific responses to worm sleep deprivation may indicate ancient functions of sleep. We found that deprivation triggers the UPR$^{\mathrm{mt}}$, which protects feeding behavior in sleep deprived worms. In contrast to the UPR$^{\mathrm{ER}}$, the UPR$^{\mathrm{mt}}$ was not strongly associated with sleep deprivation previously. This may be partly due to a focus on sleep-related changes in gene expression in the brain (Cirelli, 2006; Cirelli et al., 2005, 2004; Jones et al., 2008; Naidoo, 2009; Naidoo et al., 2005a; Shaw et al., 2000; Terao et al., 2003; Wang et al., 2011; Zimmerman et al., 2006). Nevertheless, one study found that the mitochondrial chaperones Hsp60 and Glucose-regulated protein 75 (Grp75, from the Hsp70 superfamily) were upregulated in the cerebral cortex of rats after sleep deprivation, although not as much as BiP (Cirelli and Tononi, 2000).

Broad transcriptional responses to sleep deprivation were reported in mouse livers, lungs, and hearts (Anafi et al., 2013; Maret et al., 2007). These studies demonstrate that the molecular consequences of disrupting sleep are not limited to the brain and that sleep contributes to normal function in a manner that may vary between different tissues or organs. The pharynx of *C. elegans* is a highly active organ, required to repeatedly generate powerful contractions. Neurons that regulate pumping may face a distinct cellular metabolic challenge and therefore may particularly benefit from the UPR$^{\mathrm{mt}}$ post-deprivation. Nonlethal sleep deprivation upregulates the expression of BiP in rodents and flies, thus indicating the activation of the UPR$^{\mathrm{ER}}$ (Cirelli et al., 2004; Naidoo et al., 2005a; Shaw et al., 2000; Terao et al., 2003). We have shown a similar upregulation of HSP-4/BiP in response to disrupting developmentally timed worm sleep. Furthermore, loss of function of the misfolded ER protein receptor IRE-1 affected both fecundity and the egg-laying circuit post-deprivation. These findings in *C. elegans* show that the activation of the UPR$^{\mathrm{ER}}$ is a deeply conserved response to sleep deprivation (Singh et al., 2014). It remains to be determined whether the complementing set of phenotypes exhibited by the pharyngeal and the egg-laying circuits,

whose function depended on the UPR^{mt} and the UPR^{ER} respectively, is associated with differences in their developmental states, energy expenditure, or additional factors. Several hypotheses have been offered to explain the core functions of sleep, including the notion that its utility may differ across species (Siegel, 2005). The synaptic homeostasis hypothesis proposes that continuous learning during wakefulness is bound to saturate synaptic connections. Therefore, renormalization of net synaptic strength during sleep is required to restore homeostasis (Tononi and Cirelli, 2006, 2014). Other suggestions focus on ''wear and tear' in physiologically active neurons during wakefulness due to accumulation of protein fragments, unfolded proteins, or other molecular stressors (Churchill et al., 2008; Kang et al., 2009; Varshavsky, 2012; Vyazovskiy and Harris, 2013; Xue et al., 2005). On a larger scale, metabolite clearance from the brain can increase during mammalian sleep (Xie et al., 2013). In addition, disrupting sleep is linked to abnormal glucose metabolism and appetite regulation. These findings suggest that sleep is key to normal metabolic and hormonal processes outside the brain (Knutson et al., 2007; Reutrakul and Van Cauter, 2014).

This work describes multiple pathways by which sleep deprivation can create unfavorable biochemical conditions in cells and perturb proteostasis. Specific characteristics of physiological activity and development could affect the balance between accumulation and relief of allostatic load. To the best of our knowledge, how this balance might scale with different types of metabolic loads has not been systematically studied, let alone connected to sleep. Protection of post-deprivation pharyngeal function by the UPR^{mt} is consistent with the notions that sleep reduces cellular metabolic stress and that highly active organs may invoke distinct responses in this context. Implicating the UPRs in mitigating consequences of worm sleep loss indicates that these responses are deeply conserved.

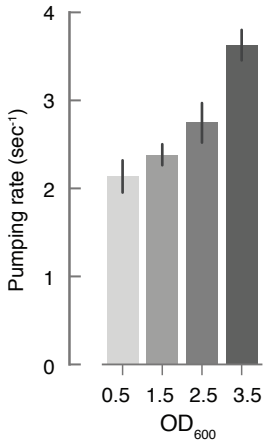

Figure 3.9: **Pumping rates increase as a function of food availability.** The average pumping rate of wild-type animals at different concentrations of ambient bacterial food (as measured by optical density, OD_{600}). Error bars depict mean ± s.e.m.

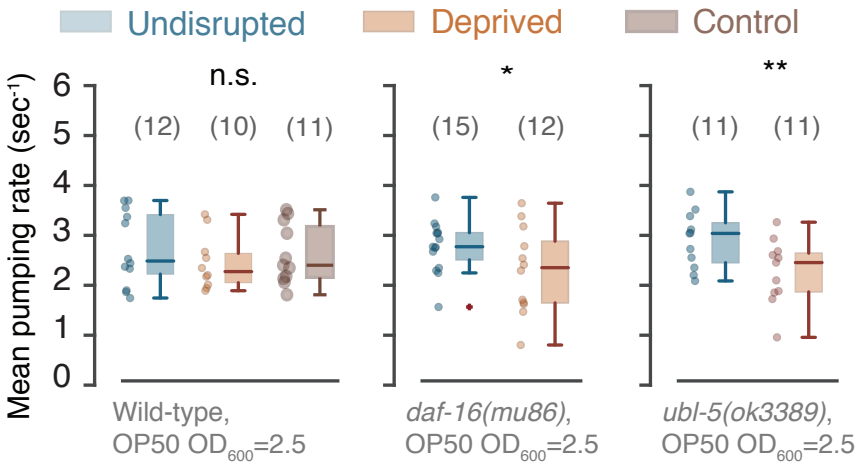

Figure 3.10: **Instantaneous pumping rates measured from EPG traces.** Instantaneous pumping rates were calculated as 1/duration between consecutive contraction peaks). Mean (per animal) rates for of wild-type animals, *daf-16(mu86)* mutants, and *ubl-5(ok3389)* mutants reproduced the phenotypes seen in the optical measurements.

3.6 Materials and Methods

3.6.1 Strains

Wild-type, transgenic, and mutant *C. elegans* strains were cultivated with OP50 bacteria according to standard protocols at 20C. The following strains were used: N2 Bristol

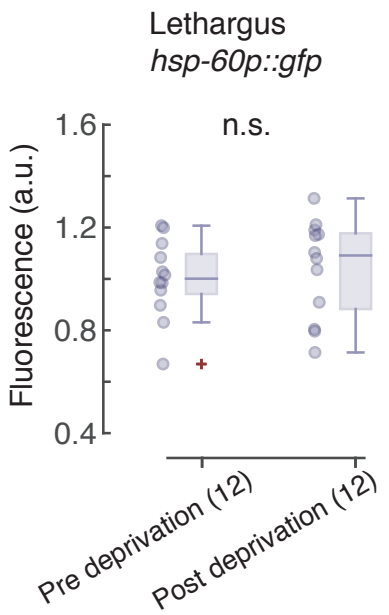

Figure 3.11: **Fluorescence of the *hsp-60p::GFP* fluorescent reporter before and after deprivation.** Elevated expression of the reporter was not observed after one hour of disrupting worm sleep without periodic vibration stimuli.

(wild-type), CF1038 *daf-16(mu86)*, GR1307 *daf-16(mgDf50)*, NQ116 *muIs211 [pNL213(ges-1p::GFP::daf-16) + rol-6(su1006)]* (Gift from Prof David Raizen), NQ441 *daf-16(mgDf50); qnIs45[Pdaf-16:GFP::daf-16; Pmyo-2:mCherry]* (Gift from Prof David Raizen at the University of Pennsylvania), SJ4151 *zcIs19 [ubl-5p::ubl-5::gfp]*, SJ4100 *zcIs13 [hsp-6::gfp]*, SJ4058 *zcIs9 [hsp-60::GFP + lin-15(+)]*, VC2564 *ubl-5(ok3389)*, SJ4200 *zcIs41 [ubl-5p::3xmyc-His tag::ubl-5 + myo-3p::gfp]*; SJ4151 *zcIs19 [ubl-5p::ubl-5::gfp]*, NQ128 *muEx169[unc-119p::GFP::daf-16 + rol-6(su1006)]* (Gift from Prof David Raizen at the University of Pennsylvania), DA184 *ser-1(ok345)*, *Is[Pmec-10::deg-3(u662)]* (Gift from Prof Millet Treinin at the Hebrew University of Jerusalem), MT3002 *ced-3(n1286)*, MD701 *bcIs39 [lim-7p::ced-1::GFP + lin-15(+)]*, SJ4005 *zcIs4 [hsp-4::gfp]* , RE666 *ire-1(v33)*, SJ17 *xbp-1(zc12)*, SJ30 *ire-1(zc14) II; zcIs4 V*, SJ17 *xbp-1(zc12) III; zcIs4 V*, RB925 *ire-1(ok799)*, VC1099 *hsp-4(gk514)II*, UX564 *jnSi118[Pcomp-1::GFP::H2B::3'comp-1; Cb-unc-119(+)]; him-5(ok1896)* (Gift from Prof Gillian Stanfield at the University of Utah), LX1938 *egl-1(n986dm)V; vsIs164 X; lite-*

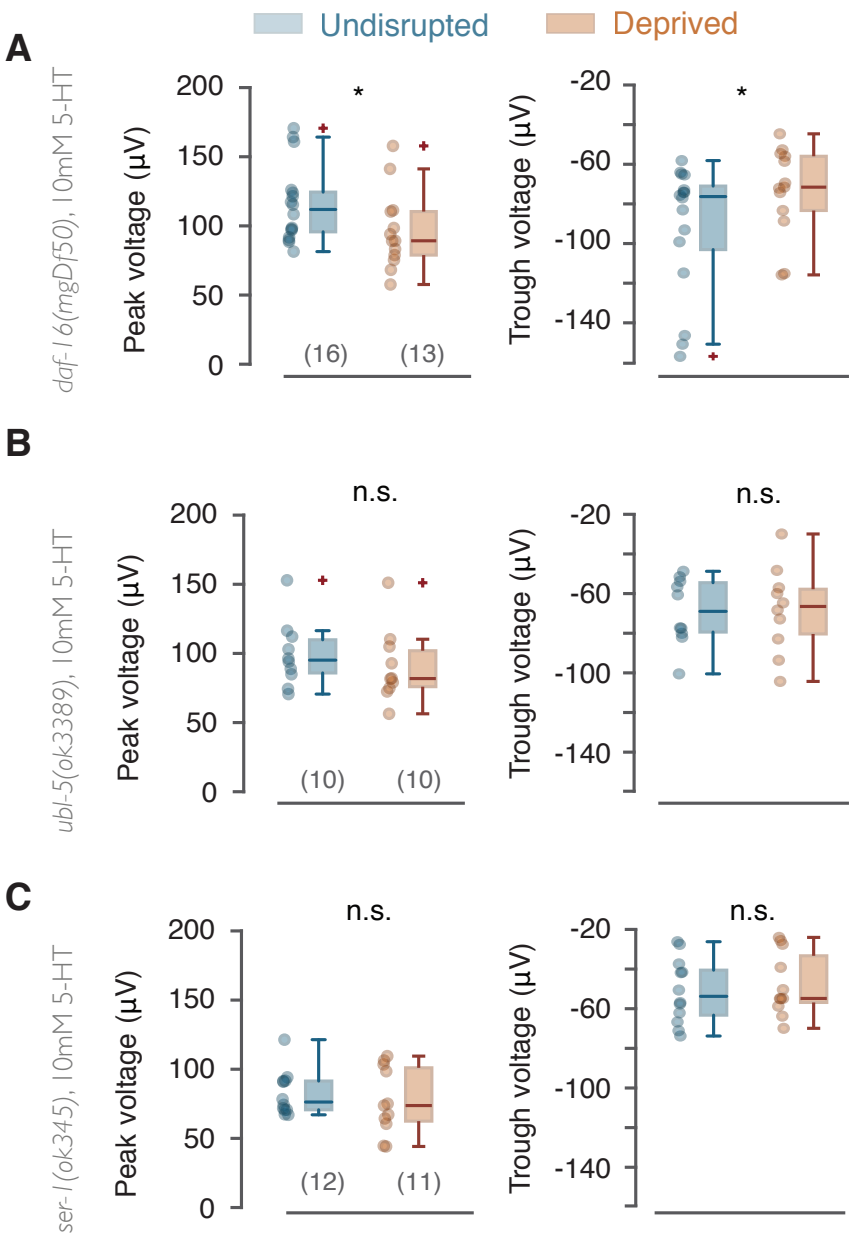

Figure 3.12: **Characteristics of 5-HT induced electropharyngeograms.** Mean (per animals) EPG peak and trough amplitudes for undisrupted *daf-16*, *ubl-5*, and *ser-1* mutants in the presence of 10 mM 5-HT. Sample sizes are noted in parentheses and asterisks denote significant differences ($p<0.05$).

1(ce314) X; lin-15(n765ts) X (Gift from Prof Kevin Collins at the University of Miami), LX1918 *vsIs164 X; lite-1(ce314) X; lin-15(n765ts) X* (Gift from Prof Kevin Collins at the University of Miami).

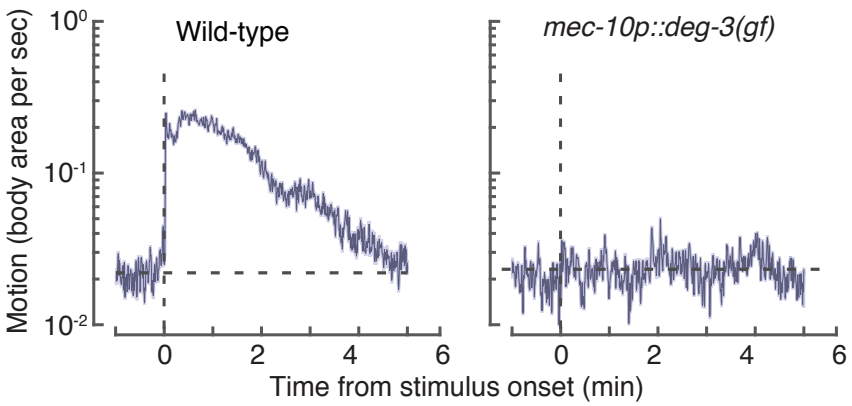

Figure 3.13: **Mean responses to the 3-minute vibration stimulus.** Locomotion in response to 1 kHz vibrations was quantified as the fraction of the body area the animal transversed per second. Wild-type animals (left) responded robustly to the stimulus while touch-insensitive *mec-10p::deg-3(gf)* transgenics (right) did not exhibit a detectable response. N=20 animals from each genotype were assayed and shaded areas depict mean±s.e.m.

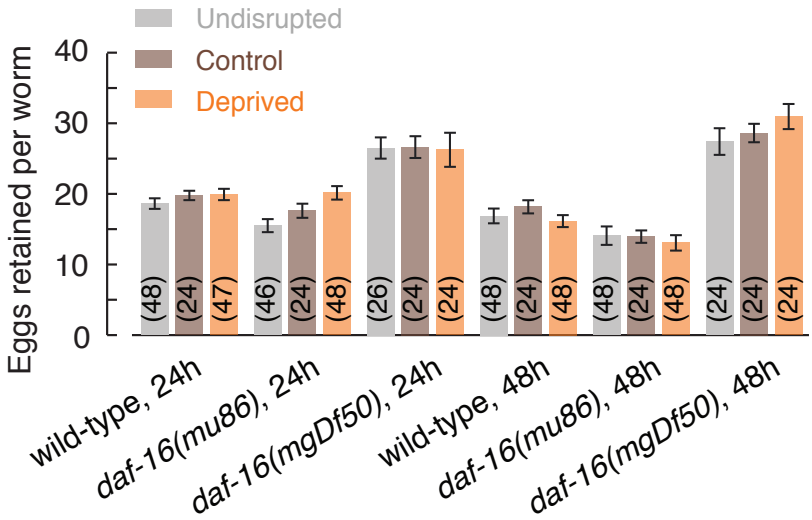

Figure 3.14: **Nonlethal deprivation does not increase egg retention.** The numbers of fertilized eggs retained in the uterus of wild-type animals and daf-16 mutants 24 hours and 48 hours after L4 lethargus. Deprived animals were exposed to the stimulus before, during, and after L4 lethargus. Control animals were exposed to the stimulus before and after L4 lethargus.

3.6.2 Severe nonlethal deprivation protocol

Motion and quiescence were identified using the image difference method as described in (Nagy et al., 2014a). To disrupt quiescence during lethargus, mid-L4 animals were trans-

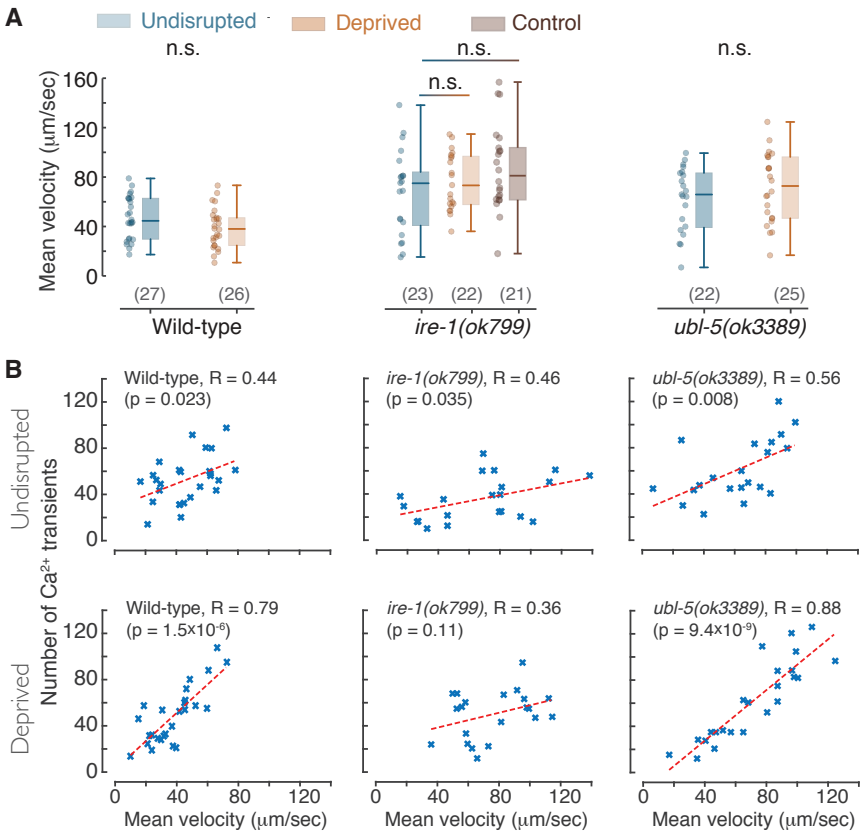

Figure 3.15: **Long-term mean velocities are not affected by deprivation but correlate with vm twitching.** (A) No significant differences were found between mean velocities (averaged over the 30 minutes of the assay) of undisrupted or deprived wild-type animals, *ire-1* mutants, or *ubl-5* mutants. Horizontal lines, boxes, and bars depict medians, 1st and 3rd quartiles, and 5 and 95 percentiles, respectively. Sample sizes are noted in parentheses. (B) Mean velocities and vm twitching were significantly correlated in wild-type animals, *ubl-5* mutants, and undisrupted *ire-1* mutants. Notably, these correlations were stronger in deprived wild-type animals and *ubl-5* mutants as compared to undisrupted worms of the corresponding genotype. However, correlations did not increase in *ire-1* mutants, suggesting that secreted proteins may be required for deprivation-induced enhancement of coordination between vm activity and locomotion.

ferred to 60 mm NGM plates containing 10 mL of medium and seeded with 50 μl of saturated OP50 culture. Vibrations (1kHz) were delivered as described in (Nagy et al., 2014). A square wave stimulus with a period of 6 minutes and duty cycle of 50% was delivered for 12 hours. To stimulate animals outside of lethargus, we similarly mechanically stimulated mid-L4 animals for 5 hours followed by a 5-hour pause and an additional 5 hours of stimulation.

3.6.3 Optical measurements of pharyngeal pumping

Post-stimulus (see above) young adults were picked into liquid NGM and loaded into a WormSpa microfluidic device (Kopito and Levine, 2014; Scholz et al., 2016a). An *E. coli* OP50 overnight culture, concentration-adjusted in NGM to $OD_{600} = 2.5$ (an intermediate food concentration) was flown through the device at a constant rate throughout the assay. After an hour of acclimation in the device, the animals were imaged for one additional hour at a magnification of 10x and 62.5 frames per second using a Basler acA1920-25um cMOS camera mounted on Celestron 44104 microscopes (Lynch and Biron, 2015). Pumping events were identified using a custom Python script which aligned and subtracted consecutive images and calculated the entropy of the difference image. A pumping event resulted in a characteristic spike in this entropy (Jing et al., 2004; Scholz et al., 2016a).

3.6.4 Electropharyngeograms (EPGs)

Worms were loaded to a Nemametrix ScreenChip System microfluidic device (NemaMetrix, Inc., Eugene, OR) on a standard dissection microscope and allowed to acclimate for at least 30 min before recording. The device was filled with either bacterial food ($OD_{600} = 2.5$) or a solution of 10mM 5-HT in NGM buffer. Immediately before the onset of the measurement the output tube was disconnected to reduce electromagnetic noise. Pumping frequency was measured as described in the ScreenChip User Guide and each recording lasted 5-10 min (measurements that terminated prematurely were discarded).

3.6.5 Imaging of GFP fluorescent reporters

The one-hour deprivation protocol consisted of 3-minute long vibration pulses interspersed with 3 minute long pauses, starting during the first 30 minutes of L4 lethargus and lasting a total of one hour. Animals expressing a fluorescent reporter were exposed to these mechanical stimuli in artificial dirt microfluidic devices placed inside a standard petri dish. They

were imaged in the device immediately before and after the one-hour period of disruptions. Imaging was performed at a magnification of 20X (0.5 NA) using a Nikon Eclipse Ti microscope and an Andor iXon X3 EMCCD camera. Fluorescence intensity was determined using custom Python scripts.

3.6.6 Calcium imaging in freely behaving animals

To reduce background fluorescence, calcium imaging was performed in artificial dirt microfluidic devices (Lockery et al., 2008). Animals co-expressing GCaMP5 and mCherry in their vms were mounted in the presence of bacterial food on an epi-fluorescence Nikon Eclipse Ti inverted microscope (Nikon Inc., Melville, NY). Each worm was imaged at a magnification of 20X (0.5 NA) and a frame rate of 6 frames per second. Images were captured by an Andor iXon X3 EMCCD camera. A Dualview (DV2) two-channel system was used for simultaneous imaging of the red and green channels (Photometrix, Tucson, AZ). Each animal was tracked manually and continuously imaged for a total period of 30 minutes. Calcium transients were analyzed using custom Matlab scripts (Mathworks Inc., Natick, MA).

3.6.7 Brood size

Brood size was counted by visual inspection: ten hours after mechanical stimulation ended, animals were transferred to individual 60 mm NGM plates seeded with 50 Îijl drop of OP50 (two animals per plate). Plate were scored in the morning and evening of the following three days. To avoid the accumulation of hatched offspring, animals were transferred to new plates prior to the evening counts each day. For male mating, two males and two hermaphrodites were transferred to each plate.

3.6.8 Sperm counting

Adult *Pcomp-1::GFP::H2B::3'comp-1* animals 24 hours post-L4 lethargus were sealed into individual 'artificial dirt' chambers filled with NGM medium and 10 ÎijM levamisole. Confocal images of fluorescently labeled sperm were obtained using a Zeiss LSM 880 microscope with a Plan-Apochromat 40x/1.4 oil DIC objective. Image stacks were analyzed using the FARSIGHT Nucleus Editor (`http://www.farsight-toolkit.org/wiki/NucleusEditor`). We note that when the fluorescent marker was crossed to a *daf-16* mutant background, it was not confined to the nuclei. However individual sperm cells were still detectable. We observed this in all *daf-16(mgDf60)* mutants and 25% of the *daf-16(mu86)* mutants.

3.6.9 Real time PCR

The *lmn-1* gene, encoding the *C. elegans* nuclear laminin, was chosen as the endogenous control gene. Primers (except for *lmn-1*, used previously by the Shaham lab at Rockefeller University) were designed using Wormbase.org and the NCBI Primer BLAST software. They were tested for specificity using NCBI BLAST and by agarose gel electrophoresis (using gDNA) and purchased from Integrated DNA Technologies (IDT, Coralville, IA). The primer used for *lmn-1* and *hsp-4* were TCGAGGCGGAAAAGGCTC (Fwd), GCTCCAGCGAGTTCTCTCTC (Rev), GCCGACAAGGAAAAACTCGG (Fwd), and GTGGGGTTGGGTTGGGAAA (Rev), respectively. Real-time quantitative PCR amplifications were performed using 25 μL of QuantiTect SYBR Green Real-Time PCR master mix (QIAGEN, Hilden, Germany), 2 μL of diluted reverse transcription product (2 ng/reaction), 1.5 μL each of forward and reverse primer and 20 μL of DNase/RNase free water in a total volume of 50 μL. Amplification was carried out in a AB 7900 HT Real-Time PCR cycler (Applied Biosystems, Foster City, CA) with initial polymerase activation at 95 °C for 15 min, followed by cycles of: 94 °C for 15 sec denaturation, 57°C for 30 sec for primer-specific annealing and 72 °C for 30 sec for extension. A melting curve analysis was carried out (60 °C to 95 °C) to verify the specificity of amplicons, i.e., the absence of

primer dimers and nonspecific products. Each assay included 6 technical replicates and a no-template control for every primer pair.

3.6.10 Statistical analysis

Pairwise comparisons of data represented in bar or box plot was done using the student t-test. In the case of multiple comparisons, significance was calculated using a one-way ANOVA test and the Bonferroni post-hoc correction. Distributions represented by histograms were compared using the k-sample Anderson-Darling test and the Bonferroni post-hoc correction for multiple comparisons (when applicable).

CHAPTER 4

STOCHASTIC FEEDING DYNAMICS ARISE FROM THE NEED FOR INFORMATION AND ENERGY

4.1 Overview

Animals, who frequently face decisions that affect their survival, evolved mechanisms for gathering information from the environment and using it to make apt decisions. An important example is feeding behavior, where animals need to weigh the nutritional value of the food with the associated energetic costs. In many species, animals feed in short bursts, yet the function and advantages of a burst feeding strategy are unknown. We suggest that these bursts are used both to collect food and to gather information. Based on the quantifiable feeding behavior of the roundworm *C. elegans* we develop a model of the animal's decision process. The model shows that burst feeding is advantageous in conditions where information about the expected food is noisy. This conceptualization is usefuld to understand responses to multiple conflicting inputs, and to determine optimal feeding strategies.

The work presented in this chapter was developed with my co-authors Aaron Dinner, Erel Levine and David Biron.

4.2 Abstract

Animals regulate their food intake in response to the available level of food. Failure to do so can have severe consequences for health and fitness. Recent observations of the feeding dynamics in small animals have shown feeding patterns of bursts and pauses. However, the function of these dynamics is unknown. Here, we present a data-driven decision-theoretical model of feeding in *Caenorhabditis elegans*. Our central assumption is that food intake serves a dual purpose: To gather information about the external food level and to ingest food when the conditions are good. The model recapitulates experimentally observed feeding patterns.

It naturally implements trade-offs between speed versus accuracy, and exploration versus exploitation in responding to a dynamic environment. We find that the model predicts three distinct regimes in responding to a dynamical environment, with a transition region where animals respond stochastically to periodic signals. This type of stochastic response accounts for previously unexplained experimental data.

4.3 Introduction

egulation of food intake is important for maintaining energy balance in animals. Failure can lead, for example, to reduced fitness, metabolic disorders, and cardiovascular diseases (Hill and Peters, 1998; Woods et al., 2000). To successfully regulate their feeding, animals need to assess the availability or expected availability of food in their environment.

Recent advances in automated longitudinal imaging of small animals make the acquisition of large-scale quantitative feeding data possible. Data from worms (Lee et al., 2017; Scholz et al., 2016b) and flies (Itskov et al., 2014) reveal complex dynamics that are responsive to the availability of food in the animal's environment. These data suggest that food uptake occurs in bouts of high-rate feeding, whose duration and frequency increase with the presence of food. Whether these dynamics serve a function is not known.

In this paper we hypothesize that the dynamics of feeding observed in small animals are intimately related to a decision-making process. Since feeding behaviors are costly in energy and can expose animals to toxins and pathogens, the decision to feed carries consequences and should be considered carefully by the animal. We posit that food uptake from the environment serves two purposes: to provide the animal with information about the food that is available in the environment, and to take up nutrients. To explore the implications of this assertion, we develop, analyze and experimentally test a quantitative model.

We focus on the regulation of feeding by the roundworm *Caenorhabditis elegans*, a free-living nematode that is found predominantly in fruit composts and feeds on bacteria. The feeding organ of the worm, the pharynx, is a simple neuromuscular pump. Each pump brings

a small number of bacteria suspended in water into the pharyngeal lumen. The pharynx then expels the water, grinds the bacteria, and sends them into the intestine. Pumping is therefore a proxy for the behavioral dynamics of feeding. Supported by microfluidics technology, time traces of pumping in individual worms can be obtained over long periods of time using either optical (Lee et al., 2017; Scholz et al., 2016b) or electrophysiological (Lockery et al., 2012) methods.

Decision making is a process for committing to an action, based on an estimate of the current (and perhaps future) conditions. A hallmark of decision making is integration of evidence to estimate the likelihood of each condition, and to gauge the cost and benefit of possible choices. In feeding, this evidence takes the form of ingesting small samples from the environment. The concentration and composition of each sample provides the animal with information to update its estimate of the availability and quality of food in the environment.

We formulate and analyze a model of feeding dynamics within the framework of sequential decision theory (also known as sequential analysis). The success of this theoretical framework in conceptualizing the process of evidence integration has been demonstrated in cells, insects, rodents, primates and humans (Ratcliff et al., 2003; Audley and Pike, 1965; Bogacz et al., 2010; LaBerge, 1962; Link and Heath, 1975; Reddi et al., 2003; Siggia and Vergassola, 2013; Vergassola et al., 2007). Within this model, we find that worms balance several trade-offs, including speed vs. accuracy and exploration vs. exploitation. We highlight predictions of these models, and reinterpret existing data in this new light. Finally, we discuss in detail commonalities between the feeding decision process and neuronal mechanisms of decision making.

4.4 Results

4.4.1 C. elegans feeding is a bursty stochastic process

To measure feeding dynamics we confined worms to small chambers of a microfluidic device and provided them with bacteria at a fixed density. We tested ambient bacteria densities in the range of $5 \times 10^7 - 5 \times 10^9$ bacteria/ml ($OD_{600} = 0.05 - 5$), corresponding to $0.1 - 10$ bacteria per volume of the pharyngeal lumen (Avery and Shtonda, 2003b; Fang-Yen et al., 2009a). For each ambient density we collected feeding times series from multiple worms by automatically tracking the motion of their grinder (Scholz et al., 2016b; Lee et al., 2017). Exemplary trajectories show bursts of consecutive pumps and pauses (Fig. 4.1A, B).

Based on these trajectories, we calculated the mean instantaneous pumping rate and the duty ratio (fraction of time spent in rapid pumping). We found that the overall pumping activity correlates with the concentration of available food and that pumping does not completely cease when no food was available (Fig. 4.1 and 4.2A, B) (Avery and You, 2012; Trojanowski et al., 2014; Lee et al., 2017; Song et al., 2013). In the absence of food, worms exhibit long pauses (Fig. 4.1C), while at high food concentrations they pump at a characteristic rate of $4 - 5$ Hz (Fig. 4.1E), close to the highest physiologically possible rate (Avery, 1993b). An intermediate food concentration evokes a distribution of pumping rates that can be approximated by a linear combination of the high- and no food distributions, Fig. 4.1D,F.

At all food concentrations pharyngeal pumping showed bursts of rapid feeding interspersed with pauses. We define a burst of rapid pumping as a series of continuous pumps not more than 500 ms apart. The observed rise in pumping rate with increased food concentration resulted both from a broader distribution of bursts and a narrower distribution of pauses (Fig. 4.2C,D). The mean burst duration positively correlated with the mean pumping rate in individual animals (Table 4.1). Together, our data suggest that pharyngeal pumping can be described in terms of two states — rapid-pumping and pauses — and the dynamics of switching between them.

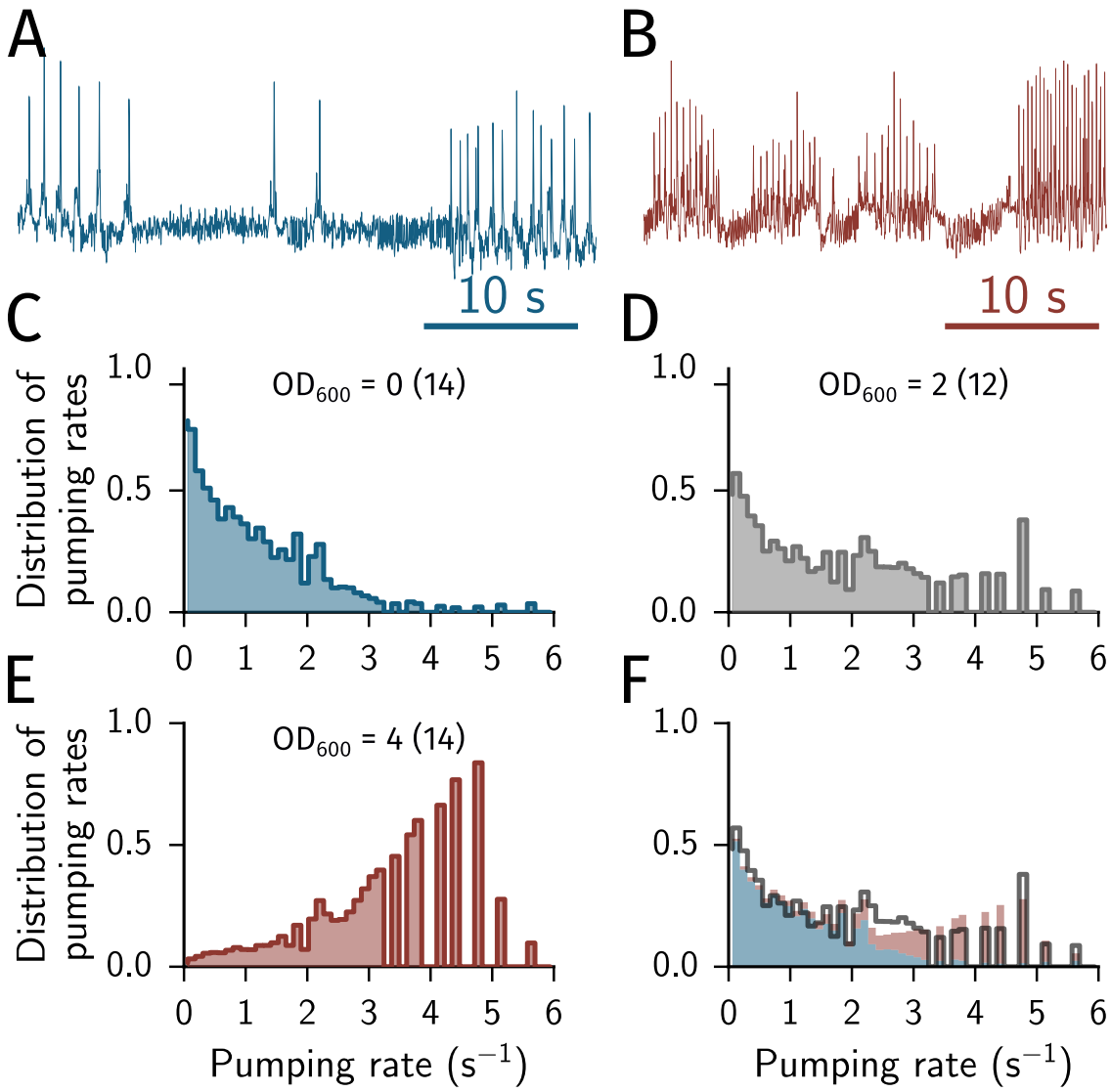

Figure 4.1: ***C. elegans* feeding can be approximated by a two-state system.** (A, B) Raw feeding trajectories at low and high food (OD_{600} = 0 and 4, respectively). The sharp peaks indicate pumping events. (C, D, E) Distribution of instantaneous pumping rates for low, medium and high food concentrations (OD_{600} = 0, 2, 4, respectively). (F) Weighted combination of the pumping rate distribution at low and high food (blue and red) compared with the medium food concentration (black). The weighting factor was found by χ^2 minimization. The best fit is $Y = \alpha Y_{\mathrm{Low}} + (1-\alpha)Y_{\mathrm{High}}$, with $\alpha = 0.687 \pm 0.023$ and $\chi^2/\mathrm{dof} = 44.28/48$. The rate distribution at intermediate food is shown in black. The panels are reproduced from data presented in (Scholz et al., 2016b).

4.4.2 A decision theory based model for adaptive feeding

The bursty feeding behavior described above appears in several small animals, raising the question of whether regulation of food intake through bursts and pauses is an advantageous strategy. To investigate this question, we frame feeding behavior as a decision process: An animal has to integrate (potentially noisy) information from the environment to decide whether the benefits of feeding exceed the costs.

A model of pharyngeal pumping should reflect the stochastic switching between bursts and pauses observed experimentally. Our data suggest that the durations of bursts and pauses are not distributed exponentially (Fig. 4.2C,D), excluding a two-state Markov process with concentration-dependent rates, arguably the simplest possibility. Thus, we instead formulate a three-state decision theory model where animals adjust the transition rates to environmental conditions in a memory-dependent process.

In our model, feeding dynamics cycles through three states: *sampling*, *committed*, and *resetting*. During the sampling state, the animal samples the environment by pumping, until it collects enough information to make a decision whether to commit to pumping or pausing. Based on this decision, it enters a committed state for a finite period. It then resets its estimate of the environment and the cycle restarts.

Sampling. In the sampling state, the worm is gathering information about the environment. With each pump, an animal ingests a small number of bacteria from the surrounding population. At low densities, the number of bacteria per pump is modeled as a random variable that obeys a Poisson distribution with a mean proportional to the ambient food concentration. We denote the energy required for the pharyngeal motion associated with a pump by $T\epsilon$, where ϵ is the nutritional value of a single bacterium, *i.e.* the energy gained from digesting it. The value of T sets a threshold: a single pump only proves beneficial if the total energy gain resulting from the ingested bacteria exceeds $T\epsilon$. To decide whether to commit to pumping or to pausing, the worm needs to decide whether the ambient food concentration μ (measured in units of number of bacteria per volume of a single pump) is

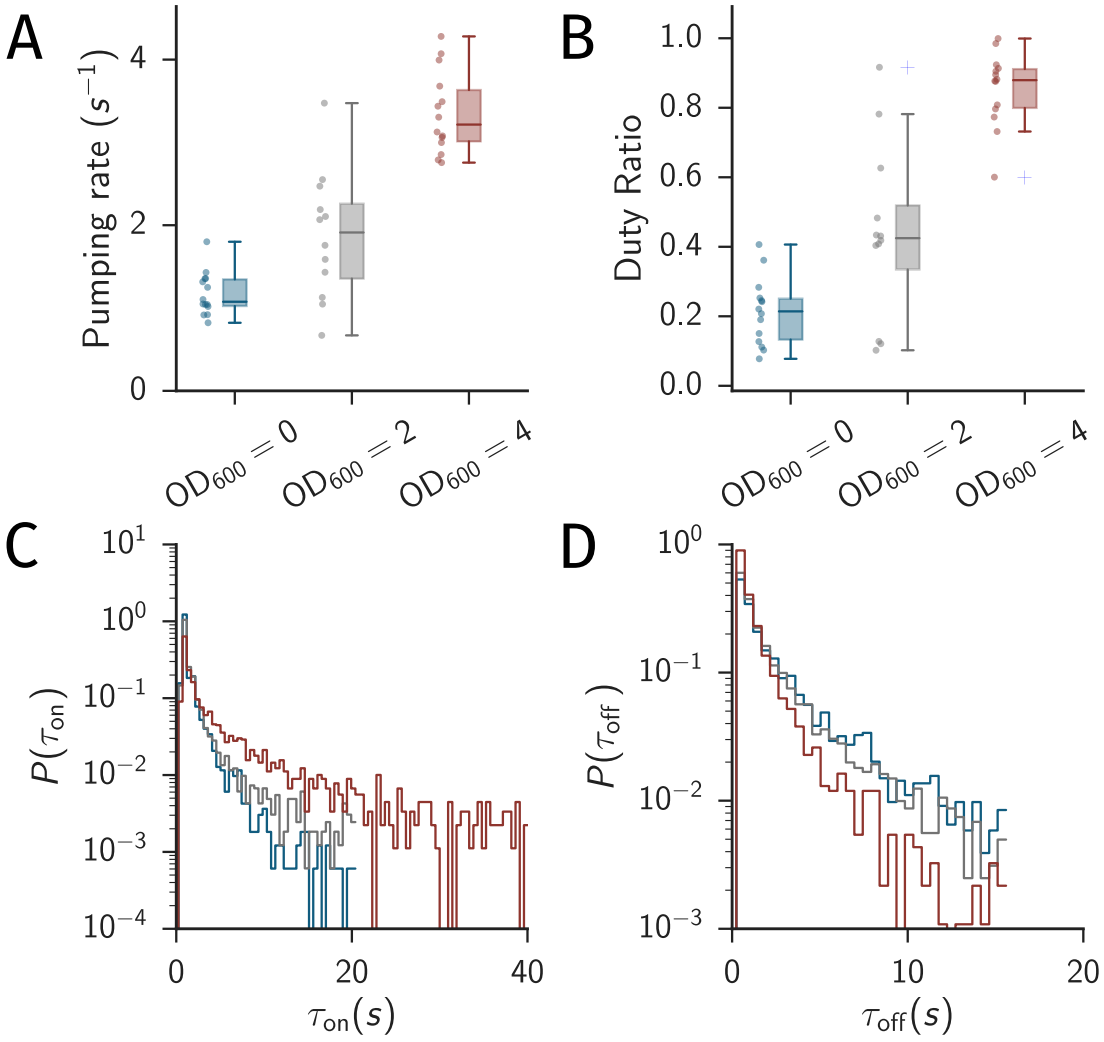

Figure 4.2: ***C. elegans* feeding is a stochastic process.** (A)Pumping rate as a function of food level. Error bars denote 5 and 95 percentiles. The boxes show the upper and lower quartiles. $N = 14, 12, 14$ for food levels of OD_{600} 0,2 and 4, respectively. (B) Duty ratio (fraction of rapid pumping) as a function of food level. The duty ratio was defined as the fraction of time during which consecutive pumps were ≤ 500 ms apart. Error bars show 5 and 95 percentiles. (C, D) Duration of bursts τ_{on} and pauses τ_{off} for the three food levels. Bursts are defined as series of continuous pumps ≤ 500 ms apart. Colors are the same as in (A, B). Panels (A) and (B) are reproduced from data presented in(Scholz et al., 2016b).

respectively higher or lower than T.

We model the sampling state as a sequential decision process. In this framework, decision-making starts with a prior $\mathcal{P}_0(x)$ which summarizes the innate belief of the animal that the ambient food density is x. This prior is set by evolution and refined through epigenetics, learning and memory, all occurring on time-scales much longer than the process considered here (see Discussion). The animal then samples the environment and uses the evidence it collects to update this belief, which after t samples takes the form $\mathcal{P}(x;t)$. Most important in this formulation is the decision variable (DV), which summarizes the current belief of the animal into a single number. This number is used to make the decision. Typically, if the DV is *larger* than some threshold, the animal concludes that the condition belongs to one set, which justifies one action. If the DV is *smaller* than another threshold, the animal concludes a different condition, and takes a different action. Otherwise, if the DV takes some intermediate value, the animal makes no decision and goes on to collect further evidence.

In our model, the evidence collected in each sample is the number of ingested bacteria. The probability for a sample of size x_t follows a Poisson distribution $P(x_t|\mu)$ with a parameter μ, the true ambient bacteria density. It is convenient to assume that the prior distribution $\mathcal{P}(x;t)$ of the ambient food concentration x takes the form of a Gamma distribution, which is the conjugate prior to the Poisson distribution:

$$\mathcal{P}(x;t) = f(x;a_t,b_t) \equiv \frac{b_t^{-a_t}}{\Gamma(a_t)} x^{a_t-1} e^{x/b_t} \tag{4.1}$$

where $\Gamma(a)$ is the Gamma function and a_t and b_t are the shape and scale parameters of the Gamma distribution. The time dependence of this probability can therefore be tracked through the time evolution of a_t and b_t.

We assume that the worm updates the probability distribution using a Bayesian rule, where $\mathcal{P}(x;t)$ serves as the prior for $\mathcal{P}(x;t+1)$ and the number of bacteria ingested in a

single pump, x_t, is the evidence. The decision dynamics is therefore

$$\begin{aligned}\mathcal{P}(x;t+1) = \mathcal{P}(x;t)\,P(x_t|x) &\sim x^{a_t-1}e^{x/b_t} \times \frac{x^{x_t}}{x_t!}e^{-x} \\ &\sim x^{a_t+x_t-1}e^{x(1/b_t-1)} \qquad \text{(up to normalization).} \quad (4.2)\end{aligned}$$

Thus after each pump the posterior remains a Gamma distribution, with new shape and scale parameters

$$a_{t+1} = a_t + x_t \qquad \text{and} \qquad b_{t+1} = \frac{b_t}{b_t+1}\,. \tag{4.3}$$

From $\mathcal{P}(x;t)$ we can define the decision variable as

$$DV = Pr\{\mu \geq T\} = \int_T^\infty \mathcal{P}(x;t)\,.$$

Sampling continues until either $DV > 1-p_H$ or $DV < p_L$, where the thresholds p_H and p_L set the level of confidence with which the alternative hypothesis is rejected (Fig. 4.3A, dashed black lines). An exemplary time evolution of the DV and $\mathcal{P}(x;t)$ is illustrated in Fig. 4.3A,B. The initial prior is set such that neither threshold criterion is fulfilled. For simplicity, we take $p_H = p_L \equiv p$. We note that for Poisson-distributed samples, this procedure is equivalent to a uniformly most powerful statistical test (Lehmann and Romano, 2005).

Committed. In the committed phase, the worm takes the action implied by the hypothesis of choice for a finite duration. The duration of the commitment is drawn from an exponential distribution with mean τ_b if the action of choice is to pump and τ_p if it is to pause.

Resetting. In the wild, an animal should expect the environment to be dynamic. To enable adaptation to changes in the environment the animal needs to keep reevaluating its decision once the commitment step is concluded. In our model, we do this by resetting $\mathcal{P}(x;t)$ to the initial prior by assigning $a_t = a_0$ and $b_t = b_0$. All information gathered from previous samples is thus erased and our model does not include long-term memory or

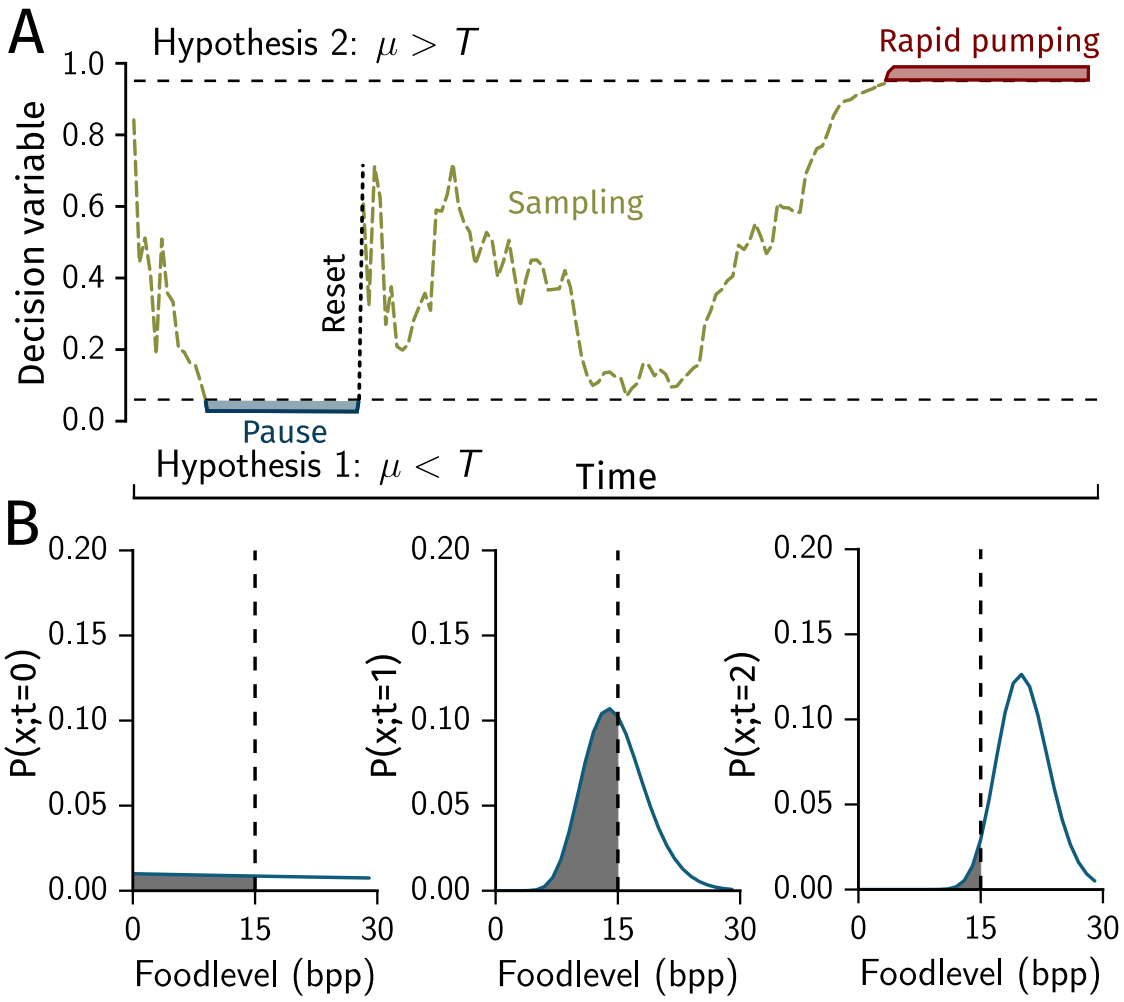

Figure 4.3: **A decision theory based model for adaptive feeding.** (A) Schematic evolution of the decision variable in time. (B) Evolution of the belief function $\mathcal{P}(x;t)$ with samples. The gray area shows the value of the decision variable. The dashed line indicates the cost T. Graphs are from simulations at food level 20 bpp.

learning (see Discussion).

It should be noted that in our model at any given time a worm may be sampling, committed to pumping, or pausing. However, when observing the time trace of pumping, one can only discern pumping from pausing. Thus, the duration of a burst of pumping observed experimentally may be composed of two parts that cannot be distinguished: sampling and commitment. The burst duration distribution is therefore directly affected by the distribution of sampling periods.

Simulating the model. The pumping time series has an inherent physiological timescale set by the maximal speed of the pump. Therefore, the procedure described above can be naturally simulated in a discrete-time framework (see Methods). For a maximum rate of 6 Hz, each time step of the model corresponds to 167 ms of real time. We define the optimal energy gain as the result of a hypothetical perfect series of decisions made by a worm fully aware of the ambient food concentration. In each simulation, we evaluated the performance of the simulated worm by comparing to this optimum.

4.4.3 The required confidence level affects performance when resources are scarce

The threshold p used to make a decision determines the number of required experimental observations (pumps). A stringent decision process defined by a small value of p requires prolonged sampling before committing and reduces the number of wrong decisions. Conversely, larger values of p shorten the sampling process, which can prevent excess pumping at low densities but increases the chances of erroneous decisions.

To quantitatively address this trade-off between the accuracy and speed of decision-making, we simulated our model with several values of p, using the default parameter values in Table 4.2 and a range of constant food concentrations (0 to 30 bacteria per liquid volume of a single pump). When the concentration of available food was similar to the threshold T, the time spent in the sampling state was longest. In all feeding environments, the model

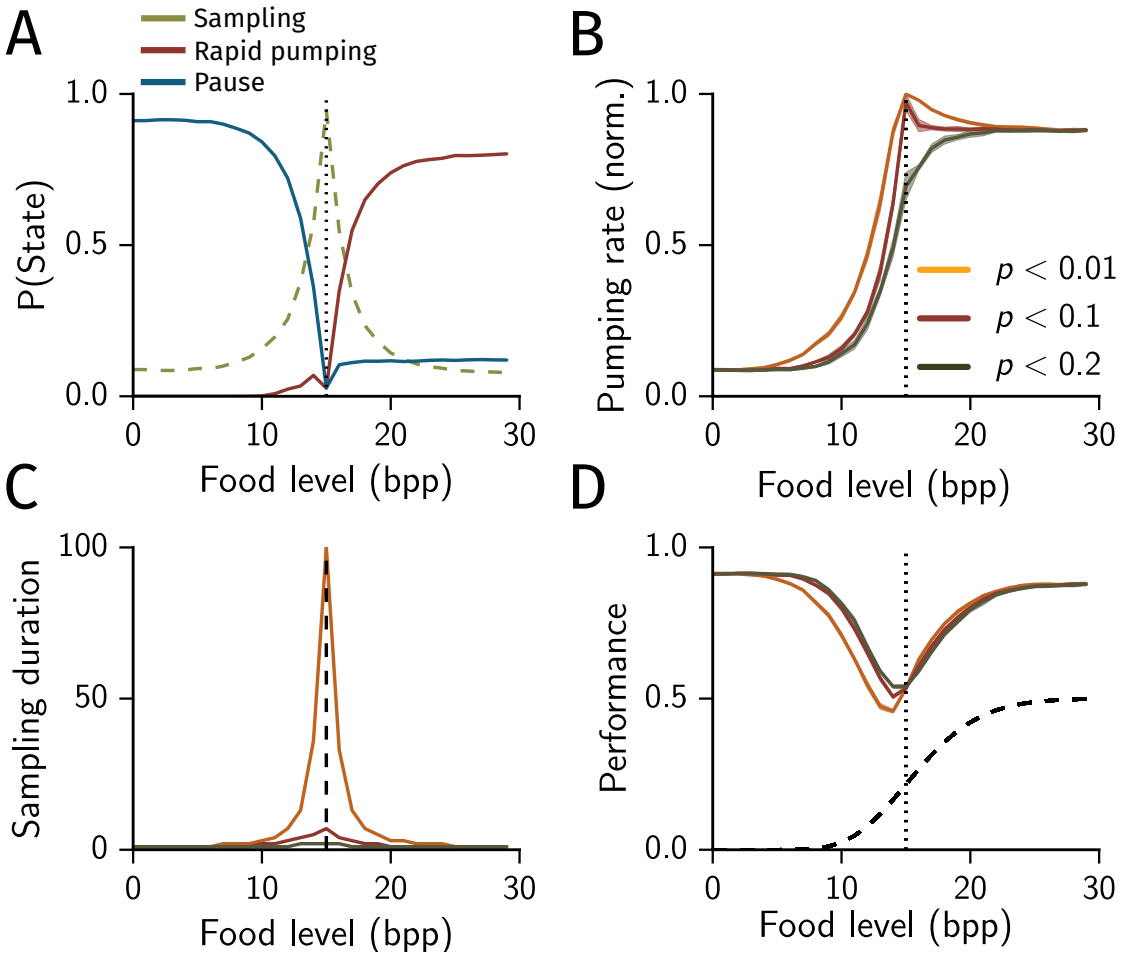

Figure 4.4: **Decision model response to food concentration.** (A) Fraction of time spent in sampling, committed and pausing states for a stringency of $p \leq 0.1$. (B) Pumping rate as a function of food concentration. (C) Duration of the sampling state for stringency. (D) Performance (fraction of correct decisions) as a function of food concentration. For comparison the performance of a random model with a 50% chance of pumping at every time step (black dashed line).

switched from mostly pausing to mostly rapid pumping when the concentration of food exceeded the cost (Fig. 4.4A). For stringent (small) values of p, the pumping rate was maximized near the threshold (Fig. 4.4B), where the worm spent considerable time on sampling (Fig. 4.4C). At higher or lower food concentrations the time spent in sampling was suppressed. Indeed, the pumping rate approaches 1 at $\mu = T$ as p becomes smaller. We note that in previous experiments no such maximum was observed, suggesting that *C. elegans* follows a less stringent rule (Lee et al., 2017; Scholz et al., 2016b).

We termed the decisions to pump (pause) 'correct' when the resulting food intake satisfied $x_t > T$ ($x_t < T$). We then defined the performance of the model as the average fraction of correct decisions. The decision model outperformed a random model (with a 50% chance of pumping at each time step) at all food levels (Fig. 4.4D). At high confidence levels, performance at low food levels $\mu < T$ was reduced, but not affected when food availability was high $\mu \geq T$. The coincidence of sampling and feeding produces asymmetric effects on performance because prolonged sampling is wasteful in harsh environments but inconsequential in plentiful ones.

4.4.4 Resetting is important in fluctuating environments

Feeding landscapes can be dynamic and spatially heterogeneous (McCann et al., 2005; Durham et al., 2013; Baker and Brown, 2014). The concatenation of decision processes naturally takes into account the fact that the environment may change. Therefore, we asked how the structure of our model affects responses to changes in food availability. Since many of our parameters merely set a timescale, we focused on the role of resetting. We compared the full model with a reduced version, where the prior parameters a and b were not reset to their initial values after the commitment step. The two models were simulated in the presence of a step increase in available food, from below- to above-threshold levels. Two differences are apparent: At the low food concentration, the non-resetting model developed a high accuracy. Consequently, the sampling was minimized and wasteful pumping was reduced. However, when food became plentiful, the non-resetting model lagged in responding to the change: the high confidence in what became a wrongfully bleak estimate resulted in a drawn out sampling process and slow detection of the change. After the step increase in food availability, the suppression of pumping was unproductive and inferior to the full model (Fig. 4.5 A,B). The duration of the lag was not sensitive to changes in the confidence level required for decision, p, suggesting that this parameter is more important when external dynamics are slow (Fig. 4.5 C,D). These results show that the resetting step serves to confer

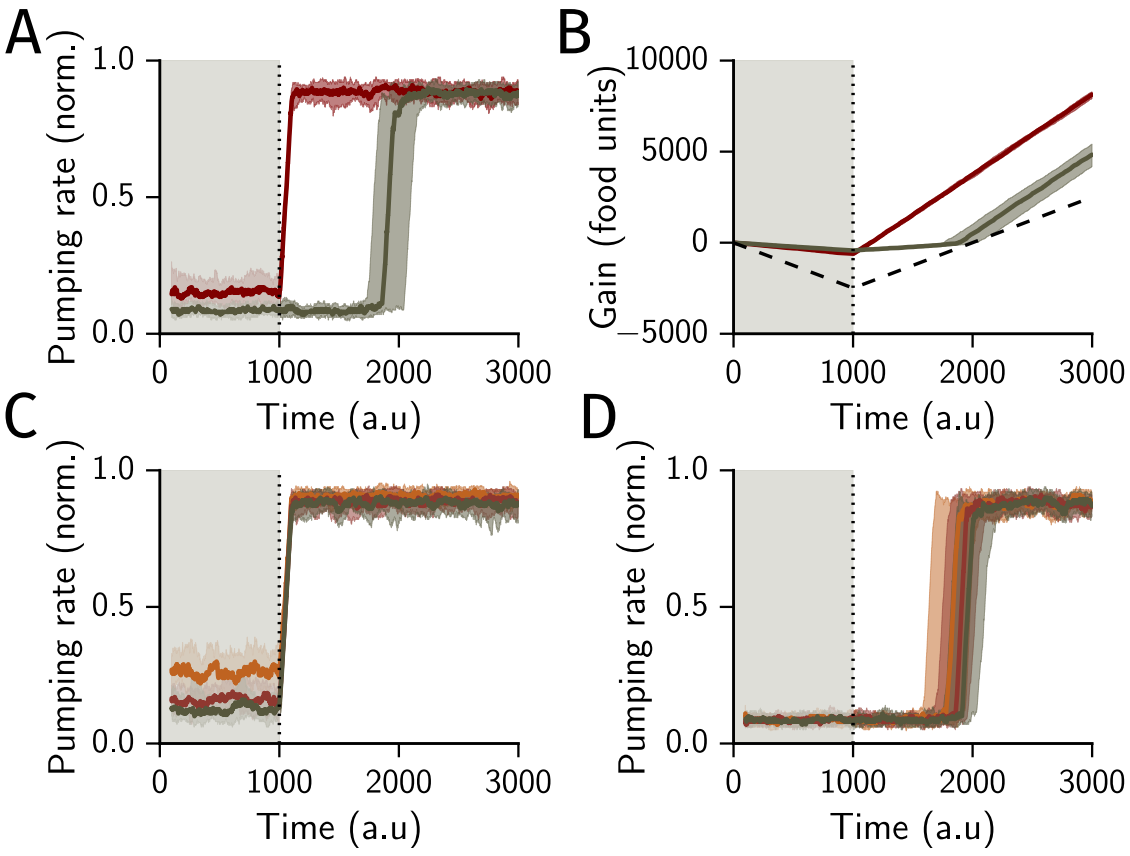

Figure 4.5: **Resetting improves adaptive feeding in a dynamic environment.** (A) Pumping rate in response to a step increase in mean food level from 10 to 20 units, for a model with and without resetting (red and olive, respectively). The step happens at $t = 1000$ (dashed line and after shading). The shaded area shows the standard deviation as calculated from 30 simulated trials. (B) Cumulative net food intake (gain) over the simulated time. The width of the curve indicates the standard deviation as calculated from 30 simulated trials. A random model with a 50% chance of pumping performs worse (dashed black line).(C) Response of the full model to a step in food level from 10 to 20 units for stringency $p = 0.01, 0.1, 0.2$, yellow, red and olive, respectively. (D) Response of the non-resetting model to a step in food level from 10 to 20 units for stringency $p = 0.01, 0.1, 0.2$, yellow, red and olive, respectively.

flexibility and assist the adaptation response to an external change. In spatially heterogeneous or temporally dynamic environments, resetting would positively affect the net energy balance and thus the overall fitness.

4.4.5 Food oscillations evoke stochastic switching

To gain insight into feeding behavior in a fluctuating environment, we considered oscillating food levels. We expected one of three possibilities: (i) pumping that faithfully tracks the oscillations, (ii) response to a time average of the concentration, or (iii) intervals of high or low pumping that are longer than the half-period of the environmental oscillations. We recently observed that *C. elegans* do not track oscillations of food concentration perfectly, even when these oscillations are slower than the typical duration of a burst. Rather, they switch between tracking and non-tracking modes on a timescale of ~ 100 sec (Scholz et al., 2016b). We asked whether our model exhibits such behavior by simulating environments where the concentration of food oscillated between $T - \Delta T$ and $T + \Delta T$, with $T = 15$ and $\Delta T = 2, 5$ or 15 bacteria.

Optimal net energy gain would be achieved by perfectly tracking the oscillations. Fast oscillations with respect to the timescales of bursts and pauses, τ_b and τ_p, resulted in partial or no tracking of the periodic stimulus (Fig. 4.6A). In particular, the combination of a short period and small amplitude yielded continuous pumping (yellow stripe at periods shorter than $\sim 3 \times \tau_b$ in Fig. 4.6C). This likely reflects the inability of the worm to complete the sampling process and commit to a decision. Very slow oscillations were perfectly tracked, as expected. When the amplitude was not too low, the model achieved 80% of perfect performance (Fig. 4.6B). Given resetting, this was optimal: the cost of starting to sample from the prior accounted for the missing 20%. This indicates that a soft reset that partially retains the gathered information could improve performance. The reduced performance at lower amplitudes can be attributed to the fact that the decision problem in this case is harder and requires more sampling.

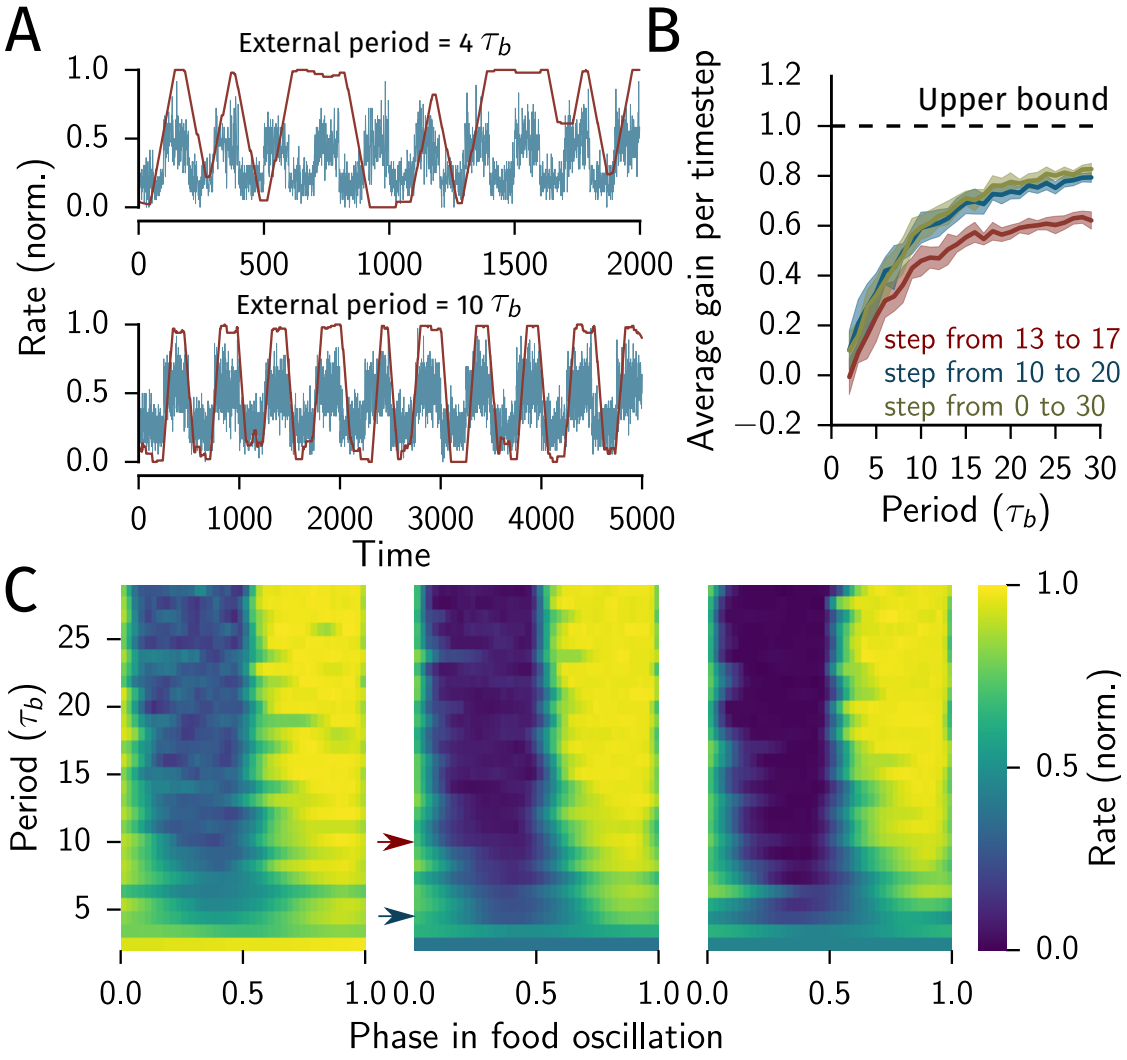

Figure 4.6: **Feeding in a dynamic environment depends on the timescale of change.** (A) Pumping response to periodic low-to-high food steps with a fast and slow period compared to the committed and pause lengths ($\tau_b = \tau_p = 50$) and instantaneous food level x_t (red and blue, respectively). (B) Fraction of food gained per bite (normalized to the theoretical maximum). (C) Periodogram showing the average pumping rate in response to periodic steps from 13 to 17, 10 to 20 and 0 to 30 ($T = 15$). The location of the trajectories shown in (A) are indicated as blue and red arrows (top and bottom of panel (A), respectively. The committed and pause durations for all panels are $\tau_b = \tau_p = 50$).

In contrast, at intermediate periods substantially slower than τ_b and τ_p, we observed stochastic switching between tracking and non-tracking. In Fig. 4.6C good tracking of the oscillatory stimulus manifests as a clear distinction between the light and the dark parts of the heat maps. The transition between stochastic switching and good tracking occurs near a period of $\sim 7\tau_b$. Together, these results mirror our previous experimental observations (Scholz et al., 2016b), although this feature was not considered in the development of our model.

Discussion

In this paper we propose that bursty feeding dynamics stem from the need to acquire both energy and information. For *C. elegans*, we assume that the mechanical act of pumping bacteria into the pharyngeal lumen is economical only when the number of bacteria captured exceeds a threshold, which depends on their nutritional content. However, instead of pumping strictly when expecting the reward to exceed the threshold, we propose that worms also pump when the outcome is uncertain. This is done to alleviate the uncertainty.

The sampling assumption necessitates the ability to sense and estimate the nutritional value of a single volume of the pharyngeal lumen. Our model is indifferent to the mechanisms used for this estimate, which may depend on mechanical and chemical cues, but it strictly requires pumping. Although short term history dependence is built into the model, individual measurements of food concentration do not have to be stored in a physical memory and need not be accessible at any time. Rather, they are instantaneously used to evolve an abstract state variable which can be encoded in a single cell or a small circuit. The biological implementation of a dynamic state variable may be more plausible than a random access memory, where individual data points (i.e., samples of the food level) are stored and can be accessed repeatedly.

Decision making has long been described as a statistical inference problem in which animals collect information about the environment until a decision can be reached (Gold

and Shadlen, 2007). Our model sequentially repeats a generic decision cycle. Each cycle is initiated with a naive prior: a probability distribution for possible ambient concentrations of bacteria that represents a standard prediction in the absence of evidence. The animal then collects samples through a sequence of pumps, which are used to update its assessment of the environment. Once it estimates that the amount of food is above or below a threshold, the worm makes a short-term commitment to initiate a burst of fast pumping or to pause, respectively.

We formulate and analyze our model in the framework of sequential analysis.This framework is particularly useful when the starting point of the decision process is well-defined, the statistics of the incoming information are stable, and the timescale over which information accrues can be identified. These conditions are not guaranteed to be satisfied in neural circuits which routinely exhibit adaptation, non-linear responses, and refractory periods. However, they are satisfied by the time series of pumping events: the size of each sample is dictated by the properties of the pharynx and its timing is directly observable (Lee et al., 2017; Lockery et al., 2012; Scholz et al., 2016b). We can thus identify the starting point of each decision cycle unambiguously as the end of a long pause or of a burst of fast pumping.

The decision process described here involves trade-offs. First, the accuracy of the decisions is determined by the stopping criterion p and measured as the frequency of correct decisions. Increasing it requires longer sampling. This is known as the speed-accuracy trade-off (Chittka et al., 2009; Barack and Gold, 2016). The sampling procedure considered in our model, which can be viewed as a biased diffusion of the DV between two absorbing boundaries, strikes an optimal balance between speed and accuracy (Bogacz et al., 2006). Second, the duration of the commitment period (set by τ_b and τ_p) manifests as an explore-exploit trade-off (Sutton and Barto, 1998; Cohen et al., 2007; Barack and Gold, 2016; Vergassola et al., 2007; Humphries and Sims, 2014). On one hand, an animal aims to maximize (in the short term) the benefit from the knowledge obtained from recent measurements. Exploitation however makes it hard to respond to a change in the environment, which can be

deleterious if conditions are highly fluctuating. Despite its simplicity, this model provides mechanisms for tuning these characteristic trade-offs.

Resetting the prior at the end of each cycle allows flexibility in responding to dynamic or heterogeneous environments. Alternative strategies for coping with heterogeneous environment have been proposed, e.g., in bacteria and worms (Celani and Vergassola, 2010; Clausznitzer et al., 2014; Iwanir et al., 2016; Greene et al., 2016). In our model, we assume that after resetting the worm returns to a constant prior that does not change. This prior can be encoded genetically and epigenetically, and therefore change on evolutionary or generational time scales. Moreover, it is known that food preference and feeding behavior are learned behavior that can be modulated by life history (Song et al., 2013; Calhoun et al., 2014). Thus, the parameters a_0 and b_0 which characterize the baseline prior are changing dynamically on time scales much greater than the process considered here. Our model can therefore be incorporated into a multi-scale model which includes the effect of learning and evolutionary adaptation.

We have assumed that pumping in the sampling state occurs at the same rate as pumping during bursts (5 Hz), which is only limited by pharyngeal physiology. Physiological limits on the speed of sampling are known to be important for determining animal sampling strategies (Uchida et al., 2006; Gold and Shadlen, 2007). However, additional factors may contribute to the choice of sampling rate. For example, the size of individual samples is correlated with the amount of information they provide. Animals with a larger pharynx could reduce their sampling frequency. Moreover, a high sampling frequency may produce highly correlated consecutive samples. This would reduce the information gained per pump. Indeed, we have observed that in many cases worms pump more irregularly and somewhat slower before initiating bursts of continuous rapid pumping (Lee et al., 2017; Scholz et al., 2016b).

Finally, the framework we develop here provides a starting point for investigating more elaborate and realistic scenarios, theoretically and experimentally. In particular, if feeding dynamics are indeed dictated in part by a decision process then harder decisions would change

it in a predictable manner. This can be tested by feeding worms with mixtures of bacteria species of varying nutritional contents, more closely resembling an actual ecological niche. Since worms in the wild experience spatially and temporally heterogeneous environments, it is of interest to understand how the acquisition of information affects responses to changing conditions. Microfluidic approaches are particularly suitable for addressing such questions experimentally (Ben-Yakar et al., 2009), and the framework of sequential analysis is well-suited to develop them theoretically (Nassar et al., 2010; Behrens et al., 2007; Tartakovsky, 2015).

4.5 Materials and Methods

4.5.1 Pumping experiments

C. elegans adults were loaded into the WormSpa microfluidic device. An overnight culture of *E. coli* OP50 was spun down and resuspended in NGM buffer. The culture was concentration-adjusted to a given optical density (OD_{600}) and flown through the microfluidic device at 5 μl/min. After an hour of acclimation in the device, the animals were imaged for 30 minutes at a magnification of 4x and 62.5 frames per second. Pumping events were identified using a custom Python script which aligned and subtracted consecutive images and calculated the entropy of the difference image. A pumping event results in a characteristic spike in this entropy (Scholz et al., 2016b). The data in Fig. 4.1 and Fig. 4.2A,B and is reproduced from (Scholz et al., 2016b).

4.5.2 Simulations

The simulations were implemented in Python 2.7. At the start, the prior is initialized with the values given in Table S2 (unless otherwise indicated). To get a time series of the feeding decisions, we use a discrete time approach. At each time step t, we draw a food value x_t from a Poisson distribution with mean μ. The change of the decision variable is then calculated

using the update rules given in [4.3]. At each time step, we assess whether a decision can be made or sampling continues by using the built-in numerical integration of the Gamma function to obtain the value of p_H or p_L. If a decision is made, we draw a commitment time from an exponential distribution of mean τ_b or τ_p, depending on the decision. When the commitment is finished, we reset the decision variable and restart the process.

4.6 Discussion

In this paper we propose that bursty feeding dynamics stem from the need to acquire both energy and information. For *C. elegans*, we assume that the mechanical act of pumping bacteria into the pharyngeal lumen is economical only when the number of bacteria captured exceeds a threshold, which depends on their nutritional content. However, instead of pumping strictly when expecting the reward to exceed the threshold, we propose that worms also pump when the outcome is uncertain. This is done to alleviate the uncertainty.

The sampling assumption necessitates the ability to sense and estimate the nutritional value of a single volume of the pharyngeal lumen. Our model is indifferent to the mechanisms used for this estimate, which may depend on mechanical and chemical cues, but it strictly requires pumping. Although short term history dependence is built into the model, individual measurements of food concentration do not have to be stored in a physical memory and need not be accessible at any time. Rather, they are instantaneously used to evolve an abstract state variable which can be encoded in a single cell or a small circuit. The biological implementation of a dynamic state variable may be more plausible than a random access memory, where individual data points (i.e., samples of the food level) are stored and can be accessed repeatedly.

Decision making has long been described as a statistical inference problem in which animals collect information about the environment until a decision can be reached (Gold and Shadlen, 2007). Our model sequentially repeats a generic decision cycle. Each cycle is initiated with a naive prior: a probability distribution for possible ambient concentrations of

bacteria that represents a standard prediction in the absence of evidence. The animal then collects samples through a sequence of pumps, which are used to update its assessment of the environment. Once it estimates that the amount of food is above or below a threshold, the worm makes a short-term commitment to initiate a burst of fast pumping or to pause, respectively.

We formulate and analyze our model in the framework of sequential analysis.This framework is particularly useful when the starting point of the decision process is well-defined, the statistics of the incoming information are stable, and the timescale over which information accrues can be identified. These conditions are not guaranteed to be satisfied in neural circuits which routinely exhibit adaptation, non-linear responses, and refractory periods. However, they are satisfied by the time series of pumping events: the size of each sample is dictated by the properties of the pharynx and its timing is directly observable (Lee et al., 2017; Lockery et al., 2012; Scholz et al., 2016b). We can thus identify the starting point of each decision cycle unambiguously as the end of a long pause or of a burst of fast pumping.

The decision process described here involves trade-offs. First, the accuracy of the decisions is determined by the stopping criterion p and measured as the frequency of correct decisions. Increasing it requires longer sampling. This is known as the speed-accuracy trade-off (Chittka et al., 2009; Barack and Gold, 2016). The sampling procedure considered in our model, which can be viewed as a biased diffusion of the DV between two absorbing boundaries, strikes an optimal balance between speed and accuracy (Bogacz et al., 2006). Second, the duration of the commitment period (set by τ_b and τ_p) manifests as an explore-exploit trade-off (Sutton and Barto, 1998; Cohen et al., 2007; Barack and Gold, 2016; Vergassola et al., 2007; Humphries and Sims, 2014). On one hand, an animal aims to maximize (in the short term) the benefit from the knowledge obtained from recent measurements. Exploitation however makes it hard to respond to a change in the environment, which can be deleterious if conditions are highly fluctuating. Despite its simplicity, this model provides mechanisms for tuning these characteristic trade-offs.

Resetting the prior at the end of each cycle allows flexibility in responding to dynamic or heterogeneous environments. Alternative strategies for coping with heterogeneous environment have been proposed, e.g., in bacteria and worms (Celani and Vergassola, 2010; Clausznitzer et al., 2014; Iwanir et al., 2016; Greene et al., 2016). In our model, we assume that after resetting the worm returns to a constant prior that does not change. This prior can be encoded genetically and epigenetically, and therefore change on evolutionary or generational time scales. Moreover, it is known that food preference and feeding behavior are learned behavior that can be modulated by life history (Song et al., 2013; Calhoun et al., 2014). Thus, the parameters a_0 and b_0 which characterize the baseline prior are changing dynamically on time scales much greater than the process considered here. Our model can therefore be incorporated into a multi-scale model which includes the effect of learning and evolutionary adaptation.

We have assumed that pumping in the sampling state occurs at the same rate as pumping during bursts (5 Hz), which is only limited by pharyngeal physiology. Physiological limits on the speed of sampling are known to be important for determining animal sampling strategies (Uchida et al., 2006; Gold and Shadlen, 2007). However, additional factors may contribute to the choice of sampling rate. For example, the size of individual samples is correlated with the amount of information they provide. Animals with a larger pharynx could reduce their sampling frequency. Moreover, a high sampling frequency may produce highly correlated consecutive samples. This would reduce the information gained per pump. Indeed, we have observed that in many cases worms pump more irregularly and somewhat slower before initiating bursts of continuous rapid pumping (Lee et al., 2017; Scholz et al., 2016b).

Finally, the framework we develop here provides a starting point for investigating more elaborate and realistic scenarios, theoretically and experimentally. In particular, if feeding dynamics are indeed dictated in part by a decision process then harder decisions would change it in a predictable manner. This can be tested by feeding worms with mixtures of bacteria species of varying nutritional contents, more closely resembling an actual ecological niche.

Since worms in the wild experience spatially and temporally heterogeneous environments, it is of interest to understand how the acquisition of information affects responses to changing conditions. Microfluidic approaches are particularly suitable for addressing such questions experimentally (Ben-Yakar et al., 2009), and the framework of sequential analysis is well-suited to develop them theoretically (Nassar et al., 2010; Behrens et al., 2007; Tartakovsky, 2015).

4.7 Supplementary information

4.7.1 Animal to animal variation in feeding behavior

Despite the genetic similarity between individuals in an isogenetic population, we observed animal–to–animal variability in feeding behavior (Fig. 4.7). From each animal's pumping time series, we calculated burst durations τ_{on} and the mean pumping rate over the whole trajectory. The burst duration of individual animals is correlated with the mean pumping rate (Table 4.1). These correlations indicating that the variablility in pumping dynamics seen in Fig. 4.7 could arise from heterogeneity in the animal population. These differences correlate with a parameter of the decision process: the average duration of the commitment step (Table 4.1). It is interesting to ask to what extent are the decision parameters genetically encoded as opposed to tuned by adaptation and learning. The values of these parameters influence the prior estimate of the environment and the tuning of different trade-offs. If the behavior of a single animal over time remains constant then animal– to– animal variability would indicate weak regulation or perhaps a population-wide diversification strategy. In contrast, adapting to external changes within the range of observed behaviors can contribute to the fitness of the individual.

Table 4.1: Correlation between mean burst duration and average pumping rate for individual animals

Foodlevel in OD_{600}	Pearson R	p-value
0	0.74	0.0024
2	0.77	0.0032
4	0.66	0.0100

4.7.2 Default model parameters

Unless otherwise noted in the main text, all simulations of the model were done with the standard parameters given in Table 4.2.

4.7.3 Resetting is important in fluctuating environments

We compare the response of the full model and a model without resetting (the prior parameters a and b remain unchanged after the commitment step). We present the models with a step decrease in food concentration (from 20 to 10 bpp). Similar to the response observed when the food level increases, we observe a key difference between the two models: While the non-resetting model intitially performs similarly, it lags in responding to the change in food availability(Fig. 4.8A). Therefore, the net food intake is less than that of the full model (Fig. 4.8B). Similar to the step increase, the lag time does not depend on the required confidence level (Fig. 4.8C,D).

Table 4.2: Default model parameters

Parameter	Value	Units
Cost (T)	15	bacteria per pump (bpp)
Initial value of decision variable ($Pr\{\mu > T\}|_{t=0}$)	0.14	–
Initial parameters of the prior ($a_0,\ b_0$)	1, 100	– , bpp
Mean rapid pumping duration (τ_b)	10	time steps
Mean pause duration (τ_p)	10	time steps
Reset duration (τ_r)	1	time steps
Confidence level (p)	0.1	–

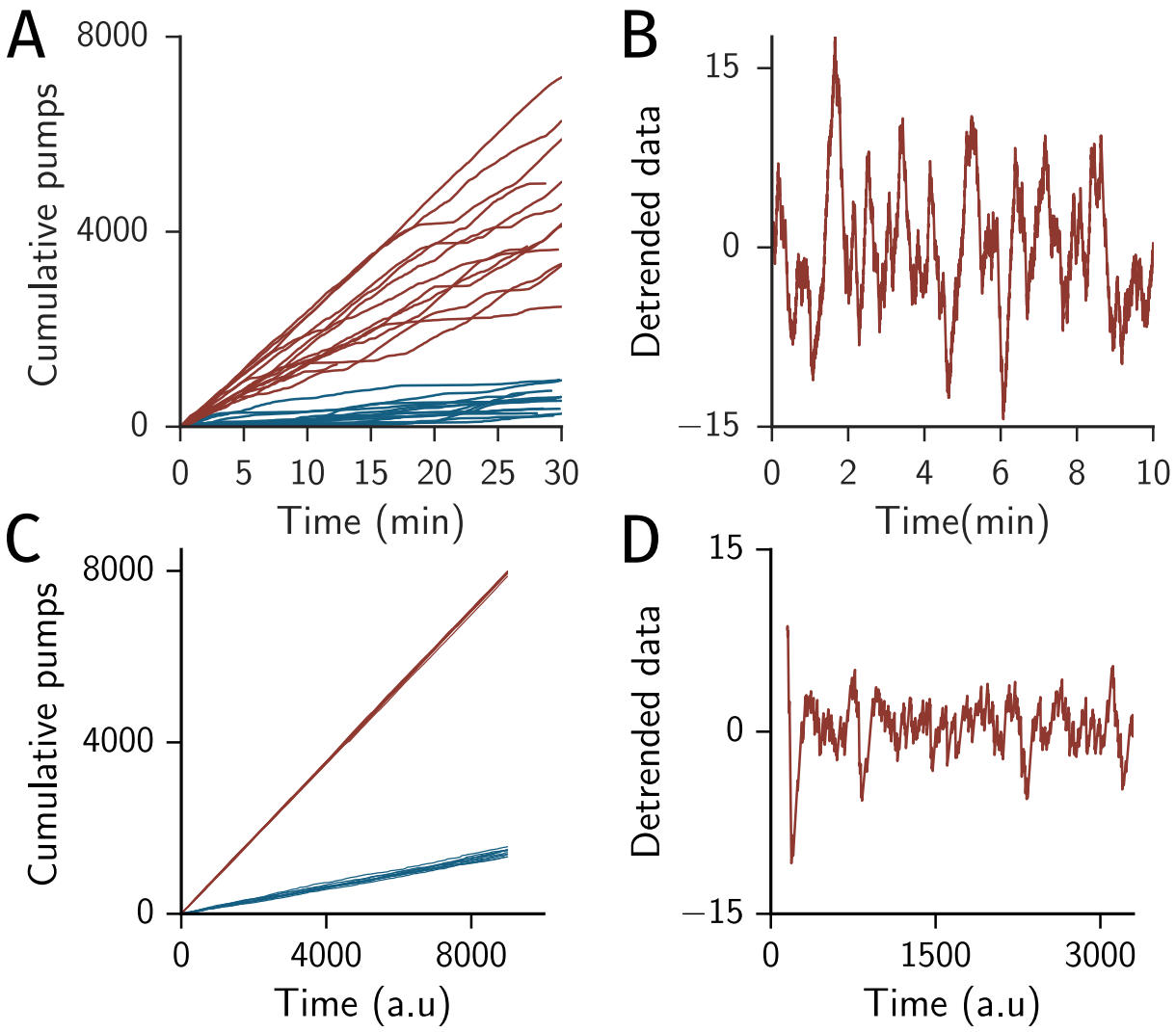

Figure 4.7: **Variability of *C. elegans* feeding.** (A) Cumulative number of pumping events over 30 minutes (OD_{600} = 0 and 4, blue and red, respectively). Individual lines are from individual animals. (B) Example of deviations from the local mean pumping rate as calculated by subtracting a local linear trend with a width of 1 minute from the data shown in (A). (C) Cumulative pumping events as obtained from simulations with standard parameters at 10 and 30 bpp mean food levels, blue and red, respectively. Each condition was simulated 10 times and is shown as individual lines. (D) Example of deviations from the local mean pumping rate, similar to (B), but for simulated trajectories.

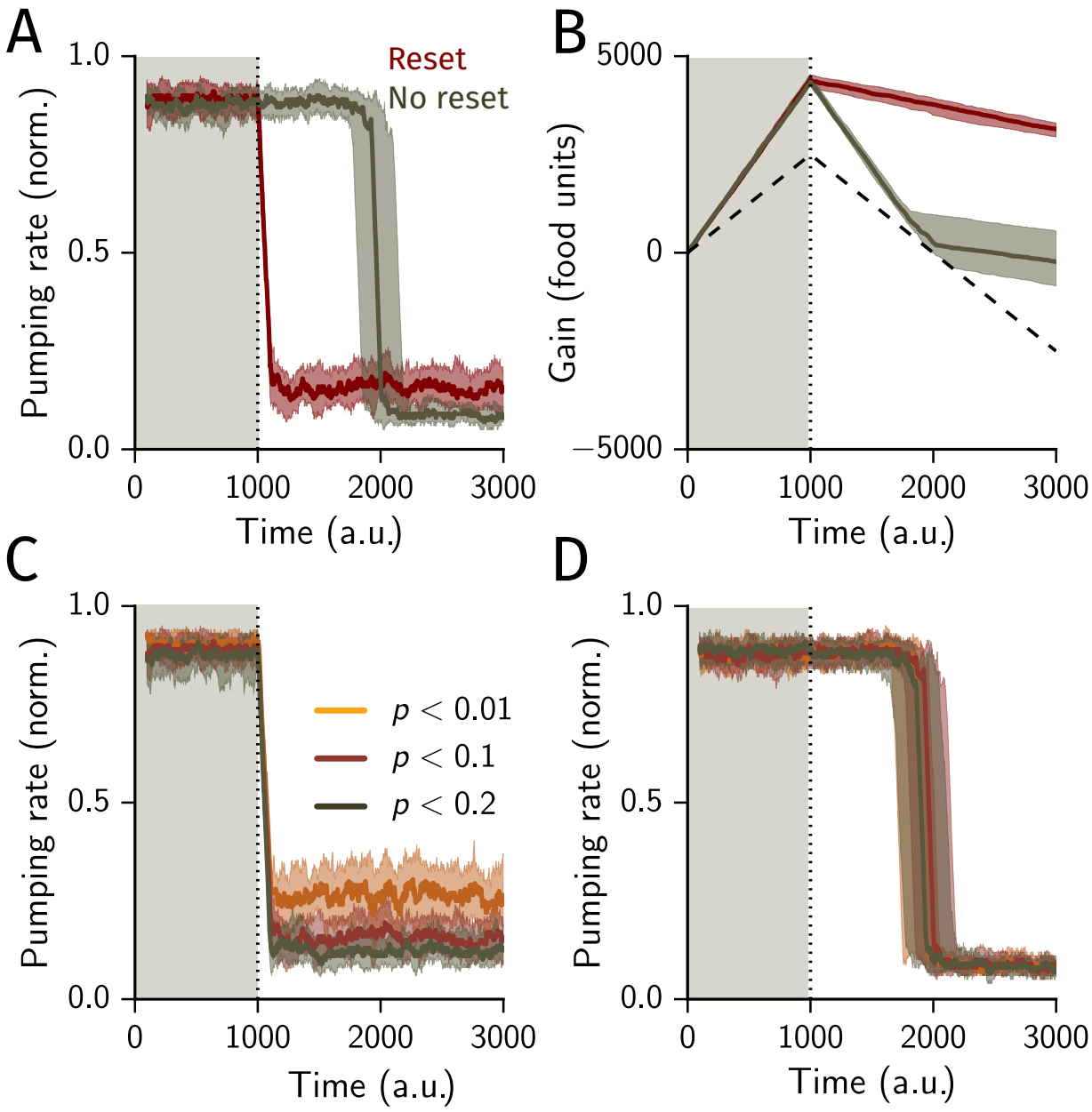

Figure 4.8: **Resetting improves adaptive feeding in a dynamic environment.** (A) Pumping rate in response to a step decrease in mean food level from 20 to 10 units, for a model with and without resetting (red and olive, respectively). The step happens at $t = 1000$ (dashed line and after shading). The shaded area shows the standard deviation as calculated from 30 simulated trials. (B) Cumulative net food intake (gain) over the simulated time. The width of the curve indicates the standard deviation as calculated from 30 simulated trials. A random model with a 50% chance of pumping performs worse (dashed black line).(C) Response of the full model to a step in food level from 10 to 20 units for stringency $p = 0.01, 0.1, 0.2$, yellow, red and olive, respectively. (D) Response of the non-resetting model to a step in food level from 20 to 10 units for stringency $p = 0.01, 0.1, 0.2$, yellow, red and olive, respectively.

CHAPTER 5

CONCLUSION AND FUTURE DIRECTIONS

5.1 Inference of regulatory principles from precise behavioral quantification

Behavior determines how animals interact with the world and each other. Often the most interesting behaviors to an observer are those whose function or implementation are not immediately obvious. For example, how do fish school (Katz et al., 2011)? Or why do some worker ants appear to be lazy (Charbonneau and Dornhaus, 2015)? Despite the advances in molecular biology and cellular neuroscience, to ultimately understand these behaviors requires careful observation and quantification [1]. Inference from behavioral data allows us to define the purpose, regulation and constraints that act on a behavior and shape it. In this thesis I describe how we used precise quantitative measurements to investigate feeding behavior in the nematode *C. elegans*.

In Chapter 2, I presented a new method to quantify feeding behavior. By enabling us to observe the temporal dynamics of feeding over long times, we found a new description of feeding behavior as a burst process. With tight control of environmental parameters, such as food levels, we observed that *C. elegans* adapts its feeding rate to the environmental food concentration. These results contradict the previous notion that feeding behavior is essentially binary, the animal pumps at a maximum rate on food and ceases or reduces pumping when off food. The animals' response to rapidly varying food levels was stochastic, which was an unexpected outcome and indicates a complex level of regulation underlying the response to food. Using these novel tools, we were able to find a quantitative description of feeding behavior.

In the following chapter, we analyzed the effects of sleep deprivation on adult feeding

1. What does it mean to 'understand' a behavior? In the words of Nikolaas Tinbergen, it is an answer to the question: 'What is the causal structure underlying the observed phenomena' (Tinbergen, 1963).

behavior. The method presented in Chapter 2 enabled high-throughput experiments and allowed us to perform a reverse-genetic screen of genes involved in feeding defects following sleep deprivation. We found that mild sleep deprivation causes feeding defects in adult worms. The effects of sleep deprivation are mitigated by a protective pathway which involved the mitochondrial unfolded protein response. By comparing the effects of sleep deprivation between two tissues with different functions, we found that the effects of sleep-deprivation are tissue-specific. Likely, the requirements of the active neuromuscular pump of the pharynx which needs to function with fast, coordinated contractions are distinct from the requirements of the reproductive tissue. It is interesting to note that the pharynx is completely inactivated during sleep, and damage accumulates despite the tissue not being in use at the time of sleep deprivation. We found that the damage is neuronal, indicating that regulatory circuits do play a role in the function of the pharynx and need to be shielded from damage by protective mechanisms. It could also indicate that neuronal remodeling, as observed in the neuron NSM, might be happening during sleep. In this chapter we showed that development and life-history affect feeding behavior later in life.

In Chapter 4 we used the quantitative description of feeding behavior to define a model of feeding behavior. The model describes how the animal uses information gathered from the environment to adapt its feeding behavior to external conditions. We found that the constraints that the data place on potential models can help identify a possible computational mechanism, which describes in general terms how an animal integrates information. The assumptions of the model, namely that the animal acquires information while feeding strongly predict a sensory neuron or circuit in the pharynx that can estimate the amount of food gained per pump. The model performs well under conditions where the animal faces a hard sampling problem; the noise on the incoming information obscures any direct inference about the environment. It also performs well in situations where the food levels change dynamically, and it captures the stochastic response to external conditions observed in the experiments. The model is useful for testing assumptions and making predictions, since it describes the

steps and animal undergoes to make a decision in algorithmic form. It can be generalized to describe more complex decision problems, such as environments with multiple food sources.

5.2 Role of the nervous system in feeding

Inference from behavior can give insight into the regulation of feeding behavior and its essential components. Given the description of feeding, the next step would be to connect the behavioral level to the underlying neuronal computation. The temporal regulation of feeding is complex, and it is responsive to a range of external signals. Previous experiments have only been able to identify a small number of neurons as essential for pumping. The remainder might have a more subtle function that could not be identified by manual counting or electrophysiology. The requirements for adaptive feeding defined in Chapter 4 can serve as a starting point to investigate neuronal regulation. For example, the model requires that the animals are able to sense the amount of food that is ingested in a single pump. Using targeted functional ablation, one could identify the neurons required for this function. Out of the 20 pharyngeal neurons only a small subset have sensory endings, which results in a small list of putative targets. As a proof-of principle, I developed a dual color microscope which can record feeding behavior and the amount of food ingested per bite simultaneously. These experiments could shed light on the type of mechanism that animals use to detect the amount of food present in their environment. Mechanical cues certainly play a role, since these animals do feed on plastic microspheres without any nutritional value or smell. An alternative role for these neurons is the feeding regulation in scenarios we have not been able to recreate in the laboratory. These neurons might function mostly in a sensory and modulatory capacity, thus only becoming relevant in more complex feeding scenarios, with mixtures of bacterial species with varying nutritional values.

5.3 Ecologically relevant feeding

In natural environments, the animal encounters a complex landscape of food levels. The environment varies both spatially and temporally, and contains a variety of bacterial species. Recreating an ecologically relevant landscape in the laboratory requires the development of new tools. In particular, feeding is tightly coupled to foraging, and thus to locomotion. Future studies should observe pumping in freely moving animals, which requires combining a worm tracker with high-resolution imaging of the pharynx. These experiments can build on existing software I developed to measure pumping in microfluidic chips. In particular, given the stochastic nature in which animals respond to rapid switches in the external food concentration, it would be interesting to know their response time when encountering a bacterial lawn.

5.4 Future directions: Linking neuronal activities and behavior

The size and separated nature of the pharynx make it a useful model system to investigate a small neural circuit directly. Many questions in the neuroscience of mammals are investigated by measuring the activity pattern of a small fraction of neurons and inferring the function and computation occurring in a larger group of neurons. With *C. elegans*, we can use the small size of the nervous system to understand the role of a contained regulatory circuit. Recent developments allow observation of about 100 neurons at the same time (the total number of neurons in a *C. elegans* hermaphrodite is 302). The timescale of the behavior (bursts of feeding and pauses occur on the timescale of tens of seconds) makes it amenable to use physiological imaging to observe neuronal behavior. Using optical manipulation (optogenetics) and observing neuronal activity concurrently with feeding behavior (Calcium imaging) allows us to observe the action of a circuit concurrently with its behavioral output. With these tools we could approach neuroscience questions, such as how is information from the body integrated and how does the animal respond to conflicting inputs? What are the

functions of the remaining neurons in the pharynx?

An additional advantage in using *C. elegans* as a model for answering these particular questions is the fact that the 'wiring diagram' is known [2]. However, in *C. elegans* and many other organisms, it has become clear that the connections between neurons are not sufficient to describe the resulting behaviors. Underlying the connectome is a 'shadow' map, where neuromodulators, such as neuropeptides, act to modify the resulting output of the neural network (Bargmann, 2012). This type of signaling can alter the function of a neural circuit completely and dynamically, depending on the presence or absence of such neuromodulators. In the worm, the number of known neuropeptides alone exceeds 100. Having a well-characterized system, such as the pharynx, allows investigation of the role of such neuromodulators. Combining neuronal activity imaging with genetics would allow us to separate the contribution of the synaptic connections versus the humoral connections to feeding behavior.

2. The quality of the connectome is vastly better for the rest of the body, but recently the pharynx connectome has been updated with new electronmicrographs (Bhatla et al., 2015).

APPENDIX A

PIA - PHYSIOLOGICAL IMAGE ANALYSIS TOOLS

A.1 Overview

PIA is a graphical user interface (GUI) intended for tracking and correcting cells imaged using physiological calcium imaging (GCamp). PIA is designed to load image stacks, and assist in automated and/or manual analysis. PIA can track either a single labeled cell or a pair of cells that have a constant relative distance to each other. PIA can also analyze ratiometric images. In that case, two fluorescence channels showing the same object are required. Further requirements for this type of analysis is listed below. The PIA output file contains the location of each tracked object (one or two objects), the brightness, the background level around the object and the area of the object. This program was used for the data analysis in Chapter 3.

PIA has four distinct tracking modes which are

1. Tracking a single object over time (eg. traditional GCamp images)
2. Tracking two objects in the same arrangement (rotation and translation are ok)
3. Tracking an object in two colors and showing ratiometric changes
4. Tracking two objects with ratiometric changes.

PIA can also play a series of images at as a movie and load previous PIA data files and allow the user to manually correct and update the data. The GUI is shown in A.1. The figure illustrates how the interface looks when tracking an object in two colors and calculating ratiometric changes. Ratiometric tracking is particularly useful to reduce the effects of movement in and out of the focal plane and fluctuations in illumination or camera sensitivity. One channel is recorded with the cell labeled with fluorescent molecule which is non-responsive to changes in the cellular environment. The other channel is recorded from a molecule that tracks cellular changes, such as pH or Calcium levels.

A.2 Usage

A.2.1 Object tracking

1. Download or clone the PIA repository

2. Navigate to the PIA directory and start PIA in a python console by typing

   ```
   bash python pia.py
   ```

3. Load an image stack by selecting an image folder. Check that the filetype matches the 'Image data type' set in the GUI. The left panel should show the first image of the stack.

4. Adjust tracking modus and parameters as necessary (see Table below)

5. Click ''Run tracker' and use the mouse to click on the object to be tracked.

6. The program will automatically run through the stack. The data will live update while the tracker is running.

7. Save the result by selecting a new file ('New File') and click 'Write to new file'. Data will only be written if this button is clicked to avoid accidental overwriting!

A.2.2 Correcting existing tracking data

1. Start PIA (see above)

2. Load an existing image stack (point 3. above). The first image of the stack should appear on screen.

3. Set the 'Track Mode' to the correct setting

4. Load an existing PIA data file by selecting 'Data file'. The tracking curves should be displayed in the right window.

5. Navigate to the frame(s) that require manual input by either changing the entry field 'Current index' or clicking on the top data plot.

6. Click on the neuron in the frame. The data entry will be updated.

7. If you need to return to the original data, click 'Reset Data'. This returns to the last saved version of the data.

8. Save the new data either to the existing file by clicking 'Overwrite data' or to a new file following point 7 above.

A.2.3 Input and output

PIA uses matplotlib.image's imread function. Natively, this only supports png images, however, with the help of Pillow, it can also read tif and jpg images. The input images are expected to have a 4-digit timestamp at the end of the filename, eg.,

`img_0001.jpg`

. The output file specifies four parameters for each object: Fluorescence, associated background, location in the image and area. Depending on the tracking mode, it returns this for one or two objects in one or two colors. Note that the GUI displays smoothed overlays and sometimes artificially offsets the output to improve visualization. However, the data that is recorded in the output file are the raw brightness values as obtained from the analysis, and no offset, smoothing or subtraction has been performed.

A.3 Object detection and tracking

A.3.1 Detection

The algorithm identifies the brightest object by thresholding the part of the image in the background box using the 'signal theshold' value (see Table A.1). The all distinct objects

are labeled and the one with the largest brightness is chosen. If the algorithm is tracking two objects, it will also consider the second-brightest object. The object is then masked from the background box by an area of size 'neuron box' and the fluorescence in that area is calculated as the background level. When tracking two objects, the program reports back the vector between the two objects in the coordinate system of the image, to later establish the identity of each object. An illustration of the tracking parameters and the object identification is shown in Fig. B.1.

A.3.2 Tracking

Tracking assumes that the object does not move extremely far within a frame. The size of the background box determines where the algorithm assumes the object will appear again (see Parameter table in Table A.1). The automated tracking algorithm identifies the brightest object in the background box and assumes this is the desired object. The user can also click on or in the vicinity of the object to manually assist tracking. This is particularly useful if the object moved a large distance between frames or if the sample was out of frame for a period of time. However, the exact determination of the objects location will still be performed by the tracking algorithm, which will find the brightest object in the vicinity of the user's clicked location. The following frame will take into account the previous velocity of the tracked object and move the background box in that direction. This usually ensures good tracking for slow-moving objects. For two objects, the vector between the two objects is used to establish identity: The algorithm assumes that the smallest possible rotation of the connecting vector is the likeliest movements the two objects made. This ensures that when the brightness of the two objects varies, the identity does not switch over the course of tracking.

Table A.1: PIA tracking parameters

Parameter	Description	Recommended value
Background box	Determines the search area around a location where an object is expected.	Should be larger than the expected displacement per frame
Neuron box	This area will be masked for the background calculation and should cover the entire fluroescent object	Approximately the size of the object and any halo that might appear around it
Signal threshold	In percent pixel of the background box, this determines the threshold that separates object and background.	The percentile value of brightness i.e., signal threshold = 95% all pixels with the 5% highest brightness levels are part of the object
Dual color shift	Dual color(ratiometric) imaging offset	calculate the shift between the two channels, should be constant for a given movie and a microscope setup

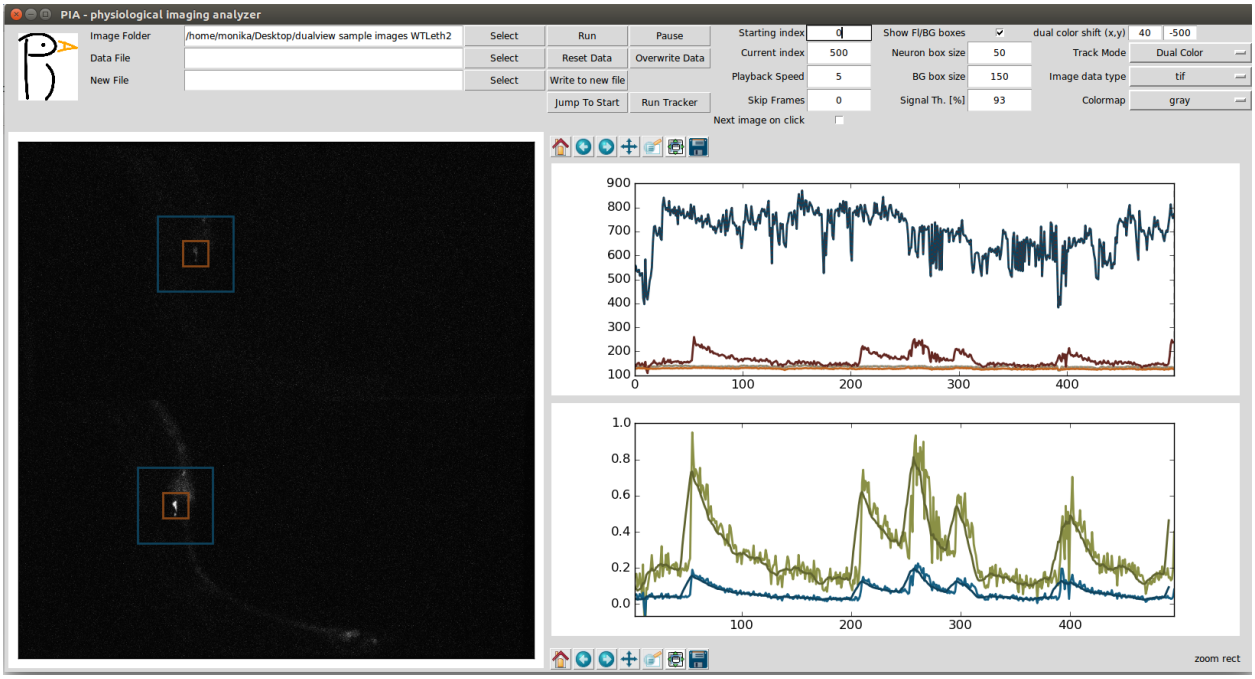

Figure A.1: **The interface during tracking of an object in ratiometric mode.** The graphical user interface for PIA shows the current frame and the analyzed data. The user can adjust parameters, load and save data, manually aid object identification and run an automated tracker. The current frame of the image stack is shown in the left panel. The top half of the image shows the fluorescence from GCamp, and the bottom half the RFP fluorescence. The ratio of the two fluorescence level is a measure of the activity of the cell, in this case a neuron. The right upper panel shows the fluorescence level of the tracked object in either channel. The top curves are the raw fluorescence values for GCamp and RFP (red and blue, respectively). The two bottom curves show the respective background levels around the objects (orange and green). The RFP channel is noticably brighter, which correspondingly shows up as higher fluorescence values in the data (blue). The background is small and shows up as flat curves in the bottom. The lower panel on the right shows the ratiometric values calculated as the background-subtracted ratio between the fluorescence levels in each channel $R = (F_{GCamp} - Bg_{GCamp})/(F_{RFP} - Bg_{RFP})$ (green).

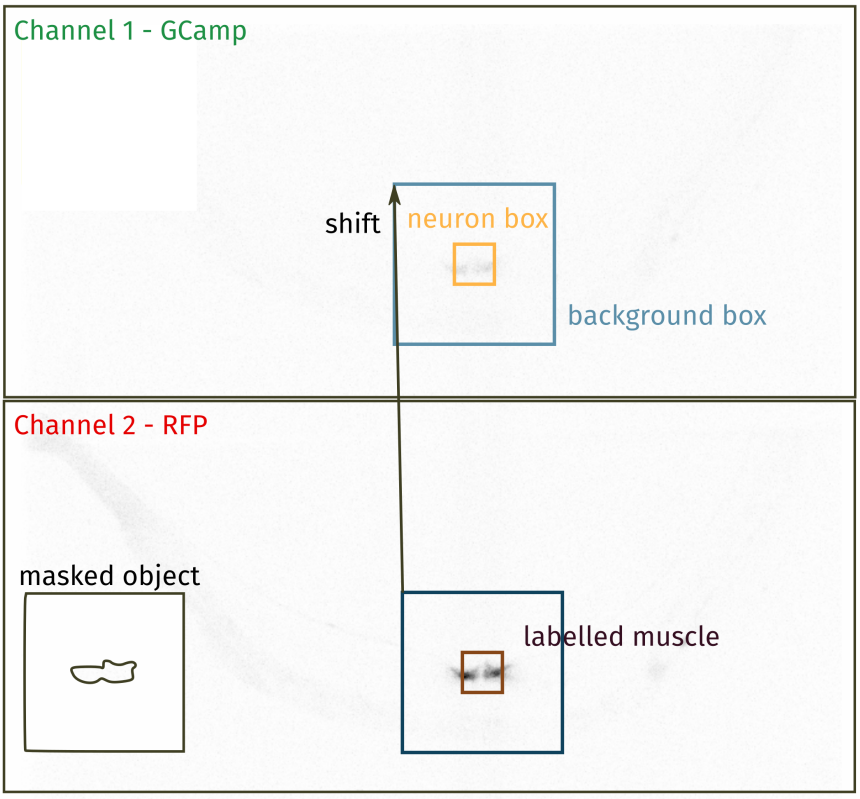

Figure A.2: **Illustration of ratiometric tracking with PIA.** PIA tracks objects that were recorded in two fluorescence channels. Here, a *C. elegans* vulva muscle is labeled in RFP and GCamp. The object is tracked in the RFP channel, which is expected to have constant fluorescence. GCamp responds to changes in Calcium levels in a cell by changing fluorescence, and therefore can track cellular activity. The neuron in the GCamp channel is found by adding a constant offset (shift) to the object in the RFP channel. The inset shows the shape of the detected muscles. Brightness and area of this object is calculated for each channel.

APPENDIX B

A FAST DUAL-COLOR MICROSCOPE FOR BEHAVIORAL IMAGING

B.1 Monitoring feeding dynamics and food intake simultaneously

The model of adaptive feeding described in Chapter 4 predicts that the pumping rate will correlate with the amount of food ingested immediately prior to initiating a burst of feeding. To test this prediction and its dependence on the concentration of food, it would be helpful to observe the food intake per bite concurrently with the feeding behavior. To this end, I developed a modified version of our imaging setup that can acquire both behavioral and food level data simultaneously and at high frame rates. Here, I describe the setup in more detail.

The goal is to simultaneously record brightfield and fluorescence images at fast (>50 Hz) frame rates for each channel. (A particular application is recording fast muscular contractions and a fluorescent marker). With LEDs, instead of using a shutter, one can rapidly flicker the LED on and off to quickly change illumination. Simultaneously triggering the camera allows recording the two frames at maximum speed. The speed is limited by the read-out speed of the camera and illumination requirements. In this setup, we use a red LED to illuminate the brightfield image, a green LED to excite red fluorescence and a long-pass filter to discriminate excitation and emission wavelengths. The long-pass filter creates the following effect:

During red illumination, all light passes through the sample and into the filter. The wavelength of 620 nm exceeds the cutoff wavelength of the filter, such that all light passes through. The image is created by the different absorption in the sample, which creates a so-called brightfield image. When the sample is illuminated with green light, the light passes through the sample and excites red fluorescent molecules. The excitation wavelength is blocked by the filter, such that only the emission (red light) can continue to the camera. This creates a fluorescence image.

B.1.1 Setup

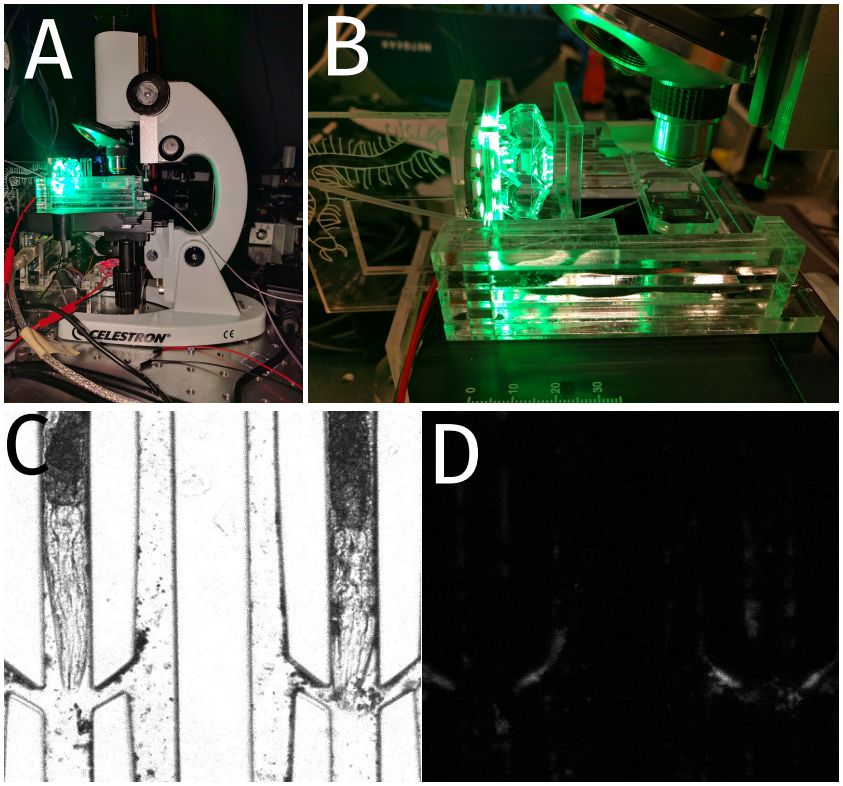

Figure B.1: **Dual color high-speed microscope.** (A) The microscope with both light-sources (red and green) switched on. (B) The sample is illuminated from the side with the green LED, creating an orthoginal lightpath to the red light source. The LEd is mounted in a custom acrylic holder. (C) Example image showing two *C. elegans* animals in the microfluidic chip. The nominal exposure time was 8 ms. (D) Fluorescence image corresponding to (C). The exposure is 8 ms, the gain of the camera was set to 25 and the image was binned (2 by 2 binning).

A basic microscope is modified with custom 3D-printed or lasercut fittings for the camera, LEDs and filter, a micro -controller and a camera. The red light source is placed below the stage to illuminate the sample from below. The green light source is placed orthogonal to the sample-camera axis. Since the longpass-filter is not perfect (0.01% transmission in the forbidden region), we need to arrange the excitation light at an angle to the camera. Otherwise, the small amount of transmitted light creates a 'shadow' brightfield image in the fluorescence channel. The camera is triggered in sync with the color-switches in the light

source, such that each frame is illuminated by exactly one color.

B.1.2 Required components

1. Arduino Uno R3 ($24.95)
2. High Flex 6 Pin Hirose Female HR10A-7P-6S Cable for Basler GIGE AVT CCD Camera ($39.99)
3. Adafruit NeoPixel NeoMatrix 8x8 - 64 RGB LED Pixel Matrix ($34.95)
4. Long Pass Filter, Cut-On Wavelength: 600 nm (eg. Thorlabs FEL0600, $73)
5. Basler camera eg. acA640-120um ($400+)
6. Breadboard-friendly 2.1 mm DC barrel jack
7. 330 Ohm resistor
8. a few breadboard-pin wires to connect to Arduino

B.1.3 Preliminary results

We imaged animals in the WormSpa microfluidic chip, as described in Chapter 2. Instead of a bacterial suspension, the animals experienced a slow flow of buffer with micron-sized polystyrene beads [1]. The beads are conjugated with a fluorescent tag with an emission maximum at 605 nm. Data was recorded with the dual-color LED scope at 100 Hz (50 Hz per channel). The data was analyzed by aligning the images in the vertical direction and calculating the fluorescence intensity in the intestine, the terminal bulb and the pharyngeal lumen. Our preliminary data indicates that beads are ingested by the animals and we can observe fluorescence levels in different parts of the animal. It is promising to see that the animals enter long pumping bursts at this bead concentration, indicating normal pumping

1. FluoSpheres Polystyrene Microspheres, 1.0 μm

behavior despite the artificial food source (Fig. B.2A). After the second burst of pumping, the accumulated food can be detected as an increase in the mean fluorescence in the bulb and in the pharynx (Fig. B.2B). Further analysis of such data sets will elucidate how food intake and behavior are coupled.

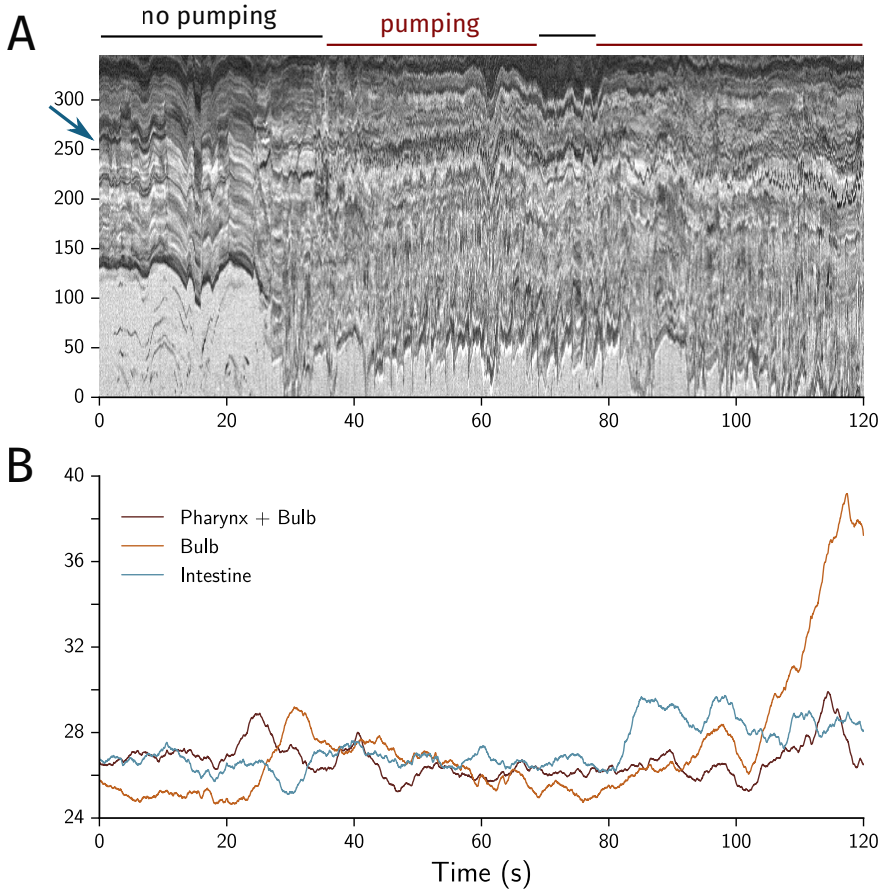

Figure B.2: **Simultaneous imaging of pumping and particle intake.** Example of an animal pumping in a solution of fluorescently-labeled polystyrene beads (1 μm diameter). (A) Kymograph showing the pumping behavior of the animal. The arrow denotes the location of the terminal bulb. The behavior was annotated manually from the kymograph. (B) Average fluorescence in different parts of the pharynx and intestine as quantified from the corresponding fluorescence images. The curves are smoothed with a Gaussian filter of width 4 seconds.

B.1.4 Issues and comments

At fast framerates the exposure time is limited by the frame rate. This leads to very low signals in the fluorescence channel. There are two solutions: A more expensive, dedicated camera for fluorescence applications with a high quantum efficiency at 600 nm, or to change the recording pattern from alternating frames to a series of fast brightfield frames followed by a longer-exposure fluorescence frame. The feasibility of this approach depends on the desired application.

Variable exposure times can arise from the LED internal clock. The Adafruit Neopixel LEDs have an internal clock that runs at 2 ms. If the light-switch data comes in during the 'off' cycle of the LED, there will be a delay in the switch by (at most) 2 ms. Considering that the exposure time at 60Hz is 8 ms (60 Hz in each channel which corresponds to 16 ms for two frames), this presents a significant change in total illumination. The problem can be solved by using faster-clocking LEDs, or it can be improved in the analysis by performing histogram equalization on the images.

APPENDIX C

RNA SEQUENCING OF THE WHOLE ANIMAL

The results presented in Chapter 3 implicate the stress-activated transcription factor DAF-16/FoxO in mitigating the effects of sleep deprivation. DAF-16/FoxO has been studied extensively and targets of the transcription factor have been found under a variety of conditions (Libina et al., 2003). To test whether we can identify differentially-expressed genes in *C. elegans* after sleep deprivation, we sequenced RNA extracted from whole animals. Animals were sleep-deprived according to the method described in Chapter 3. The control animals were treated with vibrations outside of lethargus, to separate the effects of the vibrations and sleep-specific effects. The RNA extraction was then performed using the protocol below. Due to the small sample size, the protocol needed to be optimized to reduce the loss of sample [1].

C.1 Materials

1. M9 or LNGM
2. Trizol
3. chloroform
4. RNAse free glycogen (5mg/ml stock, Ambion)
5. 2-propanol
6. 70% ethanol
7. RNAse free H_2O
8. Arcturus PicoPure RNA kit or Zymo RNA Clean & Concentrator-5

1. This protocol has been optimized for whole animal RNA extraction in adult *C. elegans* with the help of Dan Dominissini.

C.2 Protocol

C.2.1 Wash sample

1. Pick 20 worms in 100ul of M9 in an RNAse free Eppendorf tube.

C.2.2 Homogenization

1. Add 300 ul of Trizol.
2. Vortex for 30 sec by hand.
3. Vortex at 4 for 20 min or *freeze / thaw multiple times on dry ice and thaw in 37 and vortex between cycles.*
4. **Sample can be frozen at -80 until ready to proceed**.
    - For large samples: let sit at RT for 10 min.
    - Spin at 12,000 x g for 10 min at 4 .
    - The resulting pellet contains ECM, polysaccharides, and high molecular weight DNA, while the supernatant contains the RNA. In high fat content samples, a layer of fat collects above the supernatant.
    - Transfer the clear supernatant to a new tube.

C.2.3 Phase separation

1. Add 80 ul of chloroform.
2. Mix by shaking vigorously for 15 sec.
3. Add to phase-lock column.
4. Centrifuge at 12,000 x g for 15 min at 4 .
5. Remove the aqueous phase (clear to layer), roughly 225 ul to a new tube.

C.2.4 Zymo kit

1. Add 2 volumes RNA Binding Buffer to the sample (eg. 225 ul sample + 450 ul RNA binding buffer)

2. Add an equal volume EtOH to the sample (eg. 675 ul sample + 675 ul EtOH)

3. Transfer the mix to a column and collection tube and spin 30 sec. Don't load more than 800 ul at a time. If the total volume exceeds 800 ul, repeat the load and spin until all the sample is added.

4. Add 400 ul RNA Prep Buffer to the column and centrifuge for 30 seconds. Discard the flow-through.

5. Add 700 ul RNA Wash Buffer to the column and centrifuge for 30 seconds. Discard the flow-through.

6. Add 400 ul RNA Wash Buffer to the column and centrifuge for 2 minutes to ensure complete removal of the wash buffer. Transfer the column carefully into an RNasefree tube.

7. Add 14 ul DNase/RNase-Free Water directly to the column matrix and centrifuge for 30 seconds.

REFERENCES

Alejandro Aballay and Frederick M Ausubel. Programmed cell death mediated by ced-3 and ced-4 protects *Caenorhabditis elegans* from salmonella typhimurium-mediated killing. *Proceedings of the National Academy of Sciences*, 98(5):2735–2739, 2001.

A. Albeg, C. J. Smith, M. Chatzigeorgiou, D. G. Feitelson, D. H. Hall, W. R. Schafer, D. M. Miller, and M. Treinin. *C. elegans* multi-dendritic sensory neurons: morphology and function. *Mol Cell Neurosci*, 46:308–317, 2011. doi: 10.1016/j.mcn.2010.10.001. URL `http://dx.doi.org/10.1016/j.mcn.2010.10.001`.

Donna G Albertson and JN Thomson. The pharynx of *Caenorhabditis elegans*. *Philosophical Transactions of the Royal Society of London B: Biological Sciences*, 275(938):299–325, 1976.

Dirk R Albrecht and Cornelia I Bargmann. High-content behavioral analysis of *Caenorhabditis elegans* in precise spatiotemporal chemical environments. *Nature methods*, 8(7):599–605, 2011.

Paula Alhola and Päivi Polo-Kantola. Sleep deprivation: Impact on cognitive performance. *Neuropsychiatric disease and treatment*, 3(5):553, 2007.

Arno Alpi, Pawel Pasierbek, Anton Gartner, and Josef Loidl. Genetic and cytological characterization of the recombination protein rad-51 in *Caenorhabditis elegans*. *Chromosoma*, 112(1):6–16, 2003.

Tathiana A Alvarenga, Camila Hirotsu, Renata Mazaro-Costa, Sergio Tufik, and Monica L Andersen. Impairment of male reproductive function after sleep deprivation. *Fertility and sterility*, 103(5):1355–1362, 2015.

Victor Ambros. A hierarchy of regulatory genes controls a larva-to-adult developmental switch in *C. elegans*. *Cell*, 57(1):49–57, 1989.

Ron C Anafi, Renata Pellegrino, Keith R Shockley, Micah Romer, Sergio Tufik, and Allan I Pack. Sleep is not just for the brain: transcriptional responses to sleep in peripheral tissues. *BMC genomics*, 14(1):1, 2013.

R. J. Audley and A. R. Pike. Some Alternative Stochastic Models of Choice1. *British Journal of Mathematical and Statistical Psychology*, 18(2):207–225, November 1965. ISSN 2044-8317. doi: 10.1111/j.2044-8317.1965.tb00342.x. URL `http://onlinelibrary.wiley.com.ezp-prod1.hul.harvard.edu/doi/10.1111/j.2044-8317.1965.tb00342.x/abstract`.

L Avery and YJ You. *C. elegans* feeding (May 21, 2012), WormBook, ed. The *C. elegans* Research Community, WormBook, doi/10.1895/wormbook. 1.150. 1, 2012.

Leon Avery. The genetics of feeding in *Caenorhabditis elegans*. *Genetics*, 133(4):897–917, 1993a.

Leon Avery. Motor neuron M3 controls pharyngeal muscle relaxation timing in *Caenorhabditis elegans*. *J. Exp. Biol.*, 175(1):283–297, 1993b.

Leon Avery and H Robert Horvitz. A cell that dies during wild-type *C. elegans* development can function as a neuron in a *ced-3* mutant. *Cell*, 51(6):1071–1078, 1987.

Leon Avery and H Robert Horvitzt. Pharyngeal pumping continues after laser killing of the pharyngeal nervous system of *C. elegans*. *Neuron*, 3(4):473–485, 1989.

Leon Avery and Boris B Shtonda. Food transport in the *C. elegans* pharynx. *Journal of Experimental Biology*, 206(14):2441–2457, 2003a.

Leon Avery and Boris B. Shtonda. Food transport in the C. elegans pharynx. *Journal of Experimental Biology*, 206(14):2441–2457, July 2003b. ISSN 0022-0949, 1477-9145. doi: 10.1242/jeb.00433. URL `http://jeb.biologists.org/content/206/14/2441`.

Leon Avery and James H Thomas. 24 Feeding and Defecation. *Cold Spring Harbor Monograph Archive*, 33:679–716, 1997.

Claes Axäng, Manish Rauthan, David H Hall, and Marc Pilon. Developmental genetics of the *C. elegans* pharyngeal neurons nsml and nsmr. *BMC Developmental Biology*, 8(1):38, 2008.

Mohammad A Abu Baker and Joel S Brown. Foraging in space and time structure an African small mammal community. *Oecologia*, 175(2):521–535, 2014.

David L Barack and Joshua I Gold. Temporal trade-offs in psychophysics. *Current Opinion in Neurobiology*, 37:121–125, April 2016. ISSN 0959-4388. doi: 10.1016/j.conb.2016.01.015. URL `http://www.sciencedirect.com/science/article/pii/S0959438816300010`.

Cornelia I Bargmann. Beyond the connectome: how neuromodulators shape neural circuits. *Bioessays*, 34(6):458–465, 2012.

Timothy EJ Behrens, Mark W Woolrich, Mark E Walton, and Matthew FS Rushworth. Learning the value of information in an uncertain world. *Nature Neuroscience*, 10(9): 1214–1221, 2007.

Daniel W Belsky, Terrie E Moffitt, Karen Sugden, Benjamin Williams, Renate Houts, Jeanette McCarthy, and Avshalom Caspi. Development and evaluation of a genetic risk score for obesity. *Biodemography and social biology*, 59(1):85–100, 2013.

Adela Ben-Yakar, Nikos Chronis, and Hang Lu. Microfluidics for the analysis of behavior, nerve regeneration, and neural cell biology in *C. elegans*. *Current Opinion in Neurobiology*, 19(5):561–567, 2009.

Cristina Benedetti, Cole M Haynes, Yun Yang, Heather P Harding, and David Ron. Ubiquitin-like protein 5 positively regulates chaperone gene expression in the mitochondrial unfolded protein response. *Genetics*, 174(1):229–239, 2006.

Nikhil Bhatla, Rita Droste, Steven R Sando, Anne Huang, and H Robert Horvitz. Distinct neural circuits control rhythm inhibition and spitting by the myogenic pharynx of *C. elegans*. *Current Biology*, 25(16):2075–2089, 2015.

Rafal Bogacz, Eric Brown, Jeff Moehlis, Philip Holmes, and Jonathan D. Cohen. The physics of optimal decision making: A formal analysis of models of performance in two-alternative forced-choice tasks. *Psychological Review*, 113(4):700–765, 2006. ISSN 1939-1471, 0033-295X. doi: 10.1037/0033-295X.113.4.700. URL `http://doi.apa.org/getdoi.cfm?doi=10.1037/0033-295X.113.4.700`.

Rafal Bogacz, Eric-Jan Wagenmakers, Birte U. Forstmann, and Sander Nieuwenhuis. The neural basis of the speed–accuracy tradeoff. *Trends in Neurosciences*, 33(1):10–16, January 2010. ISSN 0166-2236, 1878-108X. doi: 10.1016/j.tins.2009.09.002. URL `http://www.cell.com/trends/neurosciences/abstract/S0166-2236(09)00155-6`.

L Byerly, RC Cassada, and RL Russell. The life cycle of the nematode *Caenorhabditis elegans*: I. wild-type growth and reproduction. *Developmental biology*, 51(1):23–33, 1976.

Marcella Calfon, Huiqing Zeng, Fumihiko Urano, Jeffery H Till, Stevan R Hubbard, Heather P Harding, Scott G Clark, and David Ron. Ire1 couples endoplasmic reticulum load to secretory capacity by processing the xbp-1 mrna. *Nature*, 415(6867):92–96, 2002.

Adam J. Calhoun, Sreekanth H. Chalasani, and Tatyana O. Sharpee. Maximally informative foraging by Caenorhabditis elegans. *eLife*, 3:e04220, December 2014. ISSN 2050-084X. doi: 10.7554/eLife.04220. URL `http://elifesciences.org/content/3/e04220`.

Filipa Carvalhal Marques, Yuli Volovik, and Ehud Cohen. The roles of cellular and organismal aging in the development of late-onset maladies. *Annual Review of Pathology: Mechanisms of Disease*, 10:1–23, 2015.

Antonio Celani and Massimo Vergassola. Bacterial strategies for chemotaxis response. *Proceedings of the National Academy of Sciences*, 107(4):1391–1396, January 2010. ISSN 0027-8424, 1091-6490. doi: 10.1073/pnas.0909673107. URL `http://www.pnas.org/content/107/4/1391`.

Daniel Charbonneau and Anna Dornhaus. Workers 'specialized' on inactivity: Behavioral consistency of inactive workers and their role in task allocation. *Behavioral ecology and sociobiology*, 69(9):1459–1472, 2015.

Michael WL Chee and Lisa YM Chuah. Functional neuroimaging insights into how sleep and sleep deprivation affect memory and cognition. *Current opinion in neurology*, 21(4):417–423, 2008.

Lars Chittka, Peter Skorupski, and Nigel E. Raine. Speed–accuracy tradeoffs in animal decision making. *Trends in Ecology & Evolution*, 24(7):400–407, July 2009. ISSN 0169-5347. doi: 10.1016/j.tree.2009.02.010. URL `http://www.sciencedirect.com/science/article/pii/S0169534709001220`.

Julie Y Cho and Paul W Sternberg. Multilevel modulation of a sensory motor circuit during *C. elegans* sleep and arousal. *Cell*, 156(1):249–260, 2014.

L Churchill, DM Rector, K Yasuda, C Fix, MJ Rojas, T Yasuda, and JM Krueger. Tumor necrosis factor α: activity dependent expression and promotion of cortical column sleep in rats. *Neuroscience*, 156(1):71–80, 2008.

Chiara Cirelli. Cellular consequences of sleep deprivation in the brain. *Sleep medicine reviews*, 10(5):307–321, 2006.

Chiara Cirelli. The genetic and molecular regulation of sleep: from fruit flies to humans. *Nature Reviews Neuroscience*, 10(8):549–560, 2009.

Chiara Cirelli and Giulio Tononi. Gene expression in the brain across the sleep–waking cycle. *Brain research*, 885(2):303–321, 2000.

Chiara Cirelli, Paul J Shaw, Allan Rechtschaffen, and Giulio Tononi. No evidence of brain cell degeneration after long-term sleep deprivation in rats. *Brain research*, 840(1):184–193, 1999.

Chiara Cirelli, Christina M Gutierrez, and Giulio Tononi. Extensive and divergent effects of sleep and wakefulness on brain gene expression. *Neuron*, 41(1):35–43, 2004.

Chiara Cirelli, Timothy M LaVaute, and Giulio Tononi. Sleep and wakefulness modulate gene expression in drosophila. *Journal of neurochemistry*, 94(5):1411–1419, 2005.

Diana Clausznitzer, Gabriele Micali, Silke Neumann, Victor Sourjik, and Robert G. Endres. Predicting Chemical Environments of Bacteria from Receptor Signaling. *PLoS Computational Biology*, 10(10):e1003870, October 2014. ISSN 1553-7358. doi: 10.1371/journal.pcbi.1003870. URL `http://dx.plos.org/10.1371/journal.pcbi.1003870`.

Jonathan D. Cohen, Samuel M. McClure, and Angela J. Yu. Should I stay or should I go? How the human brain manages the trade-off between exploitation and exploration. *Philosophical Transactions of the Royal Society of London B: Biological Sciences*, 362 (1481):933–942, May 2007. ISSN 0962-8436, 1471-2970. doi: 10.1098/rstb.2007.2098.

Kevin M Collins and Michael R Koelle. Postsynaptic erg potassium channels limit muscle excitability to allow distinct egg-laying behavior states in *Caenorhabditis elegans*. *Journal of Neuroscience*, 33(2):761–775, 2013.

Kevin M Collins, Addys Bode, Robert W Fernandez, Jessica E Tanis, Jacob C Brewer, Matthew S Creamer, and Michael R Koelle. Activity of the *C. elegans* egg-laying behavior circuit is controlled by competing activation and feedback inhibition. *eLife*, 5:e21126, 2016.

Ricki J Colman, Rozalyn M Anderson, Sterling C Johnson, Erik K Kastman, Kristopher J Kosmatka, T Mark Beasley, David B Allison, Christina Cruzen, Heather A Simmons, Joseph W Kemnitz, et al. Caloric restriction delays disease onset and mortality in rhesus monkeys. *Science*, 325(5937):201–204, 2009.

Barbara Conradt and H Robert Horvitz. The *C. elegans* protein egl-1 is required for programmed cell death and interacts with the bcl-2–like protein ced-9. *Cell*, 93(4):519–529, 1998.

Serge Dernovici, Tanja Starc, Joseph A Dent, and Paula Ribeiro. The serotonin receptor ser-1 (5ht2ce) contributes to the regulation of locomotion in *Caenorhabditis elegans*. *Developmental neurobiology*, 67(2):189–204, 2007.

Robert J Driver, Annesia L Lamb, Abraham J Wyner, and David M Raizen. Daf-16/foxo regulates homeostasis of essential sleep-like behavior during larval transitions in *C. elegans*. *Current Biology*, 23(6):501–506, 2013a.

Robert J Driver, Annesia L Lamb, Abraham J Wyner, and David M Raizen. Daf-16/foxo regulates homeostasis of essential sleep-like behavior during larval transitions in *C. elegans*. *Current Biology*, 23(6):501–506, 2013b.

Christophe Dupre and Rafael Yuste. Non-overlapping neural networks in *Hydra vulgaris*. *Current Biology*, 2017.

William M Durham, Eric Climent, Michael Barry, Filippo De Lillo, Guido Boffetta, Massimo Cencini, and Roman Stocker. Turbulence drives microscale patches of motile phytoplankton. *Nature Communications*, 4:2148 EP–, 2013.

Markus Dworak, Robert W McCarley, Tae Kim, Anna V Kalinchuk, and Radhika Basheer. Sleep and brain energy levels: Atp changes during sleep. *The Journal of Neuroscience*, 30 (26):9007–9016, 2010.

Hilary M Ellis and H Robert Horvitz. Genetic control of programmed cell death in the nematode *C. elegans*. *Cell*, 44(6):817–829, 1986.

Carol A Everson, Marcia A Gilliland, Clete A Kushida, June J Pilcher, VS Fang, S Refetoff, BM Bergmann, and A Rechtschaffen. Sleep deprivation in the rat: Ix. recovery. *Sleep*, 12 (1):60–67, 1989.

Christopher Fang-Yen, Leon Avery, and Aravinthan D. T. Samuel. Two size-selective mechanisms specifically trap bacteria-sized food particles in Caenorhabditis elegans. *Proceedings of the National Academy of Sciences*, 106(47):20093 –20096, November 2009a. doi: 10.1073/pnas.0904036106. URL `http://www.pnas.org/content/106/47/20093.abstract`.

Christopher Fang-Yen, Leon Avery, and Aravinthan DT Samuel. Two size-selective mechanisms specifically trap bacteria-sized food particles in *Caenorhabditis elegans*. *Proceedings of the National Academy of Sciences*, 106(47):20093–20096, 2009b.

Marie-Anne Félix and Christian Braendle. The natural history of *Caenorhabditis elegans*. *Current Biology*, 20(22):R965–R969, 2010.

Luigi Fontana, Linda Partridge, and Valter D Longo. Extending healthy life spanâĂŤfrom yeast to humans. *Science*, 328(5976):321–326, 2010.

Anton Gartner, Stuart Milstein, Shawn Ahmed, Jonathan Hodgkin, and Michael O Hengartner. A conserved checkpoint pathway mediates dna damage–induced apoptosis and cell cycle arrest in *C. elegans*. *Molecular cell*, 5(3):435–443, 2000.

Anton Gartner, Peter R Boag, T Keith Blackwell, et al. Germline survival and apoptosis. *WormBook*, 4:1–20, 2008.

Julia B George-Raizen, Keith R Shockley, Nicholas F Trojanowski, Annesia L Lamb, and David M Raizen. Dynamically-expressed prion-like proteins form a cuticle in the pharynx of *Caenorhabditis elegans*. *Biology open*, page BIO20147500, 2014.

Joshua I. Gold and Michael N. Shadlen. The Neural Basis of Decision Making. *Annual Review of Neuroscience*, 30(1):535–574, 2007. doi: 10.1146/annurev.neuro.29.051605.113038. URL `http://dx.doi.org/10.1146/annurev.neuro.29.051605.113038`.

Anupama Gopalakrishnan, L Li Ji, and Chiara Cirelli. Sleep deprivation and cellular responses to oxidative stress. *SLEEP-NEW YORK THEN WESTCHESTER-*, 27(1):27–35, 2004.

Roberta A Gottlieb and Aleksandr Stotland. Mitotimer: a novel protein for monitoring mitochondrial turnover in the heart. *Journal of Molecular Medicine*, 93(3):271–278, 2015.

Joshua S. Greene, Maximillian Brown, May Dobosiewicz, Itzel G. Ishida, Evan Z. Macosko, Xinxing Zhang, Rebecca A. Butcher, Devin J. Cline, Patrick T. McGrath, and Cornelia I. Bargmann. Balancing selection shapes density-dependent foraging behaviour. *Nature*, 539(7628):254–258, November 2016. ISSN 0028-0836. doi: 10.1038/nature19848. URL `http://www.nature.com/nature/journal/v539/n7628/full/nature19848.html`.

Ann C Halbower, Mahaveer Degaonkar, Peter B Barker, Christopher J Earley, Carole L Marcus, Philip L Smith, M Cristine Prahme, and E Mark Mahone. Childhood obstructive sleep apnea associates with neuropsychological deficits and neuronal brain injury. *PLoS Med*, 3(8):e301, 2006.

Jason CG Halford, Emma J Boyland, John E Blundell, Tim C Kirkham, and Joanne A Harrold. Pharmacological management of appetite expression in obesity. *Nature Reviews Endocrinology*, 6(5):255–269, 2010.

Jody M Hansen, Daniela R Chavez, and Gillian M Stanfield. Comp-1 promotes competitive advantage of nematode sperm. *Elife*, 4:e05423, 2015.

D Grahame Hardie, Simon A Hawley, and John W Scott. Amp-activated protein kinase–development of the energy sensor concept. *The Journal of physiology*, 574(1):7–15, 2006.

Yvonne Harrison and James A Horne. The impact of sleep deprivation on decision making: a review. *Journal of experimental psychology: Applied*, 6(3):236, 2000.

Kylie A Haskins, Jonathan F Russell, Nathan Gaddis, Holly K Dressman, and Alejandro Aballay. Unfolded protein response genes regulated by ced-1 are required for *Caenorhabditis elegans* innate immunity. *Developmental cell*, 15(1):87–97, 2008.

Cole M Haynes and David Ron. The mitochondrial upr–protecting organelle protein homeostasis. *J Cell Sci*, 123(22):3849–3855, 2010.

Cole M Haynes, Kseniya Petrova, Cristina Benedetti, Yun Yang, and David Ron. Clpp mediates activation of a mitochondrial unfolded protein response in *C. elegans*. *Developmental cell*, 13(4):467–480, 2007.

Michael O Hengartner, Ronald E Ellis, and H Robert Horvitz. *Caenorhabditis elegans* gene *ced-9* protects cells from programmed cell death. *Nature*, 356(6369):494, 1992.

Mark FP Heschl and David L Baillie. The hsp70 multigene family of *Caenorhabditis elegans*. *Comparative Biochemistry and Physiology Part B: Comparative Biochemistry*, 96(4):633–637, 1990.

James O. Hill and John C. Peters. Environmental Contributions to the Obesity Epidemic. *Science*, 280(5368):1371–1374, May 1998. ISSN 0036-8075, 1095-9203. doi: 10.1126/science.280.5368.1371. URL `http://science.sciencemag.org.ezp-prod1.hul.harvard.edu/content/280/5368/1371`.

Joshua B Hincks, Billyann B Monrean, Brianna Lu, Barbara E Taylor, Karsten Hueffer, and Michael B Harris. Screening Bioactivity of Virus Surface Glycoprotein Peptides using *C. elegans* Electropharyngiogram. *The FASEB Journal*, 30(1 Supplement):969–2, 2016.

Robert J Hobson, Jinming Geng, Anjali D Gray, and Richard W Komuniecki. Ser-7b, a constitutively active gαs coupled 5-ht7-like receptor expressed in the *Caenorhabditis elegans* m4 pharyngeal motorneuron. *Journal of neurochemistry*, 87(1):22–29, 2003.

Robert J Hobson, Vera M Hapiak, Hong Xiao, Kara L Buehrer, Patricia R Komuniecki, and Richard W Komuniecki. SER-7, a *Caenorhabditis elegans* 5-HT7-like receptor, is essential for the 5-HT stimulation of pharyngeal pumping and egg laying. *Genetics*, 172(1):159–169, 2006.

Nicole S Hou, Aljona Gutschmidt, Daniel Y Choi, Keouna Pather, Xun Shi, Jennifer L Watts, Thorsten Hoppe, and Stefan Taubert. Activation of the endoplasmic reticulum unfolded protein response by lipid disequilibrium without disturbed proteostasis in vivo. *Proceedings of the National Academy of Sciences*, 111(22):E2271–E2280, 2014.

Chunxiao Hu, James Dillon, James Kearn, Caitriona Murray, Vincent O'Connor, Lindy Holden-Dye, and Hywel Morgan. NeuroChip: a microfluidic electrophysiological device for genetic and chemical biology screening of *Caenorhabditis elegans* adult and larvae. *PloS one*, 8(5):e64297, 2013.

Mingxia Huang and Martin Chalfie. Gene interactions affecting mechanosensory transduction in *Caenorhabditis elegans*. *Nature*, 367(6462):467, 1994.

Nicolas E Humphries and David W Sims. Optimal foraging strategies: Lévy walks balance searching and patch exploitation under a very broad range of conditions. *Journal of Theoretical Biology*, 358:179–193, 2014.

Pavel M Itskov, José-Maria Moreira, Ekaterina Vinnik, Gonçalo Lopes, Steve Safarik, Michael H Dickinson, and Carlos Ribeiro. Automated monitoring and quantitative analysis of feeding behaviour in Drosophila. *Nature Communications*, 5:4560 EP –, 2014.

Shachar Iwanir, Nora Tramm, Stanislav Nagy, Charles Wright, Daniel Ish, and David Biron. The microarchitecture of *C. elegans* behavior during lethargus: homeostatic bout dynamics, a typical body posture, and regulation by a central neuron. *Sleep*, 36(3):385, 2013.

Shachar Iwanir, Adam S. Brown, Stanislav Nagy, Dana Najjar, Alexander Kazakov, Kyung Suk Lee, Alon Zaslaver, Erel Levine, and David Biron. Serotonin promotes exploitation in complex environments by accelerating decision-making. *BMC Biology*, 14 (1), December 2016. ISSN 1741-7007. doi: 10.1186/s12915-016-0232-y. URL `http://www.biomedcentral.com/1741-7007/14/9`.

James E Jan, Russ J Reiter, Martin CO Bax, Urs Ribary, Roger D Freeman, and Michael B Wasdell. Long-term sleep disturbances in children: a cause of neuronal loss. *european journal of paediatric neurology*, 14(5):380–390, 2010.

Guo Jing, Chng Eng Siong, and Deepu Rajan. Foreground motion detection by difference-based spatial temporal entropy image. In *TENCON 2004. 2004 IEEE Region 10 Conference*, volume 1, pages 379–382, Piscataway, N.J, 2004. IEEE, IEEE.

Ming Jing and Faramarz Ismail-Beigi. Role of 5prime-amp-activated protein kinase in stimulation of glucose transport in response to inhibition of oxidative phosphorylation. *American Journal of Physiology-Cell Physiology*, 290(2):C484–C491, 2006.

Stephany Jones, Martha Pfister-Genskow, Ruth M Benca, and Chiara Cirelli. Molecular correlates of sleep and wakefulness in the brain of the white-crowned sparrow. *Journal of neurochemistry*, 105(1):46–62, 2008.

Christopher M Jung, Edward L Melanson, Emily J Frydendall, Leigh Perreault, Robert H Eckel, and Kenneth P Wright. Energy expenditure during sleep, sleep deprivation and sleep following sleep deprivation in adult humans. *The Journal of physiology*, 589(1): 235–244, 2011.

Jae-Eun Kang, Miranda M Lim, Randall J Bateman, James J Lee, Liam P Smyth, John R Cirrito, Nobuhiro Fujiki, Seiji Nishino, and David M Holtzman. Amyloid-β dynamics are regulated by orexin and the sleep-wake cycle. *Science*, 326(5955):1005–1007, 2009.

Yael Katz, Kolbjørn Tunstrøm, Christos C Ioannou, Cristián Huepe, and Iain D Couzin. Inferring the structure and dynamics of interactions in schooling fish. *Proceedings of the National Academy of Sciences*, 108(46):18720–18725, 2011.

Matthew S Kayser, Zhifeng Yue, and Amita Sehgal. A critical period of sleep for development of courtship circuitry and behavior in drosophila. *Science*, 344(6181):269–274, 2014.

Kenji Kimura, Nozomu Tanaka, Nobuhiro Nakamura, Syuichi Takano, and Shoji Ohkuma. Knockdown of mitochondrial heat shock protein 70 promotes progeria-like phenotypes in *Caenorhabditis elegans*. *Journal of Biological Chemistry*, 282(8):5910–5918, 2007.

Kristen L Knutson, Karine Spiegel, Plamen Penev, and Eve Van Cauter. The metabolic consequences of sleep deprivation. *Sleep medicine reviews*, 11(3):163–178, 2007.

Ronen B Kopito and Erel Levine. Durable spatiotemporal surveillance of *Caenorhabditis elegans* response to environmental cues. *Lab on a Chip*, 14(4):764–770, 2014.

John W Krakauer, Asif A Ghazanfar, Alex Gomez-Marin, Malcolm A MacIver, and David Poeppel. Neuroscience needs behavior: correcting a reductionist bias. *Neuron*, 93(3): 480–490, 2017.

David LaBerge. A recruitment theory of simple behavior. *Psychometrika*, 27(4):375–396, December 1962. ISSN 0033-3123, 1860-0980. doi: 10.1007/BF02289645. URL `http://link.springer.com.ezp-prod1.hul.harvard.edu/article/10.1007/BF02289645`.

Arnaud Labrousse, Sophie Chauvet, Carole Couillault, C Léopold Kurz, and Jonathan J Ewbank. *Caenorhabditis elegans* is a model host for salmonella typhimurium. *Current Biology*, 10(23):1543–1545, 2000.

Kyung Suk Lee, Shachar Iwanir, Ronen B. Kopito, Monika Scholz, John A. Calarco, David Biron, and Erel Levine. Serotonin-dependent kinetics of feeding bursts underlie a graded response to food availability in *C. elegans*. *Nature Communications*, 8:14221 EP –, Feb 2017. URL `http://dx.doi.org/10.1038/ncomms14221`. Article.

Raymond YN Lee, Jürgen Hench, and Gary Ruvkun. Regulation of *C. elegans* daf-16 and its human ortholog fkhrl1 by the daf-2 insulin-like signaling pathway. *Current Biology*, 11 (24):1950–1957, 2001.

E. L. Lehmann and Joseph P. Romano. *Testing statistical hypotheses*. Springer texts in statistics. Springer, New York, 3rd ed edition, 2005. ISBN 978-0-387-98864-1.

Sarah F Leibowitz. The role of serotonin in eating disorders. *Drugs*, 39(3):33–48, 1990.

George A. Lemieux and Kaveh Ashrafi. Neural Regulatory Pathways of Feeding and Fat in *Caenorhabditis elegans*. *Annu. Rev. Genet*, 49(1):413–438, 2015. doi: 10.1146/annurev-genet-120213-092244. URL `http://dx.doi.org/10.1146/annurev-genet-120213-092244`. PMID: 26473379.

Guillaume Lettre and Michael O Hengartner. Developmental apoptosis in *C. elegans*: a complex cednario. *Nature Reviews Molecular Cell Biology*, 7(2):97–108, 2006.

Maxwell CK Leung, Phillip L Williams, Alexandre Benedetto, Catherine Au, Kirsten J Helmcke, Michael Aschner, and Joel N Meyer. *Caenorhabditis elegans*: an emerging model in biomedical and environmental toxicology. *Toxicological sciences*, 106(1):5–28, 2008.

Mor Levi-Ferber, Yehuda Salzberg, Modi Safra, Anat Haviv-Chesner, Hannes E Bülow, and Sivan Henis-Korenblit. It's all in your mind: determining germ cell fate by neuronal ire-1 in *C. elegans*. *PLoS Genet*, 10(10):e1004747, 2014.

Daniel A Levitis, William Z Lidicker, and Glenn Freund. Behavioural biologists do not agree on what constitutes behaviour. *Animal behaviour*, 78(1):103–110, 2009.

Zhaoyu Li, Yidong Li, Yalan Yi, Wenming Huang, Song Yang, Weipin Niu, Li Zhang, Zijing Xu, Anlian Qu, Zhengxing Wu, et al. Dissecting a central flip-flop circuit that integrates contradictory sensory cues in *C. elegans* feeding regulation. *Nat. Commun*, 3:776, 2012.

Nataliya Libina, Jennifer R Berman, and Cynthia Kenyon. Tissue-specific activities of *C. elegans* daf-16 in the regulation of lifespan. *Cell*, 115(4):489–502, 2003.

Kui Lin, Jennie B Dorman, Aylin Rodan, and Cynthia Kenyon. daf-16: An hnf-3/forkhead family member that can function to double the life-span of *Caenorhabditis elegans*. *Science*, 278(5341):1319–1322, 1997.

Xueying Lin, Akiko Taguchi, Sunmin Park, Jake A Kushner, Fan Li, Yedan Li, and Morris F White. Dysregulation of insulin receptor substrate 2 in β cells and brain causes obesity and diabetes. *The Journal of Clinical Investigation*, 114(7):908–916, 2004.

S. W. Link and R. A. Heath. A sequential theory of psychological discrimination. *Psychometrika*, 40(1):77–105, March 1975. ISSN 0033-3123, 1860-0980. doi: 10.1007/BF02291481. URL `http://link.springer.com.ezp-prod1.hul.harvard.edu/article/10.1007/BF02291481`.

ZC Liu and Victor Ambros. Heterochronic genes control the stage-specific initiation and expression of the dauer larva developmental program in *Caenorhabditis elegans*. *Genes & Development*, 3(12b):2039–2049, 1989.

Shawn R Lockery, Kristy J Lawton, Joseph C Doll, Serge Faumont, Sarah M Coulthard, Tod R Thiele, Nikolaos Chronis, Katherine E McCormick, Miriam B Goodman, and Beth L Pruitt. Artificial dirt: microfluidic substrates for nematode neurobiology and behavior. *Journal of neurophysiology*, 99(6):3136–3143, 2008.

Shawn R Lockery, S Elizabeth Hulme, William M Roberts, Kristin J Robinson, Anna Laromaine, Theodore H Lindsay, George M Whitesides, and Janis C Weeks. A microfluidic device for whole-animal drug screening using electrophysiological measures in the nematode *C. elegans*. *Lab on a Chip*, 12(12):2211–2220, 2012.

Sarah Luedtke, Vincent O'Connor, Lindy Holden-Dye, and Robert J. Walker. The regulation of feeding and metabolism in response to food deprivation in *Caenorhabditis elegans*. *Invertebrate Neuroscience*, 10(2):63–76, 2010. ISSN 1439-1104. doi: 10.1007/s10158-010-0112-z. URL `http://dx.doi.org/10.1007/s10158-010-0112-z`.

Dylan Lynch and David Biron. *C. elegans: Methods and Applications*. Humana Press, New York, US, 2015.

Pablo Mardones, Gabriela Martínez, and Claudio Hetz. Control of systemic proteostasis by the nervous system. *Trends in cell biology*, 25(1):1–10, 2015.

Stéphanie Maret, Stéphane Dorsaz, Laure Gurcel, Sylvain Pradervand, Brice Petit, Corinne Pfister, Otto Hagenbuchle, Bruce F O'Hara, Paul Franken, and Mehdi Tafti. Homer1a is a core brain molecular correlate of sleep loss. *Proceedings of the National Academy of Sciences*, 104(50):20090–20095, 2007.

Kevin S McCann, JB Rasmussen, and James Umbanhowar. The dynamics of spatially coupled food webs. *Ecology Letters*, 8(5):513–523, 2005.

Kazutoshi Mori. Signalling pathways in the unfolded protein response: development from yeast to mammals. *Journal of biochemistry*, 146(6):743–750, 2009.

Stanislav Nagy, Nora Tramm, Jarred Sanders, Shachar Iwanir, Ian A Shirley, Erel Levine, and David Biron. Homeostasis in *C. elegans* sleep is characterized by two behaviorally and genetically distinct mechanisms. *Elife*, 3:e04380, 2014.

Nirinjini Naidoo. Cellular stress/the unfolded protein response: relevance to sleep and sleep disorders. *Sleep medicine reviews*, 13(3):195–204, 2009.

Nirinjini Naidoo. Roles of endoplasmic reticulum and energetic stress in disturbed sleep. *Neuromolecular medicine*, 14(3):213–219, 2012.

Nirinjini Naidoo, William Giang, Raymond J Galante, and Allan I Pack. Sleep deprivation induces the unfolded protein response in mouse cerebral cortex. *Journal of neurochemistry*, 92(5):1150–1157, 2005a.

Nirinjini Naidoo, William Giang, Raymond J Galante, and Allan I Pack. Sleep deprivation induces the unfolded protein response in mouse cerebral cortex. *Journal of neurochemistry*, 92(5):1150–1157, 2005b.

Nirinjini Naidoo, Vincent Casiano, Jacqueline Cater, John Zimmerman, and Allan I Pack. A role for the molecular chaperone protein bip/grp78 in drosophila sleep homeostasis. *SLEEP-NEW YORK THEN WESTCHESTER-*, 30(5):557, 2007.

Matthew R Nassar, Robert C Wilson, Benjamin Heasly, and Joshua I Gold. An approximately Bayesian delta-rule model explains the dynamics of belief updating in a changing environment. *The Journal of Neuroscience*, 30(37):12366–12378, 2010.

Elena V Nikonova, Nirinjini Naidoo, Lin Zhang, Micah Romer, Jacqueline R Cater, Matthew T Scharf, Raymond J Galante, and Allan I Pack. Changes in components of energy regulation in mouse cortex with increases in wakefulness. *Sleep*, 33(7):889–900, 2010.

Anders Olsen, Maithili C Vantipalli, and Gordon J Lithgow. Using *Caenorhabditis elegans* as a model for aging and age-related diseases. *Annals of the New York Academy of Sciences*, 1067(1):120–128, 2006.

Judith Owens, Rhoda Au, Mary Carskadon, Richard Millman, Amy Wolfson, Paula K Braverman, William P Adelman, Cora C Breuner, David A Levine, Arik V Marcell, et al. Insufficient sleep in adolescents and young adults: an update on causes and consequences. *Pediatrics*, 134(3):e921–e932, 2014.

June J Pilcher and Allen J Huffcutt. Effects of sleep deprivation on performance: a meta-analysis. *Sleep: Journal of Sleep Research & Sleep Medicine*, 19(4):318–326, 1996.

PS Prado-Lima, CHA Cruz, CA Netto, and J Licinio. Human food preferences are associated with a 5-ht2a serotonergic receptor polymorphism. *Molecular psychiatry*, 11(10):889–891, 2006.

David M Raizen and Leon Avery. Electrical activity and behavior in the pharynx of *Caenorhabditis elegans*. *Neuron*, 12(3):483–495, 1994.

David M Raizen, RY Lee, and Leon Avery. Interacting genes required for pharyngeal excitation by motor neuron mc in *Caenorhabditis elegans*. *Genetics*, 141(4):1365–1382, 1995a.

David M Raizen, RY Lee, and Leon Avery. Interacting genes required for pharyngeal excitation by motor neuron MC in *Caenorhabditis elegans*. *Genetics*, 141(4):1365–1382, 1995b.

David M Raizen, John E Zimmerman, Matthew H Maycock, Uyen D Ta, Young-jai You, Meera V Sundaram, and Allan I Pack. Lethargus is a *Caenorhabditis elegans* sleep-like state. *Nature*, 451(7178):569–572, 2008.

Catherine H Rankin, Christine DO Beck, and Catherine M Chiba. *Caenorhabditis elegans*: a new model system for the study of learning and memory. *Behavioural brain research*, 37 (1):89–92, 1990.

Roger Ratcliff, Anil Cherian, and Mark Segraves. A comparison of macaque behavior and superior colliculus neuronal activity to predictions from models of two-choice decisions. *Journal of Neurophysiology*, 90(3):1392–1407, 2003.

B. a. J. Reddi, K. N. Asrress, and R. H. S. Carpenter. Accuracy, Information, and Response Time in a Saccadic Decision Task. *Journal of Neurophysiology*, 90(5):3538–3546, November 2003. ISSN 0022-3077, 1522-1598. doi: 10.1152/jn.00689.2002. URL `http://jn.physiology.org.ezp-prod1.hul.harvard.edu/content/90/5/3538`.

Sirimon Reutrakul and Eve Van Cauter. Interactions between sleep, circadian function, and glucose metabolism: implications for risk and severity of diabetes. *Annals of the New York Academy of Sciences*, 1311(1):151–173, 2014.

LS Salinas, E Maldonado, and RE Navarro. Stress-induced germ cell apoptosis by a p53 independent pathway in *Caenorhabditis elegans*. *Cell Death & Differentiation*, 13(12): 2129–2139, 2006.

Jarred Sanders, Stanislav Nagy, Graham Fetterman, Charles Wright, Millet Treinin, and David Biron. The *Caenorhabditis elegans* interneuron ala is (also) a high-threshold mechanosensor. *BMC Neuroscience*, 14(1):156, 2013. ISSN 1471-2202. doi: 10.1186/1471-2202-14-156. URL `http://dx.doi.org/10.1186/1471-2202-14-156`.

Matti Saraste. Oxidative phosphorylation at the fin de siecle. *Science*, 283(5407):1488–1493, 1999.

Monika Scholz. pWARP: analyzing *C.elegans* pumping behavior, April 2016a. URL `http://dx.doi.org/10.5281/zenodo.49982`.

Monika Scholz. Device specifications: Automatic measuring of pharyngeal pumping, Jul 2016b. URL `osf.io/uv8tz`.

Monika Scholz, Dylan J Lynch, Kyung Suk Lee, Erel Levine, and David Biron. A scalable method for automatically measuring pharyngeal pumping in *C. elegans*. *Journal of Neuroscience Methods*, 274:172–178, 2016a.

Monika Scholz, Dylan J Lynch, Kyung Suk Lee, Erel Levine, and David Biron. A scalable method for automatically measuring pharyngeal pumping in *C. elegans*. *Journal of Neuroscience Methods*, 274:172–178, 2016b.

Björn Schumacher, Momoyo Hanazawa, Min-Ho Lee, Sudhir Nayak, Katrin Volkmann, Randall Hofmann, Michael Hengartner, Tim Schedl, and Anton Gartner. Translational repression of *C. elegans* p53 by gld-1 regulates dna damage-induced apoptosis. *Cell*, 120(3): 357–368, 2005.

Juliane Schwarz, Jan-Philipp Spies, and Henrik Bringmann. Reduced muscle contraction and a relaxed posture during sleep-like lethargus. 1(1):12–14, 2012.

Paul J Shaw, Chiara Cirelli, Ralph J Greenspan, and Giulio Tononi. Correlates of sleep and waking in drosophila melanogaster. *Science*, 287(5459):1834–1837, 2000.

Paul J Shaw, Giulio Tononi, Ralph J Greenspan, and Donald F Robinson. Stress response genes protect against lethal effects of sleep deprivation in drosophila. *Nature*, 417(6886): 287–291, 2002.

Xiaohua Shen, Ronald E Ellis, Kyungho Lee, Chuan-Yin Liu, Kun Yang, Aaron Solomon, Hiderou Yoshida, Rick Morimoto, David M Kurnit, Kazutoshi Mori, et al. Complementary signaling pathways regulate the unfolded protein response and are required for *C. elegans* development. *Cell*, 107(7):893–903, 2001.

Boris Borisovich Shtonda and Leon Avery. Dietary choice behavior in *Caenorhabditis elegans*. *J. Exp. Biol.*, 209(1):89–102, 2006.

Jerome M Siegel. Clues to the functions of mammalian sleep. *Nature*, 437(7063):1264–1271, 2005.

Eric D. Siggia and Massimo Vergassola. Decisions on the fly in cellular sensory systems. *Proceedings of the National Academy of Sciences of the United States of America*, 110(39): E3704–E3712, September 2013. ISSN 0027-8424. URL `http://www.ncbi.nlm.nih.gov/pmc/articles/PMC3785727/`.

Komudi Singh, Michael Y Chao, Gerard A Somers, Hidetoshi Komatsu, Mark E Corkins, Jonah Larkins-Ford, Tim Tucey, Heather M Dionne, Melissa B Walsh, Emma K Beaumont, et al. *C. elegans* notch signaling regulates adult chemosensory response and larval molting quiescence. *Current Biology*, 21(10):825–834, 2011.

Komudi Singh, Jennifer Y Ju, Melissa B Walsh, Michael A DiIorio, and Anne C Hart. Deep conservation of genes required for both drosophila melanogaster and *Caenorhabditis elegans* sleep includes a role for dopaminergic signaling. *Sleep*, 37(9):1439, 2014.

RN Singh and JE Sulston. Some observations on moulting in *Caenorhabditis elegans*. *Nematologica*, 24(1):63–71, 1978.

Bo-mi Song and Leon Avery. Serotonin activates overall feeding by activating two separate neural pathways in *Caenorhabditis elegans*. *Journal of Neuroscience*, 32(6):1920–1931, 2012.

Bo-Mi Song and Leon Avery. The pharynx of the nematode *C. elegans*: a model system for the study of motor control. In *Worm*, volume 2, pages 1920–1931. Taylor & Francis, Milton Park, Abingdon-on-Thames, Oxfordshire United Kingdom, 2013.

Bo-Mi Song, Serge Faumont, Shawn Lockery, and Leon Avery. Recognition of familiar food activates feeding via an endocrine serotonin signal in *Caenorhabditis elegans*. *Elife*, 2: e00329, 2013.

Mircea Steriade. Impact of network activities on neuronal properties in corticothalamic systems. *Journal of neurophysiology*, 86(1):1–39, 2001.

Fleur L Strand. Neuropeptides: general characteristics and neuropharmaceutical potential in treating cns disorders. In *Peptide Transport and Delivery into the Central Nervous System*, pages 1–37. Springer, New York, US, 2003.

Richard S. Sutton and Andrew G. Barto. *Reinforcement Learning: An Introduction*. MIT Press, 1998. ISBN 978-0-262-19398-6. Google-Books-ID: CAFR6IBF4xYC.

Alexander G Tartakovsky. On Asymptotic Optimality in Sequential Changepoint Detection: Non-iid Case. *arXiv preprint arXiv:1510.03827*, 2015.

Rebecca C Taylor and Andrew Dillin. Xbp-1 is a cell-nonautonomous regulator of stress resistance and longevity. *Cell*, 153(7):1435–1447, 2013.

LH Tecott and L Abdallah. Mouse genetic approaches to feeding regulation: serotonin 5-ht2c receptor mutant mice. *CNS spectrums*, 8(8):584, 2003.

A Terao, TL Steininger, K Hyder, A Apte-Deshpande, J Ding, D Rishipathak, RW Davis, HC Heller, and TS Kilduff. Differential increase in the expression of heat shock protein family members during sleep deprivation and during sleep. *Neuroscience*, 116(1):187–200, 2003.

Melanie C Thein, Gillian McCormack, Alan D Winter, Iain L Johnstone, Charles B Shoemaker, and Antony P Page. *Caenorhabditis elegans* exoskeleton collagen col-19: An adult-specific marker for collagen modification and assembly, and the analysis of organismal morphology. *Developmental dynamics*, 226(3):523–539, 2003.

Igor Timofeev, François Grenier, and Mircea Steriade. Disfacilitation and active inhibition in the neocortex during the natural sleep-wake cycle: an intracellular study. *Proceedings of the National Academy of Sciences*, 98(4):1924–1929, 2001.

Niko Tinbergen. *The study of instinct.* Clarendon Press/Oxford University Press, Oxford, England, U.K., 1951.

Niko Tinbergen. On aims and methods of ethology. *Ethology*, 20(4):410–433, 1963.

Giulio Tononi and Chiara Cirelli. Sleep function and synaptic homeostasis. *Sleep medicine reviews*, 10(1):49–62, 2006.

Giulio Tononi and Chiara Cirelli. Sleep and the price of plasticity: from synaptic and cellular homeostasis to memory consolidation and integration. *Neuron*, 81(1):12–34, 2014.

Marta Torres, Ricardo Laguna-Barraza, Mireia Dalmases, Alexandra Calle, Eva Pericuesta, Josep M Montserrat, Daniel Navajas, Alfonso Gutierrez-Adan, and Ramon Farré. Male fertility is reduced by chronic intermittent hypoxia mimicking sleep apnea in mice. *Sleep*, 37(11):1757–1765, 2014.

Nora Tramm, Naomi Oppenheimer, Stanislav Nagy, Efi Efrati, and David Biron. Why do sleeping nematodes adopt a hockey-stick-like posture? *PloS one*, 9(7):e101162, 2014.

M. Treinin and M. Chalfie. A mutated acetylcholine receptor subunit causes neuronal degeneration in *C. elegans*. *Neuron*, 14:871–877, 1995. doi: 10.1016/0896-6273(95)90231-7. URL `http://dx.doi.org/10.1016/0896-6273(95)90231-7`.

M. Treinin, B. Gillo, L. Liebman, and M. Chalfie. Two functionally dependent acetylcholine subunits are encoded in a single *Caenorhabditis elegans* operon. *Proc Natl Acad Sci USA*, 95:15492–15495, 1998. doi: 10.1073/pnas.95.26.15492. URL `http://dx.doi.org/10.1073/pnas.95.26.15492`.

Carol Trent, Nancy Tsung, and H Robert Horvitz. Egg-laying defective mutants of the nematode *Caenorhabditis elegans*. *Genetics*, 104(4):619–647, 1983.

Nicholas F Trojanowski and David M Raizen. Call it worm sleep. *Trends in neurosciences*, 39(2):54–62, 2016.

Nicholas F Trojanowski, Olivia Padovan-Merhar, David M Raizen, and Christopher Fang-Yen. Neural and genetic degeneracy underlies *Caenorhabditis elegans* feeding behavior. *J. Neurophysiol.*, 112(4):951–961, 2014.

Ephraim L Tsalik, Timothy Niacaris, Adam S Wenick, Kelvin Pau, Leon Avery, and Oliver Hobert. Lim homeobox gene-dependent expression of biogenic amine receptors in restricted regions of the *C. elegans* nervous system. *Developmental biology*, 263(1):81–102, 2003.

Naoshige Uchida, Adam Kepecs, and Zachary F. Mainen. Seeing at a glance, smelling in a whiff: rapid forms of perceptual decision making. *Nature Reviews Neuroscience*, 7(6):485–491, June 2006. ISSN 1471-003X. doi: 10.1038/nrn1933. URL `http://www.nature.com.ezp-prod1.hul.harvard.edu/nrn/journal/v7/n6/abs/nrn1933.html`.

Fumihiko Urano, Marcella Calfon, Takunari Yoneda, Chi Yun, Moni Kiraly, Scott G Clark, and David Ron. A survival pathway for *Caenorhabditis elegans* with a blocked unfolded protein response. *The Journal of cell biology*, 158(4):639–646, 2002.

Alexander Varshavsky. Augmented generation of protein fragments during wakefulness as the molecular cause of sleep: a hypothesis. *Protein Science*, 21(11):1634–1661, 2012.

Massimo Vergassola, Emmanuel Villermaux, and Boris I. Shraiman. 'Infotaxis' as a strategy for searching without gradients. *Nature*, 445(7126):406–409, January 2007. ISSN 0028-0836. doi: 10.1038/nature05464. URL `http://www.nature.com.ezp-prod1.hul.harvard.edu/nature/journal/v445/n7126/full/nature05464.html`.

Vladyslav V Vyazovskiy and Kenneth D Harris. Sleep and the single neuron: the role of global slow oscillations in individual cell rest. *Nature Reviews Neuroscience*, 14(6):443–451, 2013.

Laura E Waggoner, G Tong Zhou, Ronald W Schafer, and William R Schafer. Control of alternative behavioral states by serotonin in *Caenorhabditis elegans*. *Neuron*, 21(1): 203–214, 1998.

Gordon Wang, Brian Grone, Damien Colas, Lior Appelbaum, and Philippe Mourrain. Synaptic plasticity in sleep: learning, homeostasis and disease. *Trends in neurosciences*, 34(9): 452–463, 2011.

Samuel Ward and John S Carrel. Fertilization and sperm competition in the nematode *Caenorhabditis elegans*. *Developmental biology*, 73(2):304–321, 1979.

Stephen C. Woods, Michael W. Schwartz, Denis G. Baskin, and Randy J. Seeley. Food Intake and the Regulation of Body Weight. *Annual Review of Psychology*, 51(1):255–277, 2000. doi: 10.1146/annurev.psych.51.1.255. URL `http://dx.doi.org/10.1146/annurev.psych.51.1.255`.

Lulu Xie, Hongyi Kang, Qiwu Xu, Michael J Chen, Yonghong Liao, Meenakshisundaram Thiyagarajan, John OâĂŹDonnell, Daniel J Christensen, Charles Nicholson, Jeffrey J Iliff, et al. Sleep drives metabolite clearance from the adult brain. *science*, 342(6156): 373–377, 2013.

Ding Xue, Shai Shaham, and H Robert Horvitz. The *Caenorhabditis elegans* cell-death protein ced-3 is a cysteine protease with substrate specificities similar to those of the human cpp32 protease. *Genes & Development*, 10(9):1073–1083, 1996.

Xin Xue, Jiang-Hu Piao, Akihito Nakajima, Sachiko Sakon-Komazawa, Yuko Kojima, Kazutoshi Mori, Hideo Yagita, Ko Okumura, Heather Harding, and Hiroyasu Nakano. Tumor necrosis factor α (tnfα) induces the unfolded protein response (upr) in a reactive oxygen species (ros)-dependent fashion, and the upr counteracts ros accumulation by tnfα. *Journal of Biological Chemistry*, 280(40):33917–33925, 2005.

Takunari Yoneda, Cristina Benedetti, Fumihiko Urano, Scott G Clark, Heather P Harding, and David Ron. Compartment-specific perturbation of protein handling activates genes encoding mitochondrial chaperones. *Journal of cell science*, 117(18):4055–4066, 2004.

Junying Yuan and H Robert Horvitz. The *Caenorhabditis elegans* genes ced-3 and ced-4 act cell autonomously to cause programmed cell death. *Developmental biology*, 138(1):33–41, 1990.

Eva Zeiser, Christian Frøkjær-Jensen, Erik Jorgensen, and Julie Ahringer. Mossci and gateway compatible plasmid toolkit for constitutive and inducible expression of transgenes in the *C. elegans* germline. *PLoS One*, 6(5):e20082, 2011.

Kezhong Zhang and Randal J Kaufman. The unfolded protein response a stress signaling pathway critical for health and disease. *Neurology*, 66(1 suppl 1):S102–S109, 2006.

Zheng Zhou, Erika Hartwieg, and H Robert Horvitz. Ced-1 is a transmembrane receptor that mediates cell corpse engulfment in *C. elegans*. *Cell*, 104(1):43–56, 2001.

John E Zimmerman, Wendy Rizzo, Keith R Shockley, David M Raizen, Nirinjini Naidoo, Miroslaw Mackiewicz, Gary A Churchill, and Allan I Pack. Multiple mechanisms limit the duration of wakefulness in drosophila brain. *Physiological genomics*, 27(3):337–350, 2006.